NTNU

Norwegian University of
Science and Technology

Recovery Mechanisms in Naturally Fractured Carbonate Reservoirs: A Case Study of the Barents Sea Alta Discovery using Dual Porosity Model Simulations

Tonje Løland Bjerga

Petroleum Geoscience and Engineering
Submission date: June 2017
Supervisor: Jon Kleppe, IGP

Norwegian University of Science and Technology
Department of Geoscience and Petroleum

Abstract

The Barents Sea Alta discovery consists primarily of fractured carbonate formations from the Mid-Carboniferous to Permian period. Significantly fractured reservoirs are subject to different recovery mechanisms than conventional ones including gravity drainage, spontaneous imbibition, fluid expansion and diffusion. The reservoirs are commonly analyzed as two porous systems and the main objective lies in optimized oil transfer from the tight matrix to the fracture. This process depends on characteristics of the reservoir that typically have great uncertainty, making fractured reservoir development one of the most difficult technologies in oil field exploitation.

This thesis investigates oil recovery from the Alta dual porosity system with respect to key reservoir parameters; matrix block height, size / shape, capillary pressure, wettability and inter-block contact. Wettability is essential for recovery in fractured reservoirs, and as 80 % of the world's carbonate reservoirs have shown oil-wetting tendencies, this poses an important subject in the Alta field concept studies (Treiber et al., 1972; Chilingar and Yen, 1983). The impact of the listed reservoir characteristics are tested with crestal gas injection as well as water injection in the underlying aquifer. The study is performed using ECLIPSE's dual porosity/ dual permeability model of which computational aspects and validity is discussed.

Typical gas-oil capillary pressure curves for vuggy carbonates are tested with varying vertical matrix block height. The results show that block height is essential to achieve good recovery when matrix blocks are completely discontinuous. However, matrix-matrix flow corresponding to only 5 % contact area between the blocks, gives a dramatic increase in recovery. If the contact area exceeds 25 %, recovery is close to that of a completely continuous stack, while production of water from the aquifer remains lower. When the reservoir rock is strongly oil-wet, poor recovery is achieved with water injection, as entry of water into the matrix becomes a drainage process. If the reservoir is strongly water-wet, full recovery is achieved with spontaneous imbibition, and matrix block height is insignificant for the entry of water into the matrix. The examples also show that with tall matrix blocks, movement of the water front in fractures close to the producer is accelerated, which may reduce ultimate recovery due to an early water-breakthrough. The sigma factor is tested and found to have larger effect in an imbibition process compared to gravity drainage, which is important to consider in history matching of well data.

The thesis concludes that as long as either matrix shape, matrix height or reservoir wettability represent a great uncertainty in the Alta discovery, gas injection is the safest choice. However, lack of infrastructure in the Barents Sea combined with less availability of gas compared to water, is acknowledged and potential concepts briefly discussed. A simplified WAG injection example is also included and shows increased recovery compared to one phase water injection. All findings of this thesis form a solid foundation for more detailed studies of a WAG strategy.

Sammendrag

Alta-funnet i Barentshavet, med Lundin Norge AS som operatør, er gjort i oppsprukkede reservoarbergarter i karbonater fra perm og karbon alder. I slike reservoarer råder andre utvinningsmekanismer enn i de konvensjonelle, inkludert gravitasjons-drenering, spontan-imbibering, fluid-utvidelse og diffusjon. Oppsprukkede reservoarer analyseres vanligvis som to porøse systemer, der hovedmålet er å optimalisere overføring av olje fra det tette matrikkelmaterialet til sprekkenettverket. Denne prosessen er avhengig av karakteristikker i reservoaret som ofte forbindes med mye usikkerhet, noe som gjør evaluering av sprekkereservoarer til en av de vanskeligste prosessene innen petroleumsteknologi.

Denne oppgaven tar for seg utvinning av olje fra ett 'dobbel-porøsitet' system med hensyn til flere sentrale reservoar parametere; høyde av matrikkelblokk, størrelse og form, kapillærtrykk, fuktegenskaper og kontakt mellom blokker. Fukt (wettability) er essensielt for utvinning fra oppsprukkede reservoarer, og siden 80% av verdens karbonatreservoarer er oljefuktede, utgjør dette en viktig del av konseptstudiene for utnytting av Alta-ressursene (Treiber et al., 1972; Chilingar and Yen, 1983). Påvirkningen slike reservoarkarakteristikker har på oljeutvinning er testet både med gassinjeksjon i gasskappen, samt vanninjeksjon i underliggende akvifer. Studien tar i bruk ECLIPSE sin 'dual porosity/ dual permeability' model, og tilhørende beregninger samt gyldighet av modellen er diskutert.

Typiske gass-olje kapillærkurver for 'vuggy' karbonater er blitt testet for varierende høyde av matrikkelblokkene. Resultatene viser at blokkhøyden er essensiell for å oppnå høy utvinning så lenge blokkene er diskontinuerlige, men med strømning mellom matrikkelblokkene tilsvarende ett kontaktareal på 5%, øker utvinningsgraden dramatisk. Når kontaktarealet overstiger 25 %, er utvinningen tilnærmet lik den fra en fullstendig kontinuerlig matrikkelstakk. Når reservoaret er sterkt oljefuktet, gir vanninjeksjon lav utvinnningsgrad siden inntrengning av vann i matrikkelblokken blir en drenerings ('drainage') -prosess. Hvis reservoaret er sterkt vannfuktet oppnås derimot full utvinningsgrad gjennom spontanimbibiering og blokkhøyde er ubetydelig for inntreden av vann i matrikkelblokken. 'Sigmafaktoren' til matrikkelblokkene er også testet, og denne har større betydning for en imbiberingsprosess sammenlignet med gass gravitasjon-drenering prosess, noe som er viktig å ta i betrakning under historietilpasning av reservoaret.

Oppgaven konkluderer med at så lenge det er knyttet usikkerhet til form, høyde eller fuktegenskaper til matrikkelblokkene, vil gassinjeksjon være den sikreste utvinningstrategien. Mangelen på eksisterende infrastruktur i Barentshavet samt lavere tilgjengelighet på gass sammenlignet med vann for injeksjon utgjør en ekstra utfordring i valg av utvinningstrategi. Mulige konsepter for å løse disse utfordringene er kort diskutert. Ett forenklet WAG-injeksjon eksempel er også inkludert og viser økt utvinningsgrad sammenlignet med enfase vanninjeksjon. Alle observasjonene i denne oppgaven danner ett solid grunnlag for mer detaljerte studier av WAG-strategi på Alta funnet.

Acknowledgment

This thesis was written at the Department of Geoscience and Petroleum as the fulfillment of a Master's degree in Reservoir Engineering and Petrophysics at the Norwegian University of Science and Technology (NTNU). The thesis was carried out during the spring semester of 2017 and in cooperation with the Norwegian oil company, Lundin Norway AS.

I would like to thank the team at Lundin for the opportunity to conduct a thesis of current and industrial interest, and for great guidance during the course of the work. In particular Jens Petter Nørgård deserves to be thanked for his role as academic advisor, for his insight and assistance in choosing a problem description and in simulation related questions. Further, a thank you goes out to Per Øyvind Seljebotn, Kjersti Mathisen Engh, Alister MacDonald, Ingrid Piene Gianotten, Lars Sundal and Atle Dalva for assistance, good spirits and inspiring dedication for their line of work.

A special thank you to my supervisor Professor Jon Kleppe for his guidance during the course of this thesis, as well as previous semesters. His solid mentoring, good mood and always open door has been greatly and frequently appreciated.

Trondheim, June 2017

_____

Tonje L. Bjerga

Contents

List of Figures

List of Tables

Chapter 1

Introduction

In this thesis fractured reservoir recovery mechanisms are investigated through dual porosity / dual permeability simulations. The sensitivity of main fractured reservoir characteristics are studied, including matrix block height, the shape/ size factor, capillary pressure and contact area between blocks. Both gas and water flooding of the reservoir are studied and emphasis given to capillary continuity and matrix capillary pressure for gas-oil gravity drainage, and wetting-preferences in a water-injection scheme.

In 2014, Lundin Norway AS proved oil in the Alta exploration project on the southern part of the Loppa High (**Figure 1.1**). Later appraisal of the discovery has delimitated an eastern flank dominated by carbonate formations from the Permian and Carboniferous periods (330-275 Ma.). A 45 meter oil column was encountered in the Gipsdalen Group, and successful injection tests have been performed in the Ørn and Falk Formations (**Figure 1.2**). The reservoir rock is assumed to consist of naturally fractured, possibly karstified materiale, which complicates reservoir characterization and modeling compared to a conventional, un-fractured reservoir.

More than 60% of the world's oil reserves are held in carbonates, and the majority of these are defined as fractured, i.e. that fractures have a significant impact on performance and recovery. With more complex reservoir dynamics, fractured reservoirs have traditionally suffered from a low recovery compared to conventional sandstone and carbonate petroleum reservoirs (Allan et al., 2003). However, as the easiest producible oil is exploited first, 60 % of the worlds remaining proven hydrocarbon reserves are thought to be in naturally fractured(e.g. carbonates) and hydraulically fractured (e.g. shale gas) reservoirs (Chima et al., 2012).

In Norway, fractured reservoir exploitation have proven a great success with the giant Ekofisk Field in the North Sea, producing from several chalk reservoirs, e.g. deepwater carbonate depositions. Made up of entirely different mineralogy and composition, the shallow water deposited carbonates of the Alta discovery impose different challenges to the reservoir development. For example will different block size and wettability have a significant impact on the effect of the main recovery mechanisms in a fractured reservoir; gravity drainage and capillary imbibition. Wettability is a complex property, and measurements are commonly limited to experiments on small, restored core samples, which may not represent the full,

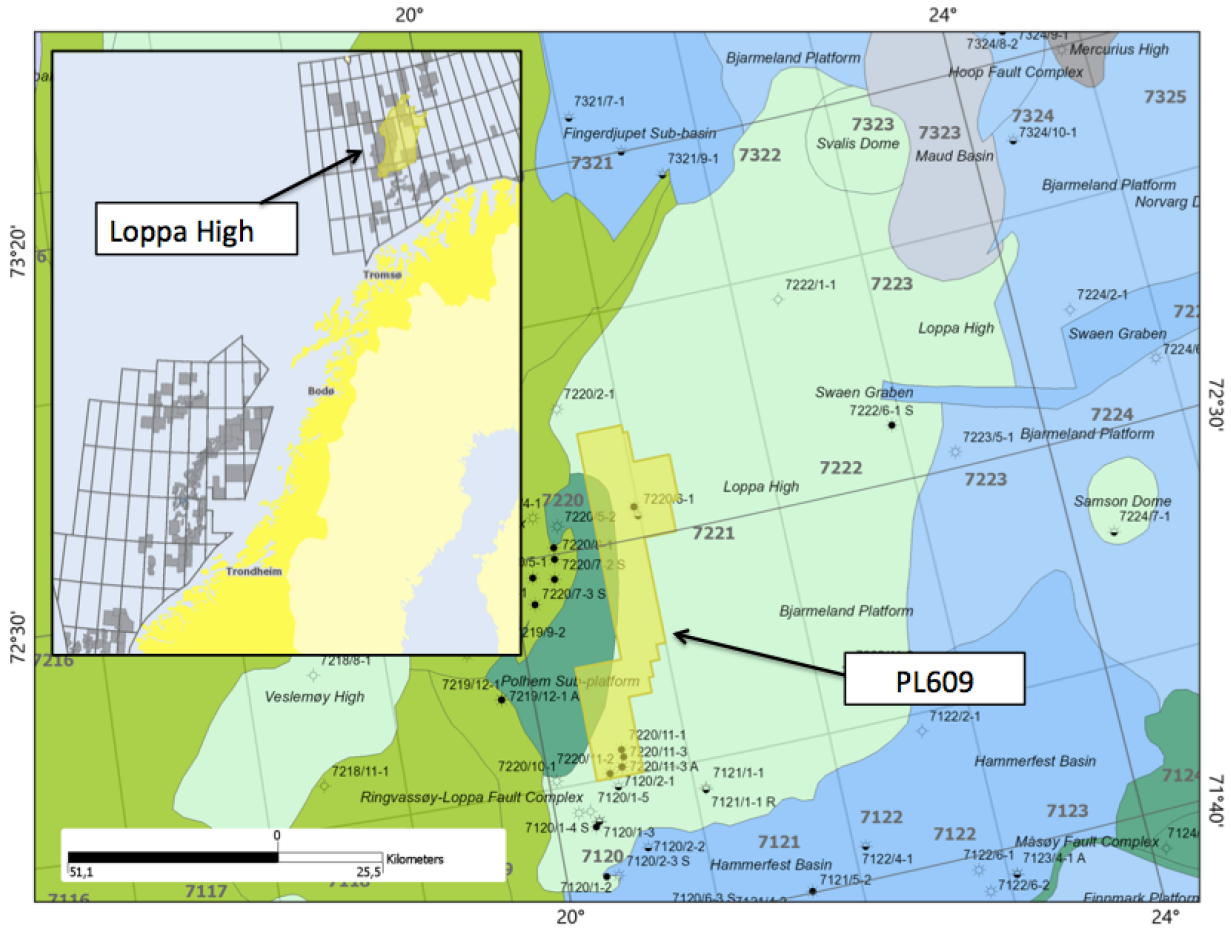

Figure 1.1: The Alta prospect is situated in the south part of the Barents Sea, roughly 160 km from the Norwegian coastline. The yellow color marks the Loppa High structure and production license 609 (PL609) where the discovery was made (NPD, 2016b).

native state reservoir. Studies suggest that more than 80 % of carbonate reservoirs have oil wet preferences (Chilingar and Yen, 1983; Treiber et al., 1972). When this is the case, the performance of water flooding is severely reduced, and may even do irreducible damage to the reservoir.

In oil wet reservoirs, gas-oil gravity drainage (GOGD) is recognized as the most successful recovery technique. When gravity drainage is the main contributor to matrix-fracture transfer, the amount of oil recovered depends largely upon the discontinuous matrices vertical height or block-to block contact, as well as capillary and threshold pressure of the matrix and fracture continuum.

The thesis starts with a description and literature study of the processes affecting recovery in a fractured reservoir; fluid expansion, capillary imbibition, gravity imbibition / drainage, diffusion and viscous displacement, as well as important parameters affecting these processes. Chapter 3 explains the principles of dual porosity modeling and specific functions and modeling limitations related to the work of this thesis. Chapter 4 describes the test model, which is a full-scale section of Lundin's Alta model and results along with preliminary discussion of the results are presented in chapter 5. Main discussion of the results and validity of those are given in Chapter 6 followed by recommendations for further work and concluding remarks.

The Alta Discovery

This section has been modified from a specialization project report written by the author.

The Alta discovery well, 7220/11-1 was the first out of currently four wells that have been spudded with Lundin's production license 609 (Figure 1.1). The last appraisal well, 7220/11-4, is currently being drilled and the drilling operation is estimated to be complete by mid-July 2017. The four wells are situated in the south-west end of the Loppa High, a structural high in the southern part of the Barents Sea (light green structure in Figure 1.1). The initial discovery was made 20 kilometers northeast of the 2013 Gohta discovery (well 7120/1-3) and 30 kilometers away from the recent Filicudi discovery (7219/12-1). Prelimenary evaluation by the Norwegian Petroleum Directorate (NPD) estimate recoverable oil and gas resources from the Alta discovery to approximately 35.8 million standard cubic meters oil equivalents (Sm^3 o.e.), and STOOIP of 26.1 Sm^3 (NPD and MPE, 2016).

The eastern flank of the Alta discovery were appraised with well 7220/11-3 in 2015. Following technical challenges the well had to be abandoned and a technical sidetrack was drilled 30-40 meters from initial trajectory, to core. A geological sidetrack (7220/11-3A) were drilled approximately 400 m southeast from the abandoned well. The well was re-deepened (7220/11-3 AR) and abandoned at 2389 m TVD seabed (NPD, 2016a). Well 7220/11-3 hit a 75 m long gas column and upper part of an oil column in Gipsdalen Group carbonates. The hydrocarbon zone proved "good to very good" reservoir quality (NPD, 2015). The sidetrack (7220/11-3A) proved a 44 m oil column, however of reduced reservoir quality.

Geological Setting

Several authors have described the geological structures of the Loppa High (Sayago et al., 2012; Elvebakk et al., 2003; Hunt et al., 2003; Carrillat et al., 2005; Fisher et al., 2010). The publications, mainly built on seismic analysis, suggests that large volumes of breccia deposits in the upper Paleozoic carbonates are derived from extensive coalesced paleocave systems formed during periodical uplift, exposure and subsequent burial and collapse.

By paleocave system it is referred to ancient karst features that have been fossilized or otherwise preserved. Karstification refers to the process where soluble carbonates (typically limestone or gypsum) have dissolved as a consequence of exposure to meteoric, acidic water, mainly rainwater. During multiple exposures several karst systems may overprint, forming cave systems in the subsurface. Depending on features such as fracture-intensity or thickness of the cave roof, the cave may collapse when subjected to burial. This process creates chaotic breccia including blocks and pieces of varying size from the bed rock. The blocks will retain their bedding from the primary depositional process, yielding a dual porosity system of primary and secondary pore systems (Loucks, 1999). Known karst-modified fractured reservoirs include include Spain's Casablanca and the Chinese Yangling Field.

The Gipsdalen Group is one of two carbonate units present at the Loppa High and consists of rocks of mid-Carboniferous to early Permian age (330-275 Ma.). The group includes three

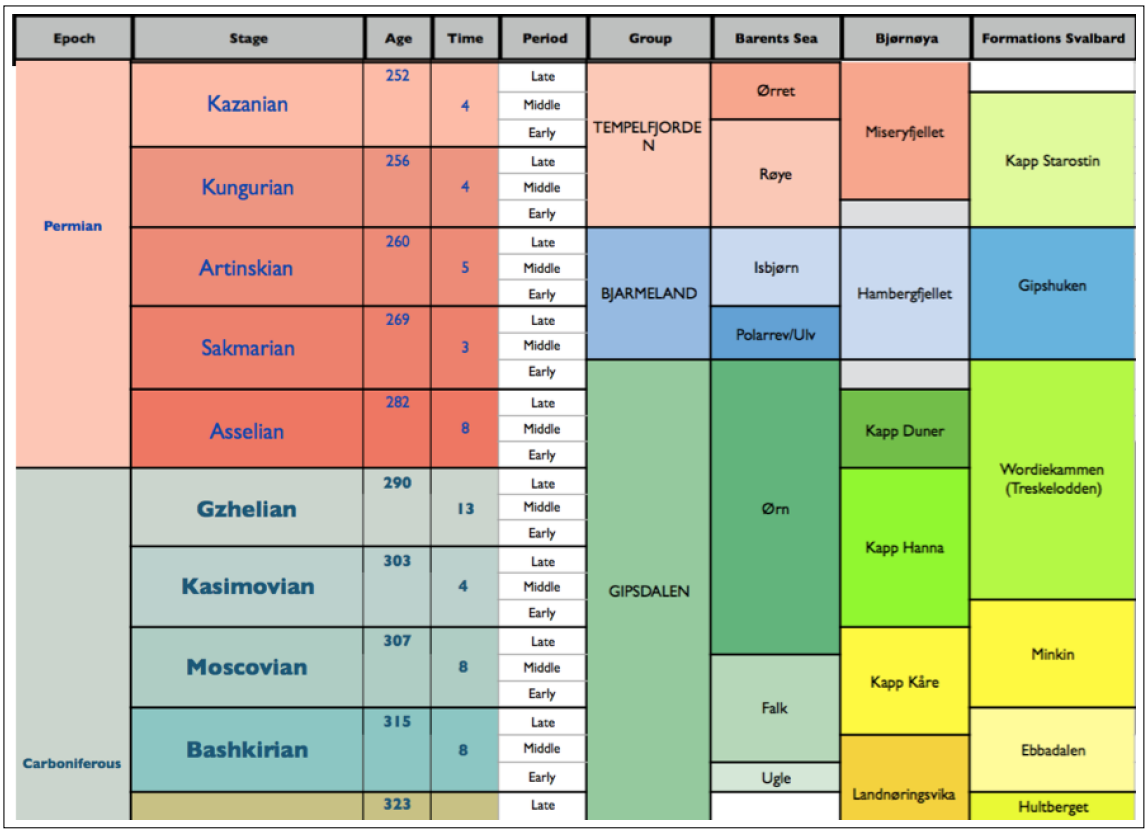

Figure 1.2: The figure depicts a section of the Paleozoic Era including the Gipsdalen Group and Ørn and Falk formations which make up the main reservoir rock in the Alta discovery. Figure from Siggerud (2015).

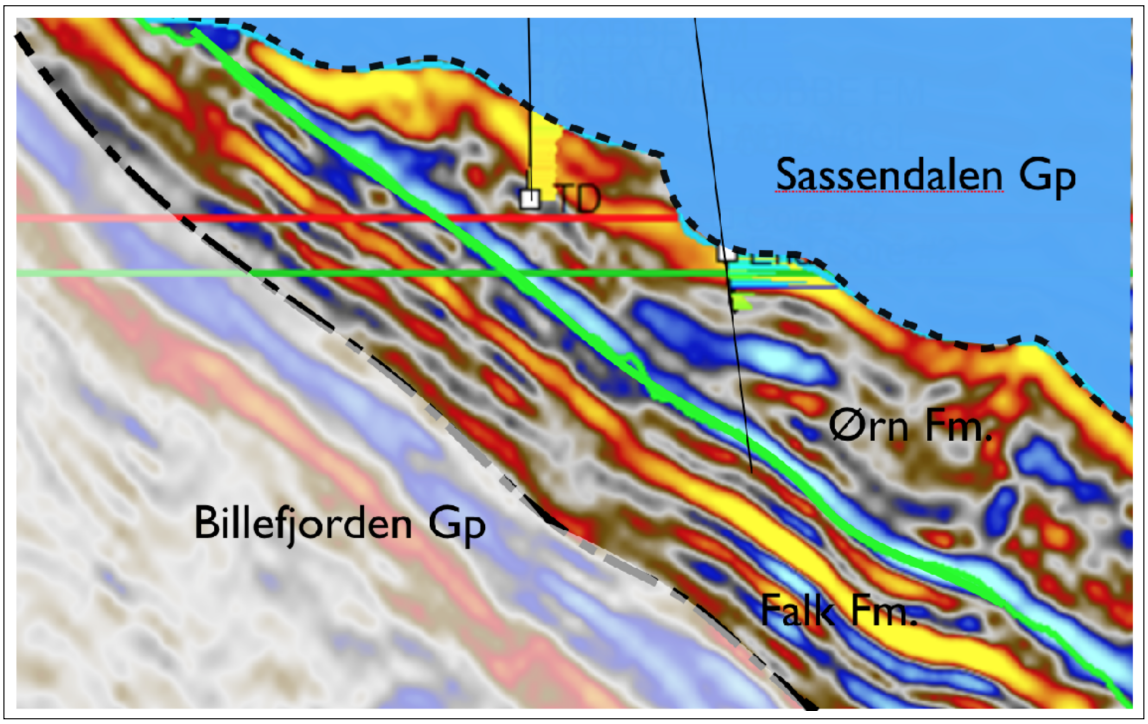

Figure 1.3: Present structural setting of the Gipsdalen Group making up the main reservoir formations of the Alta East Flank discovery. Red line indicates true depth (TD) of the initial well trajectory, 7220/11-3 (T2) which had to be abandoned at 1925 m TD. The sidetrack and subsequent re-deepening, 7220/11-3 AR, were drilled to 2389 m TVD seabed (long vertical line). Courtesy of Lundin Norway AS.

formations (Figure 1.2) and consists mainly of shallow water carbonates deposited in a marine ramp. Ørn is the youngest formation in the Gipsdalen Group, deposited in the late Gzelian to early Sakmarian age (Larssen et al., 2002). The formation is characterized by marine carbonates, ranging from supratidal evaporites to outer ramp interbedded carbonates. The surface (i.e. supratidal) to deeper marine depositions reflect a response to high frequency and high amplitude sea level fluctuations during time of deposition. On the southern margins of the Bjarmeland Platform (east of the Loppa High), the formation is over 1000 m thick, but due to erosion and updip, as illustrated in figure 1.3, only 79 m is preserved in Alta's neighbouring well 7120/2-1 (Larssen et al., 2002).

The Falk formation is suggested to have a late Bashkirian to early-middle Gzelian age and consists of a mixture of shallow marine sandstones, marine siltstones and shallow marine carbonates. In well 7120/2-1, the lower 51 m consists of stacked, less than 5 m thick rhythms of coarse-grained pebbly sandstone with minor shale and dolomite (Larssen et al., 2002).

Chapter 2

Fractured Reservoirs

A reservoir is defined as fractured only if there is a continuous network of fractures throughout the reservoir. In a fractured reservoir we would then have two distinct porous media systems called the fracture and the matrix block unit. Since around any single block a continuum (formed by the fracture network) exists, each single block will be hydrodynamically separated from adjacent blocks, i.e. the block is trapped within the fracture network. In reality these blocks are in contact through leaning points, but the hydrodynamic communication between blocks remains practically interrupted (van Golf-Racht, 1982).

Identifying a Naturally Fractured Reservoir

Identification of a continuous fracture network in carbonate reservoirs normally results from difference in total permeability, $k_{welltest}$ and matrix permeability, k_{core}:

$$\alpha = \frac{k_{welltest}}{k_{core}} >> 1 \tag{2.1}$$

The welltest / core ratio α may range from ten when a few channels are open to flow, to values of several thousand or more in the case of highly fractured reservoirs (Reiss, 1980). Other indications of a fractured reservoir include (Kjøsnes, 2012; van Golf-Racht, 1982):

1. Significant mud losses that occur during drilling operations
2. Examination of cores in the laboratory
3. Observations on outcrops during the exploration phase
4. Well pressure plotted against logarithm of time may exhibit a double slope during both pressure drawdown and build-up test
5. Low vertical temperature variation

Storage Classification

Fractured reservoir classification distinguishes between different types of reservoirs, based on the storage and flow properties of these two overlapping continua. Classification is important

to optimize reservoir management strategy, i.e. the use of secondary or tertitary (EOR) techniques, as well as choice of production rate. After evaluation of one hundred fractured fields, Allan et al. (2003) proposes the following classification to distinguish factors that control recovery in different types of reservoirs.

- Type 1: Fractures provide both storage capacity and fluid-flow pathways
- Type 2: Matrix provides some storage capacity, fractures provide permeability
- Type 3: Matrix has high porosity and low permeability (microporous)
- Type 4: Matrix has high porosity *and* permeability, fractures merely enhance permeability (macroporous)

In Type 2 (e.g the Yanling and Casablanca fields), little correlation is found between recovery factor and porosity, permeability, mobility ratio, viscosity, well spacing and residual water saturation. Several Type 2 reservoirs achieve good recovery without the need for any secondary or tertiary means, suggesting further that the recovery factor is more dependent upon the nature of the fracture network than on the matrix properties of the rock or fluid properties of the oil. The tight Type 2 reservoirs most commonly occur in rocks such as dolomite, tight limestone, tight sandstone and volcanics Allan et al. (2003). Due to the brittle nature of these lithologies, the fracture network tends to be extensive and thus commonly connected to aquifers, yielding water drive as the main drive mechanism. Fields with strong water drive are very sensitive to excessive production rates as it may lead to rapid water incursion and premature production decline. To achieve successful production from such reservoirs, water production needs to be handled carefully by reducing the choke size when water cut exceeds its limit.

The more porous Type 3 reservoir recovery show a higher correlation with rock and fluid properties than Type 2, indicating that these properties exert a more significant control on the exploitation. Type 3 reservoirs commonly occur in more ductile rocks, such as chalk, diatomite and siliceous shale. Because of its ductile nature, fractures tend to be localized around faults, and less extensive than in type 2. As these reservoirs generally do not connect to an aquifer, they are more commonly produced by solution-gas, gas-cap expansion and gravity drainage, or the application of secondary and/or EOR techniques. The application of such techniques is strongly dependent upon the reservoir rock's wettability, and comparison show that water-wet Type 3 reservoirs generally have ultimate recovery factor > 25 %, while oil-wet reservoirs have < 25 % (Allan et al., 2003).

Production Characteristics

Due to the existence of dual porosity and/ or dual permeability, the production characteristics of fractured reservoirs differ from those of conventional reservoirs in several fundamental ways (Allan et al., 2003). Type 1-3 all have low matrix permeability which would lead to

uneconomic well productivities if there were no open channels, and the channels also add a complexity to the recovery process that is absent in conventional reservoirs (Allan et al., 2003):

- Because the fracture network yields a high transmissivity, pressure gradients do not play a significant role in production and pressure drop around a producing well is very low.
- As fluid expansion, gravity drainage and imbibition supply the fracture with fluid through matrix-fracture interaction, the pressure decline during production is low compared to conventional reservoirs.
- The gas content, or GOR, of produced oil is often lower because liberated gas flows preferentially through the fractures, creating a gas cap or expanding an existing one. Maintaining a low GOR is very dependent on reservoir management.
- Fluid contacts are often sharp surfaces, since the high-permeable fracture network provides a mechanism for rapid segregation of the fluids.
- The bubble point and other PVT properties remain constant as a function of depth within the oil column. This is due to convective circulation that often occur in fractured reservoirs.

2.1 Basic Reservoir Properties

Saturation dependent functions such as the relative permeability (k_r) and the capillary pressure (P_c) are key factors for the assessment and prediction of the oil and gas production from a petroleum reservoir. Representative values are preferentially obtained through Special Core Analysis (SCAL) tests measured close to reservoir conditions in a laboratory.

2.1.1 Wettability

Wettability can affect both waterflood and gasflood performance and thus have significant impact on project economics. For instance will spontaneous imbibition of water only occur in a water-wetting reservoir. Wettability describes the preference of a solid to be in contact with one fluid rather than another (**Figure 2.1**). When two phases (gas/ oil, oil/ water, gas/ water) are present, the interfacial tension force between the phases form a curved interface, resulting in a contact angle, θ, at the solid surface. By convention, the contact angle is measured through water. For a waterwet surface, an oil drop will form a bead, minimizing its contact with the surface as compared to the surronding water phase. The contact angle for waterwet systems vary between 0 and 60 to 75 ° (left in Figure 2.2). On an oil-wet surface (right in **Figure 2.2**), the oil drop spreads, yielding a contact angle θ between 105-180 °. In the middle range of contact angles (75-105 °), a system is defined as mixed or intermediate wet.

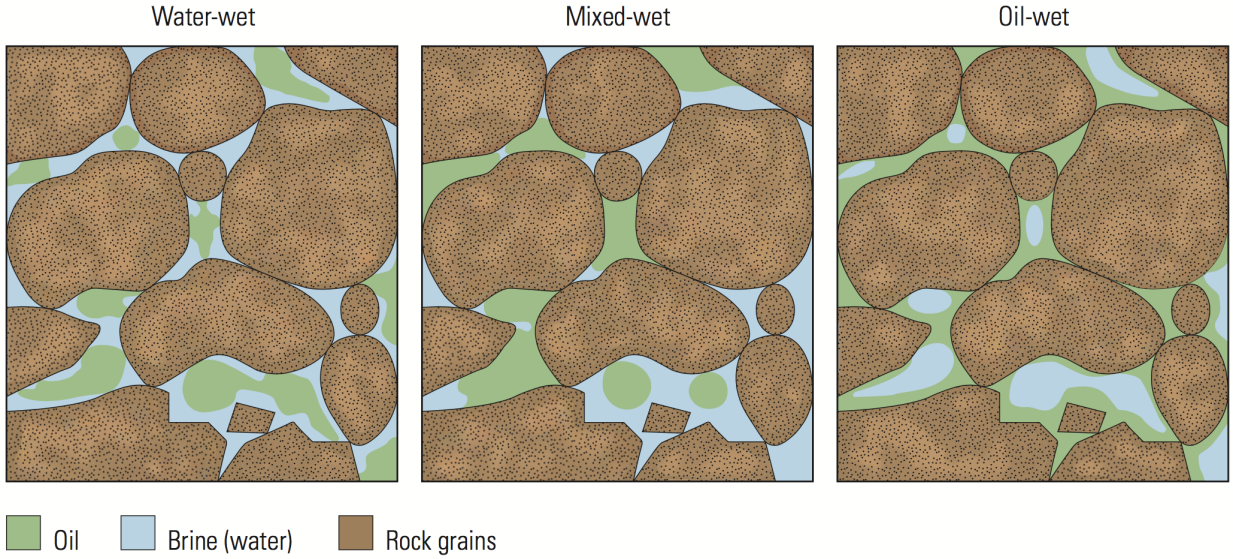

Figure 2.1: A water-wet state describes the preference of the solid to be in contact with water, and oil remains in the center of the pores (left). Vice versa, the oil adheres to the surface if the surfaces are oil-wet (right). In the mixed wet case, oil has displaced water from some of the surfaces, but is still in the centers of water-wet pores (middle). Figure from Abdallah et al. (1986).

In most cases, a formation is not either water-wet or oil-wet, but holds a range of different wetting degrees based on the rocks mineral composition, pore size, saturation history and oil composition. Several attempts have been made to find empirical trends of the wetting preferences of different petroleum-systems. Studies by Treiber et al. (1972) and Chilingar and Yen (1983) show that for the majority of carbonate reservoirs, oil wets the surface more strongly than water. Treiber et al. (1972) evaluated the contact angle of core samples from 50 different reservoirs (over half located in the US), 23 of which were carbonate reservoirs. 84 % of the carbonate samples were found to be oil-wet. More extensive work on carbonate reservoirs conducted by Chilingar and Yen (1983) found that out of 161 carbonate cores (limestones, dolomitic limestones, calcitic dolomites and dolomite) 15 % were strongly oil-wet (θ = 160°-180°), 65 % were oil-wet (θ = 100°-160°), 12 % had intermediate wettability (θ = 80°-100°), and 8 % were water-wet (θ = 0°-80°).

The impact of wettability on oil recovery extends from pore scale to reservoir scale. Hydrocarbon migration before and during production can alter the initial water saturation S_{wi}, and pore size has a different effect on the amount of recoverable oil (1 - S_{or}) depending on the wetting preference. The capillary imbibition forces resulting from interfacial tension (IFT) have a huge impact on the performance of secondary water- and/or -gasflood performance. For a water-wet reservoir water breakthrough occurs later, and more oil is produced before the water breaks through, than in an oil-wet reservoir (Abdallah et al., 1986).

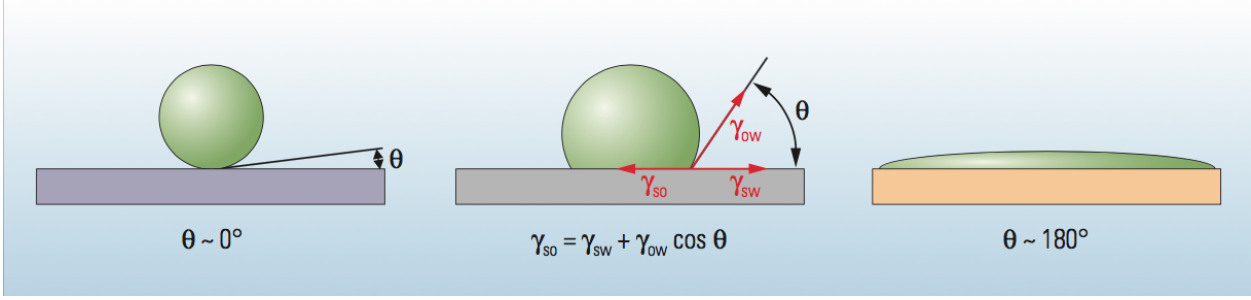

Figure 2.2: Illustration of contact angle measurement by oil drop immersed in water. Left to right shows typical water-wet, oil-wet and intermediate wet surfaces. γ is the interfacial tension between oil and gas, and θ is the measured contact angle (degrees). Figure from Abdallah et al. (1986).

2.1.2 Capillary Pressure

Wettability measurements include the capillary pressure curve, for example through the centrifuge method. In addition to permeability, the resulting curve represents the pore structure of the rock, including size, shape and the heterogeneity therein.

The capillary pressure (P_c) can be described as the pressure jump that occurs whenever an oil/water interface is curved. To balance the interfacial tension (Υ), the pressure abruptly increases and this is explained by Laplace's equation (2.1.2):

$$P_c = P_o - P_w = \Upsilon\left(\frac{1}{r_1} + \frac{1}{r_2}\right) \tag{2.2}$$

where P_o, P_w is the pressure in the oil and water phase, and r_1, r_2 is the radii of curvature of the interface, measured perpendicular to each other.

The resulting capillary force between the two phases is best explained through the surfaces in a capillary tube, illustrating pore throats in a porous formation (**Figure 2.3**). If the surface of the tube is water-wet (left inset), surface forces cause water to rise, displacing oil along the surface, - the favorable effect in waterflooding. If the inner tube is oil-wet, the water will be displaced by oil. The capillary height, h_c, is a function of the density difference ($\Delta\rho$) and the balance of wetting forces (Abdallah et al., 1986):

$$P_c = \Delta\rho g h_c \tag{2.3}$$

where g = the acceleration due to gravity.

When the pressure difference ($P_o - P_w$) is zero, only one phase is present, indicating 100 % water saturation S_w, or free water level (FWL - Figure 2.3). By convention, if the capillary pressure at the oil/water contact is positive ($P_o - P_w >$ FWL $= 0$), the rock is water-wet. If P_c is negative ($P_o - P_w < FWL = 0$) it signifies that pressure must be applied

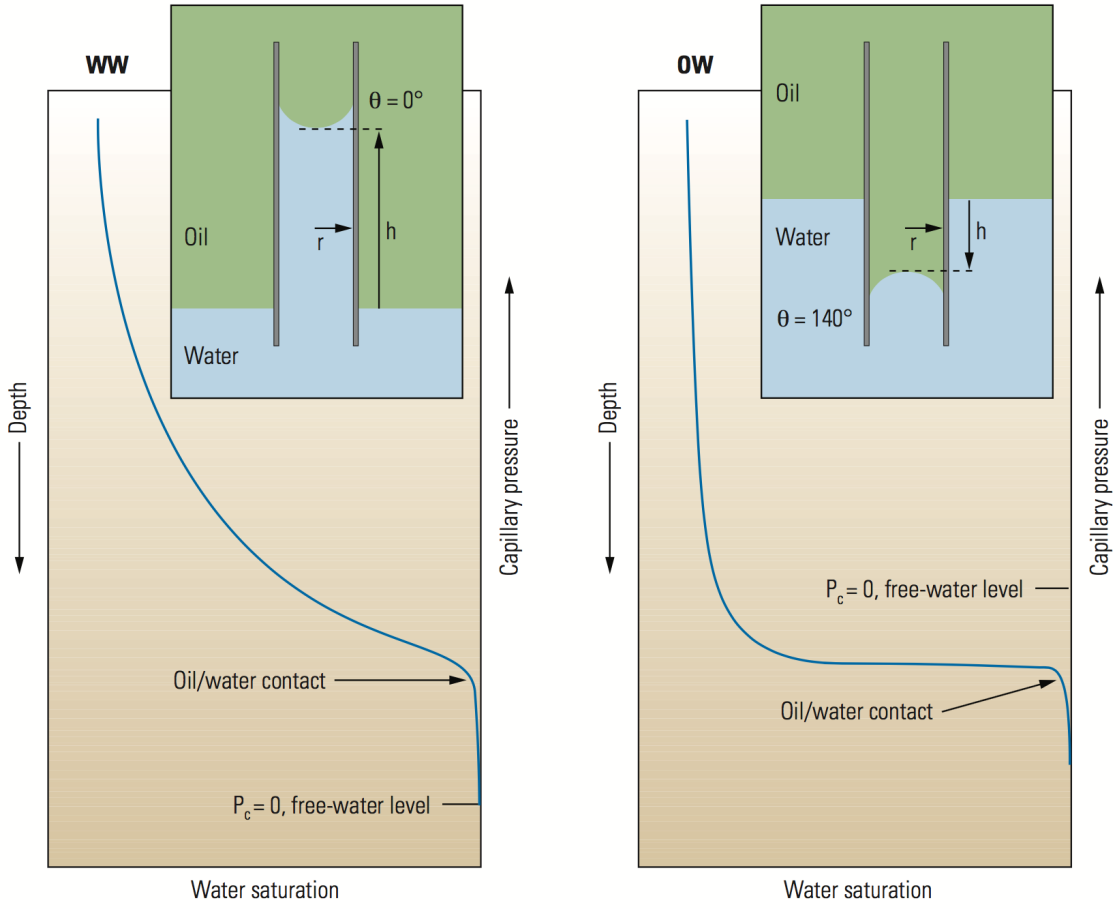

Figure 2.3: Capillary pressure curves describe the transition from a zone of high oil saturation to high water saturation at the bottom (blue curves). In a capillary tube, water-wetting (WW) surface forces cause water to rise (left inset), displacing oil, but if the tube inner surface is oil-wetting (OW), the oil will push water down (right inset). h describes the height of the capillary rise, h_c. Figure from Abdallah et al. (1986).

to force water into the largest pores, i.e. oil-wet surfaces. The oil/water contact corresponds to the displacement pressure, or capillary threshold height (h_{TH}) of the system.

2.1.3 Relative Permeability

The wetting condition of a reservoir also affects multiphase flow measurements. Due to imbibition forces, the wetting saturation increases preferantially in the smaller pores first. When the larger pores start to fill, the non-wetting phase is displaced until only one phase is flowing ($k_{r,nw} = 0$). In a water-wet case, water will initially be in the small pores and oil in the large pores, yielding a low initial relative permeability to water, k_{rw}. Since oil flows preferentially through the largest pores, the relative permeability to oil (k_{ro}) when both phases are flowing, is high. As the water saturation increases due to natural or induced water flooding, k_{rw} increases and k_{ro} decreases.The final k_{rw} (when oil stops flowing) is lower than the initial k_{ro} (when only oil was flowing) because some oil gets trapped in large pores during waterflooding (Abdallah et al., 1986).

For a less water-wet system, added water invades the largest pores first and remains in the center of those pores. As the most permeable paths fill with water, k_{ro} declines more rapidly than in a water-wet system (right inset **Figure 2.4**). However, the oil-wet condition provide a path for the oil to flow along the surfaces, so the oil does not get trapped by surrounding water filled pores.

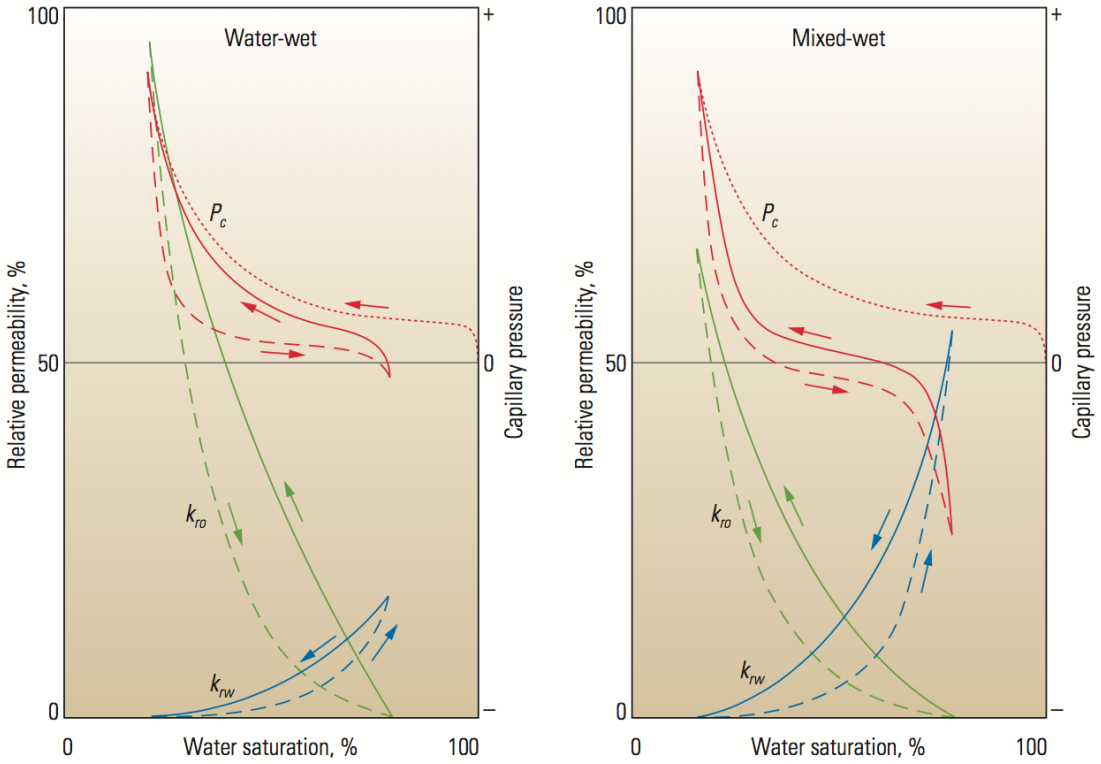

Figure 2.4: Capillary pressure and relative permeability for water-wet and mixed-wet conditions. Solid lines indicate the imbibition process, and dashed lines drainage. Mixed wet condition is indicated on the capillary pressure curve by a larger entry pressure and negative (forced) imbibition. Figure from Abdallah et al. (1986).

As wettability affects the position of relative permeabilities, the measurement is commonly used by reservoir engineers as indicators of wettability (Petrowiki, 2016). The most important indicator is the crossover-saturation point, or Craig's rule, defined as S_w^* at $k_{rw} = k_{ro}$. If water saturation where the relative permeability curves intersect is higher than 50 %, the system is likely water-wet and $S_w^* < 50$ %, indicates oil-wetting system. Ratio of wetting to nonwetting endpoints has also proved to be a good qualitative measure of wettability, but is more sensitive to the value of residual phase saturations (Lake, 1989). For his evaluation of 50 reservoirs, Treiber et al. (1972) used the following ratios:

$$\frac{k_{rw}@S_{or}}{k_{ro}@S_{wi}} = \begin{cases} 0 - 15\% >, & \text{water-wet} \\ 15 - 50\% >, & \text{intermediate / neutral wet} \\ 50 - 100\% >, & \text{oil-wet} \end{cases} \tag{2.4}$$

Such interpretation is however subject to large error because relative permeabilities also depend upon pore-size distribution, connoate water saturation, lamination and heterogeneities (Petrowiki, 2016).

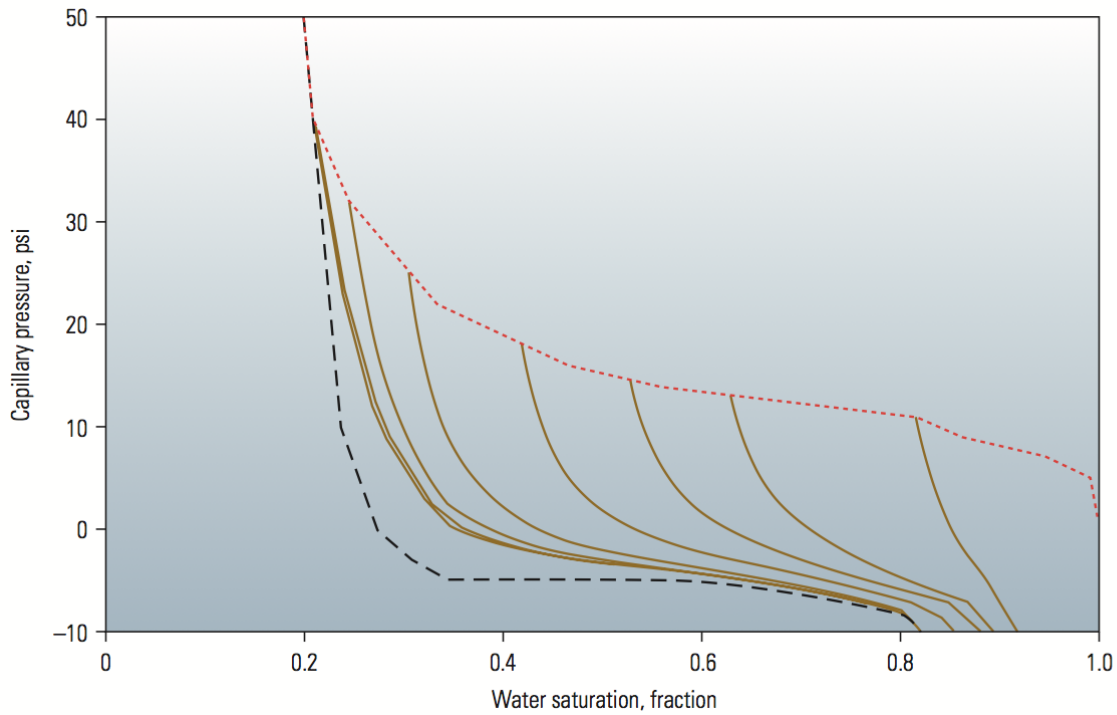

Figure 2.5: Scanning curves for an intermediate-wet carbonate. Hysteresis between the bounding primary drainage (red) and imbibition (black) curves can be represented by a series of scanning curves (gold). Figure from Abdallah et al. (1986)

2.1.4 Hysteresis

Changes in saturation that affects relative permeability and capillary pressure curves occur during both migration and production of hydrocarbons. Hysteresis describes the change in relative permeability and capillary pressure resulting from drainage (decreasing wetting phase saturation) and imbibition (increasing wetting phase saturation) processes (**Figure 2.5**). Hysteresis can be described through contact angle measurements as the difference between the contact angle when liquid is pushed over the surface and the contact angle when liquid is pushed back; $\theta_{advancing} - \theta_{receding}$. For some smooth, very homogeneous surfaces, the advancing and receding contact angle will be the same, but for most reservoir rocks saturation change results in hysteresis. A normal, heterogeneous system without hysteresis is thus a simplification, and such reservoir simulation would in general represent an overestimation of the oil recovery. Morrow et al. (1990) showed that a hysteresis curve departing from one of the bounding drainage or imbibition curves is uniquely defined by the departing point on the curve. This means that hysteresis can be represented by a series of 'scanning curves', where each branch is defined by different starting saturation point on the drainage or imbibition curve, corresponding to different heights in the transition zone (gold colored curves in Figure 2.5).

2.1.5 Saturation Functions in the Fracture

The common industry standard for saturation functions in the fractures still used today, was set by Romm (1966) who's experiments showed linear relative permeability and zero capillary pressure in the fractures. Since then, both laboratory and numerical simulations have questioned his results (Firoozabadi et al., 1990; Horie et al., 1990; de la Porte et al., 2005; Noroozi et al., 2010), but his approach is still widely used today. The fracture capillary pressure contribute to flow communication between isolated matrices and therefore have a larger impact when gravity drainage is the dominating process and / or the reservoir matrix blocks are small. The assumption of zero fracture capillary pressure is appropriate only if the matrix blocks are completely discontinuous, and de la Porte et al. (2005) found that this is a valid assumption for fractures wider than 100 microns.

Several studies (Noroozi et al., 2010; de la Porte et al., 2005) have concluded that zero capillary pressure is applicable to oil-water systems where imbibition dominates the recovery process, but for gas-oil cases, non-zero fracture capillary pressure could increase the recovery by a factor two (Noroozi et al., 2010) or 60 % (de la Porte et al., 2005). For the simplified relative permeability, water-oil systems with linear curves showed errors as high as 70 % as well as underestimated time to final recovery (de la Porte et al., 2005).

2.2 Recovery Mechanisms in Fractured Reservoirs

Production mechanisms-such as fluid expansion, diffusion, oil/water imbibition, and gas gravity drainage may all contribute to production of oil at different stages in the production life of a fractured reservoir. These mechanisms are usually explained through a simplified model of the matrix represented by single blocks. **Figure 2.6** illustrates the main oil recovery mechanism of a fractured reservoir. Matrix/ fracture transfer is considered as the sum of the contributions from these processes.

2.2.1 Fluid Expansion

In the case of fractured reservoirs, an additional elasticity, $C_{p,f}$, is added to the total effective compressibility of the reservoir, C_{et} (Reiss, 1980):

$$C_{et} = C_o + \frac{(C_w S_{w,ma} + C_{p,ma})\phi_{ma} + C_{p,f}\phi_f}{\phi_{ma}(1 - S_{w,ma}) + \phi_f} \tag{2.5}$$

For $\phi_f << \phi_m$[1] and $C_{pf} \approx C_{pm}$, equation 2.5 can be simplified:

[1]For fractured carbonate reservoirs, the presence of cement such as calcite has a huge impact on the magnitude of fracture compressibility. For cemented pores, the cement maintains the fractures open in spite of an increase in effective stress on the rock, giving fracture compressibility an order of magnitude of 10^{-5} and 10^{-6} bar (Maidebor, 1973). Calcite cement is more common in shallow water carbonates (such as the Alta discovery), than it is in chalk such as the giant Ekofisk field where compaction drive contributes significantly to oil recovery (Sylte et al., 1999).

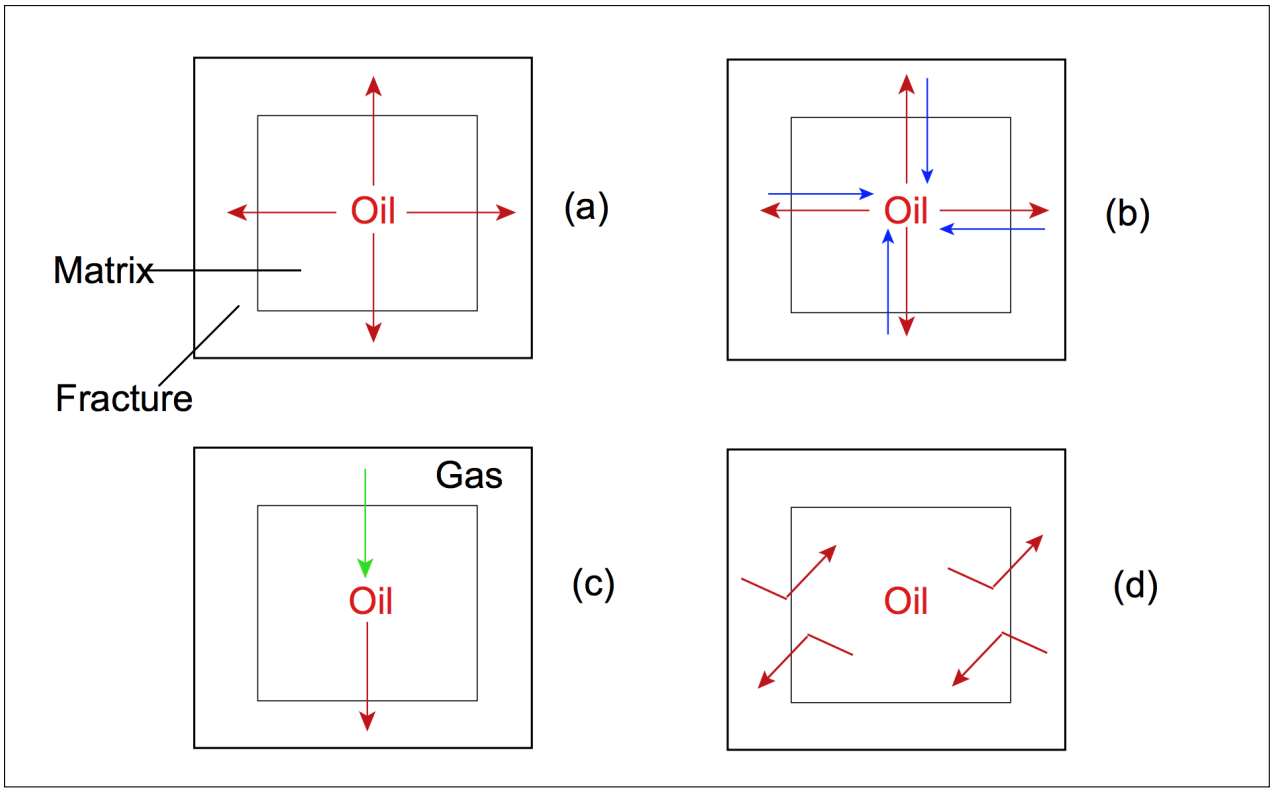

Figure 2.6: Main drive mechanisms in fractured reservoirs: a) fluid expansion, b) imbibition, c) gravity-controlled displacement, d) diffusion. Figure from Lu (2008).

$$C_{et} = C_o + \frac{C_w S_{w,ma} + C_{p,ma}}{1 - S_{w,ma}} \tag{2.6}$$

where subscripts f and ma denote the fracture and matrix continuum, and p pore, respectively. Thus, expansion is almost entirely due to the properties of the matrix and its fluid and is therefore uniform throughout the reservoir consisting of a network of fractures.

It can be shown that the pressure decline in fractured reservoirs is more uniform than is the case for conventional reservoirs, fractures therefore play a beneficial role during single phase depletion (Reiss, 1980). If gas is added to the system, for example by reservoir depletion below bubble point pressure, the total compressibility is increased, and C_{pf} has even less influence.

2.2.2 Solution Gas Drive

Solution gas drive is a function of rate of pressure decline in the reservoir, diffusion, interfacial tension between oil and gas, and the degree of heterogeneity of the rock. Heavily fracured oil reservoirs producing below their bubblepoint pressures are know to sustain high oil production rates, low rates of pressure decline, and large volumes of gas remaining in the reservoir (low GOR), signifying the importance of solution gas drive in fractured reservoirs (Festoy and van Golf-Racht, 1989). As the matrix block's are small compared to the oil column thickness, the segregated gas phase only has to travel a short distance before it reaches

the fracture system and easily joins the gas cap through the high permeable network.

Solution gas drive in fractured reservoirs is less affected by diffusion than conventional reservoirs. Homogeneous, permeable and porous networks of low porosity, such as the fracture network, encourage the formation and growth of gas bubbles, which coalesces in the fracture. By diffusion, this gas might absorb the lighter molecules in the matrix, reducing the amount of free gas in the reservoir. For this reason, even reservoirs where the pressure is depleted significantly below bubble point pressure, free gas saturation in the matrix is often less than 1 % (Reiss, 1980).

2.2.3 Sudation; Gravity Drainage & Capillary Imbibition

Sudation refers to the combined effects of two sets of forces which play a role in the substitution of oil within the matrix by the water or gas in the surronding fractures: a) Gravity forces due to the difference in densities between oil and water or oil and gas b) Capillary forces due to the interaction of surfaces within the pores. The interplay between these two forces is dependent on the wettability of the pore surfaces, and represent the main difference between conventional and fractured recovery mechanisms. Gas is always the non-wetting phase, but in case of an oil-water system, both fluids may be preferential to wetting. Both gas gravity drainage and oil/water imbibition act without depleting the reservoir (Festoy and van Golf-Racht, 1989).

Recovery by Imbibition Process

Imbibition is the process where the non-wetting fluid is displaced in favor of the wetting. Due to spontaneous imbibition of water into an oil saturated rock, imbibition is recognized as one of the main recovery mechanisms in water-wet rocks. The amount of spontaneous imbibition is ultimately controlled by the capillary pressure curve, or more accurately, the positive part of the imbibition capillary pressure curve. The shape of this curve is dictated by the wettability, as the saturation range where the capillary pressure curve is positive decreases when the wettability tends towards a less water-wet state (Fernø, 2008).

In a water-oil system, water from an injection well or natural aquifer enters the lower side of the block and displaces oil which is produced at the upper side in an oil or water environment (depending on the rate of advancement of the water-oil front in the fracture). At the initial point of displacement (when $Z = 0$), the rate of expulsion of oil, q_{om}, per unit cross section A from an element of matrix immersed in water is (van Golf-Racht, 1982):

$$q_{om} = A\frac{k}{\mu o B_o}k'_{ro,ma}\left(\Delta\gamma_{wo} - \frac{P_c}{H}\right) \tag{2.7}$$

where:
$k'_{ro,ma}$ = endpoint relative matrix permeability of oil
$\Delta\gamma_{ow}$ = difference in specific gravity between oil and water
μo = oil viscosity

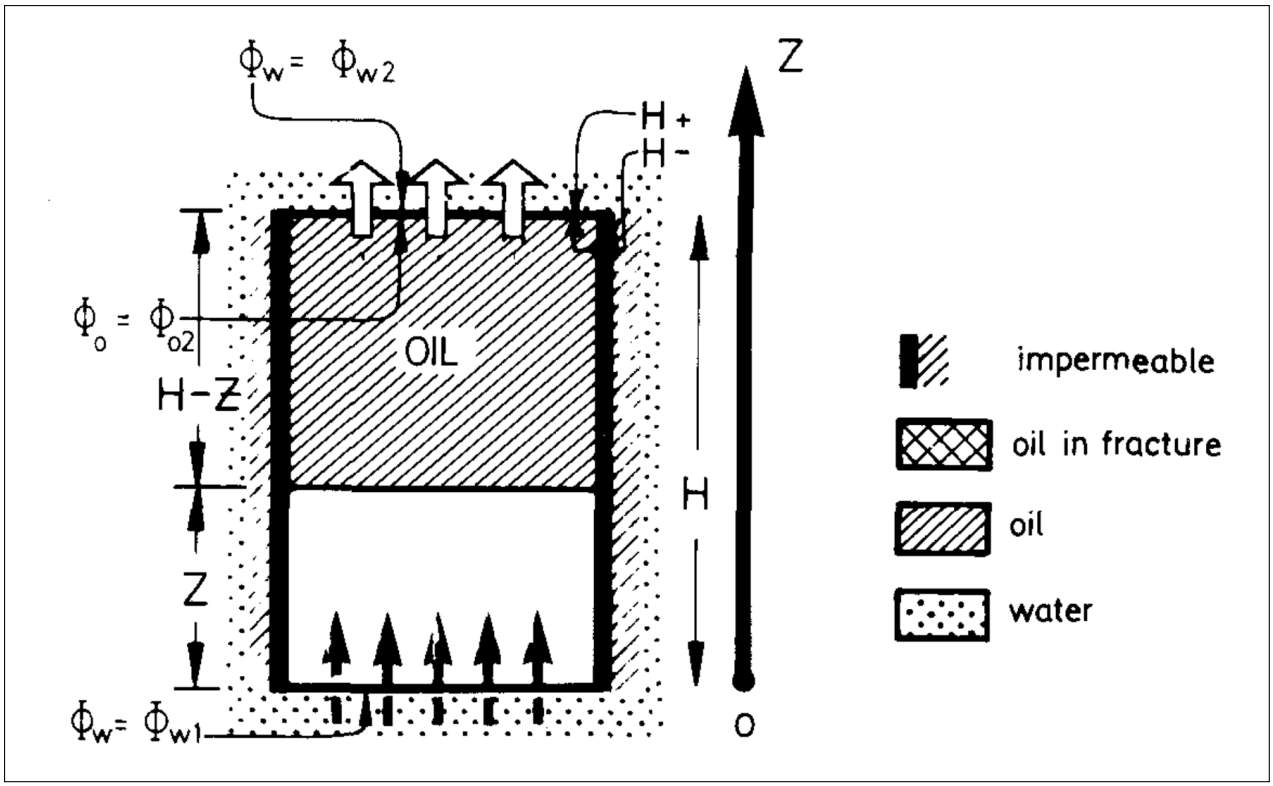

Figure 2.7: Advancement of displacement front for a block totally immersed in water. Figure from van Golf-Racht (1982).

B_o = formation volume factor of oil
H = vertical block height, and
Z = height of displacing fluid in matrix

For a water-wet system, the capillary pressure (P_c) support penetration of water into the matrix, and gravity pressure (G) additionally reinforces the matrix-fracture transfer, i.e. both terms of equation 2.8 become positive. The flow rate, q_{om} is controlled by the relationship between the two forces:

$$P_c + G = h_c \Delta\rho + (H - Z)\Delta\rho \tag{2.8}$$

If blocks are very high ($H - Z >> h_c$), Z is small (initial phase of displacement) or degree of wetting is small (h_c is low), gravitational pressure govern displacement:

$$G = (H - Z)\Delta\gamma wo >> P_c = h_c \Delta\gamma_{wo} \tag{2.9}$$

If the reservoir is intensively fractured (small blocks and no capillary continuity), or at late time when the displacement front Z is advanced, capillary pressure may be the predominant force:

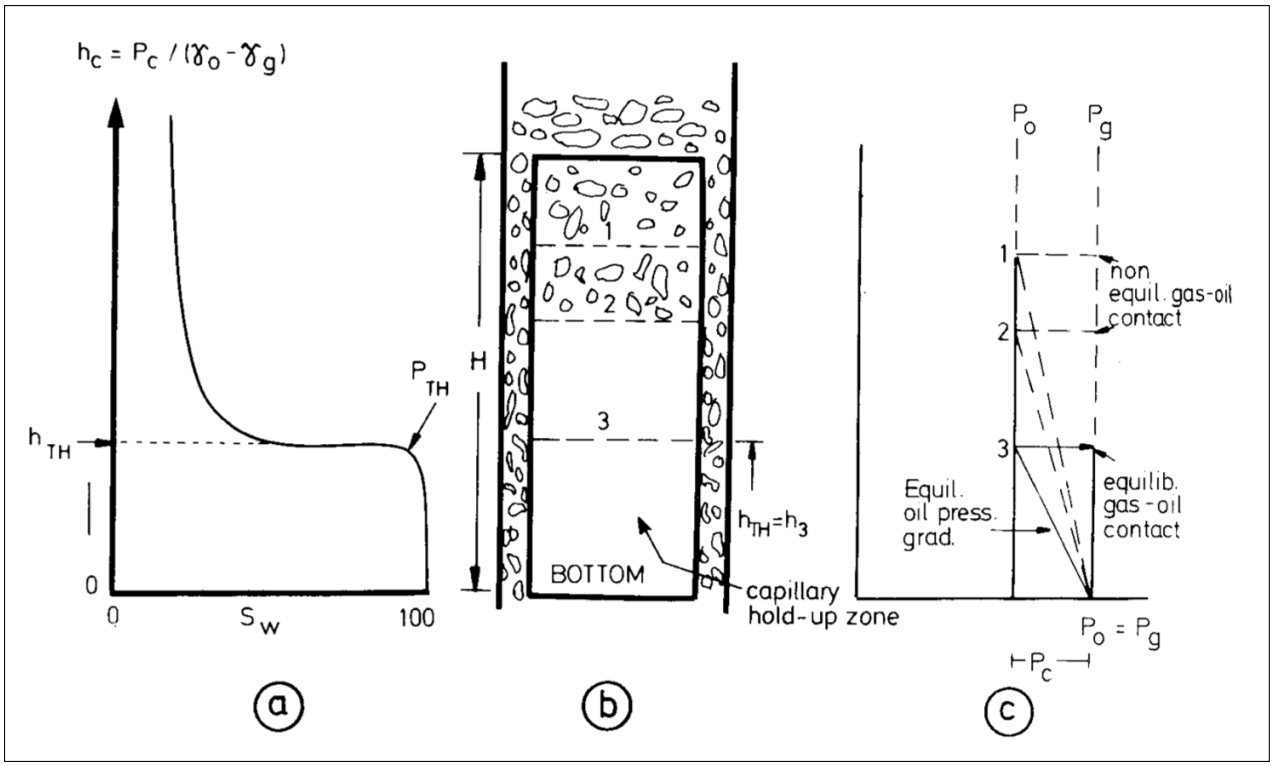

Figure 2.8: Relationship between gravity and capillary forces in drainage displacement; (a) capillary curve (b) drainage displacement in the block (c) equilibrium of gas-oil contact at matrix-fracture interface. For given capillary curve, heigh h_3 equals the capillary hold-up zone. Figure from van Golf-Racht (1982).

$$P_c = h_c \Delta\gamma_{wo} >> G = (H - Z)\Delta\gamma_{wo} \tag{2.10}$$

The regime above assumes that both the upper and lower side of the matrix block are water saturated, i.e. that the block is totally immersed in water (**Figure 2.7**). Depending on the relationship between water injection rate, and matrix transfer rate, this might not be an acceptable assumption. If the water advancement in the fractures is slow, so that the water-oil front in the block is higher than the water-oil front in the fracture, the upper face of the block is producing in an oil environment. As long as $Z <$ the water front in the fracture, H_w, gravity will contribute to displacement, but if $Z > H_w$, gravity will have a retardation effect on the displacement of oil from the matrix block (van Golf-Racht, 1982).

Recovery by Drainage Process

In a drainage process, the non-wetting fluid displaces the wetting fluid. Common drainage processes include gas cap expansion where gas (the non-wetting phase) invades the fractures and oil (the wetting phase) is drained from the matrix blocks by gravity drainage. Other drainage processes include oil-wet reservoirs being invaded by water (the non-wetting phase). In the latter process, the matrix capillary force oppose spontaneous imbibition of water, which is why many fractured carbonate fields are produced through Gas Oil Gravity Drainage

(GOGD), and not waterflooding.

If the matrix is oil-wet, the capillary force tends to oppose gravitational force, resulting in poor reservoir performance under water injection (Reiss, 1980). This is often the case for matrices with small quantities of organic matter induced, e.g. limestone. For negative capillary force, recovery of oil will reach it's maximum, in the absence of diffusion, when $G = P_c$. To optimize production, gas is often the preferred displacing fluid in such systems because of the larger gravity term. In a gas-oil system, oil is always the wetting phase, i.e. displacement of oil is a drainage process. When the fracture fills with gas, gravity forces will push oil out the bottom side of the matrix block and gas will flow into the topside. For gas to enter the block, the hydrostatic gas pressure (G) in the fracture must overcome the matrix' treshold pressure P_{TH} (**Figure 2.8**). In the case of small blocks, it is very unlikely that the gas pressure reaches this *entry value*. However, if the oil remains as a continous phase between several individual blocks, the height of the gas column to satisfy $\Delta\rho Hg > P_{TH}$ is more likely obtained, and oil will be expelled. This is the concept of *capillary continuity*.

When the gas cap expands (due to gas out of solution or injection), gas fills the permeable fractures first. At the start of a displacement process, the height of the gas-oil front in the matrix, Z, is zero, corresponding to the top of the matrix block. The displacing gas front will increase as long as $G > P_{TH}$, thus some of the oil is not recovered due to the capillary hold-up zone (**Figure 2.9**);

$$G = \Delta\rho(H - Z)g > P_{TH} = \Delta\rho h_{TH} g \tag{2.11}$$

Combining Darcy's equation and the gas-oil capillary pressure yields the initial oil rate from the matrix block as;

$$q_{om} = A\left(\frac{k}{\mu o B_o}\right) k_{ro,ma}\left(\Delta\gamma_{og} - \frac{P_{TH}}{H}\right) \tag{2.12}$$

where γ_{og} is the difference in gravity between oil and gas. As gas saturation in the block increases, both the oil relative permeability and the capillary pressure gradient ($dP_c/dz = P_{TH}/H$) decrease, and the oil production rate decreases rapidly.

2.2.4 Molecular Diffusion

Molecular diffusion of gas and oil between the matrix and fracture is the second force available to displace gas into the matrix and oil out (the other is gas gravity drainage), and may be a significant production mechanism in fractured reservoirs (Schlumberger Ltd, 2015). The presence of a high permeable fracture network accelerates the diffusion phenomen, reducing the time scale required to reach a significant effect, as compared to conventional reservoirs Reiss (1980). Diffusion is a result of different hydrocarbon composition between fracture and matrix and may occur between oil and gas, or between different oils. When diffusion takes

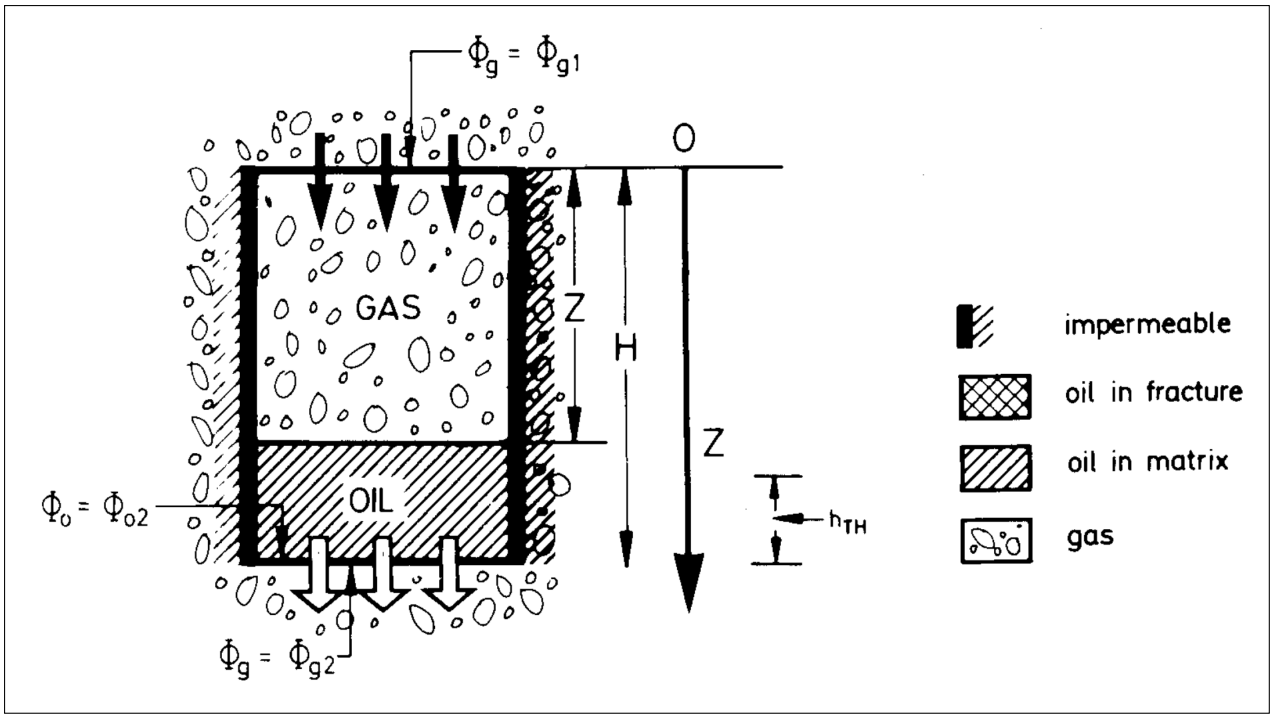

Figure 2.9: Advancement of displacement front in the case of a block totally immersed in gas. The displacing front Z will increase as long as G = $\Delta\rho Hg > P_{TH}¿$ P_{TH}. Figure from van Golf-Racht (1982).

place between gas in the fractures and oil in the matrix it enhances the sudation process. In contrast to gas gravity sudation, which results in an almost horizontal gas-oil contact in the matrix block, diffusion will push gas molecules into the matrix from all sides, and oil out. The concept of diffusion is often ignored when dealing with conventional reservoirs, as very large time scales is required before the effect becomes significant. Even though diffusion is accelerated by fractures, the effect on overall recovery is probably very small and can for most systems be neglected for practical purposes (Uleberg and Kleppe, 1996).

2.2.5 Viscous Displacement

Viscous forces are more important in an oil-water system than in a gas-oil system. Kossack et al. (2001) conducted a study of vuggy and fractured reservoir simulation, which concluded that recovery of oil from the vugs were more beneficial in a viscous environment in contrast to an environment governed by gravity forces, for an oil-water system. A viscous-dominated system is characterized by *low*-permeability fractures surronding the matrix block. In particular, the fractures parallell to the flow must be low permeability, while the perpendicular fractures may still have high permeability and yield large viscous forces.

2.3 Physical Characteristics

2.3.1 Block-to-Block Interaction

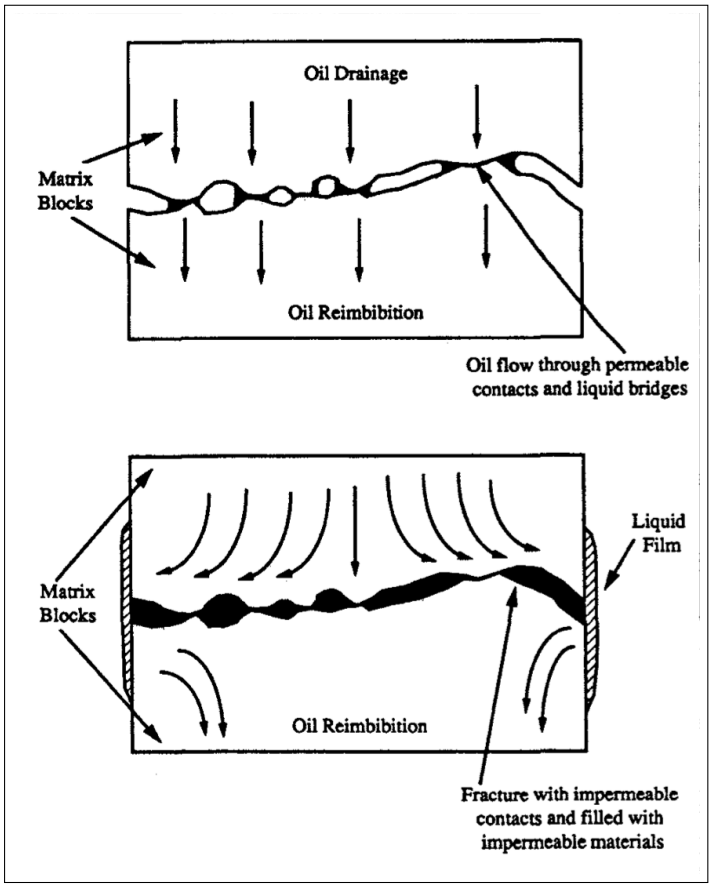

Figure 2.10: The reimbibition phenomena describes flow from matrix block to matrix block as two processes; capillary continuity (upper inset), reinfiltration (lower inset). Figure from Fung (1991).

The early single block concept of dual porosity systems, assumed completely disconnected matrix blocks where oil drained from the matrix would travel through the fracture network to the producers. Hence, the performance of a stack of blocks would be equal to the performance of a single block multiplied by the number of individual blocks. Today, the concept of block-to-block interaction, stack-of-blocks or reimbibition phenomena is widely accepted. The concept was introduced when it was realized that oil drained from the base of one block had the tendency to reinfiltrate into the block below (**Figure ??**). When one considers this phenomenon, two main reimbibition processes are distinguishable: 1) Capillary Continuity and 2) Reinfiltration (Dejam et al., 2009). The term 'reimbibition' should not be interpreted as a function of capillary effects only, as several publications (Firoozabadi et al., 1994; Barkve et al., 1992) have shown that it is a function of both gravity and capillary forces. The three terms are often mixed, but here "reimbibition" will be used as a common denominator of the two physical processes causing matrix-matrix flow, as described below. Both reimbibition processes are largely determined by the fracture thickness separating adjacent blocks (Dejam et al., 2009).

Capillary Continuity

For the case that the fracture thickness is small enough, the surface of one block will make contact with the droplets formed by oil drained from the adjacent block (upper inset in Figure 2.10). When such liquid bridges are formed, or permeable contacts exist, it causes the capillary continuity phenomenon between blocks. A schematic comparison of saturations and pressure profiles of a stack of blocks with capillary continuity vs a discontinuous stack is shown in **Figure 2.11**. When considering capillary continuity, all the blocks have only one threshold height, as indicated by the shaded region, and oil recovery is substantially more optimistic than the discontinuous case. In actual reservoirs, the degree of continuity will not be either 0 or 100 % but will vary due to permeability barriers along dip, partial

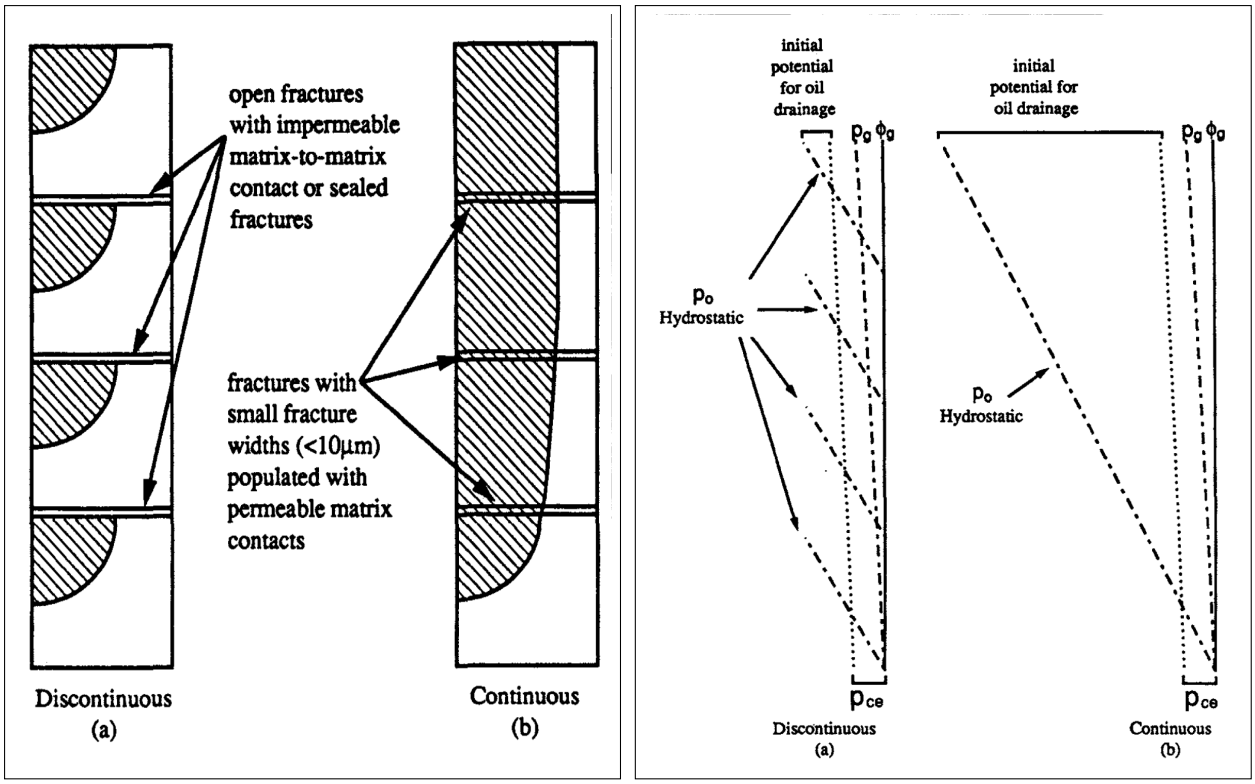

Figure 2.11: Effects of capillary continuity on oil recovery from gas gravity drainage for a stack of four matrix blocks. Right: Saturation profile for discontinuous vs continuous stack, left: pressure profile for discontinuous vs continuous stack. Figure from Fung (1991).

mineralization of the fracture wall, or more complex geometries. Therefore, Festoy and van Golf-Racht (1989) suggested that the matrix is better described as tortuously continous, and presented fine-gridded simulation results where the fracture system allowed for various degrees of interblock-contact. They found that a matrix contact area of only 25 % of the horizontal cross-sectional area would have dramatic effects on recovery.

Reinfiltration

The reinfiltration process is related to a larger fracture thickness, and/ or impermeable contacts, as illustrated by the lower inset in Figure **??**. In that case, oil movement from upper block into lower block is controlled by the formation and detachment process of oil droplets, and flow from one block to another is achieved by one of two processes: 1) film flow across contact points or 2) liquid bridges. These processes have a large impact on the rate of oil production by gravity drainage, and usually causes a time delay in the recovery process compared to the recovery predicted from a single block process (Dejam et al., 2009). In the initial stage of a gravity drainage process, liquid bridging provides the main transmissibility. When most of the oil in the fractures has been drained, main liquid transmissibility from block to block is due to film flow.

Reinfiltration affects the phase distribution of oil and gas in the matrix block which is why it traditionally has been hard to model with conventional, or dual porosity/ permeability models (Uleberg and Kleppe, 1996; Dejam et al., 2009). Fung (1991) proposed an extension

of the existing dual permeability model, where the continuous matrix capillarity phenomen were coupled with block-to-block reinfiltration pseudo capillary potentials, separating it from the usual potential calculation with a gravity head based on the depth difference between the two gridblocks.

2.3.2 Matrix Block Shape

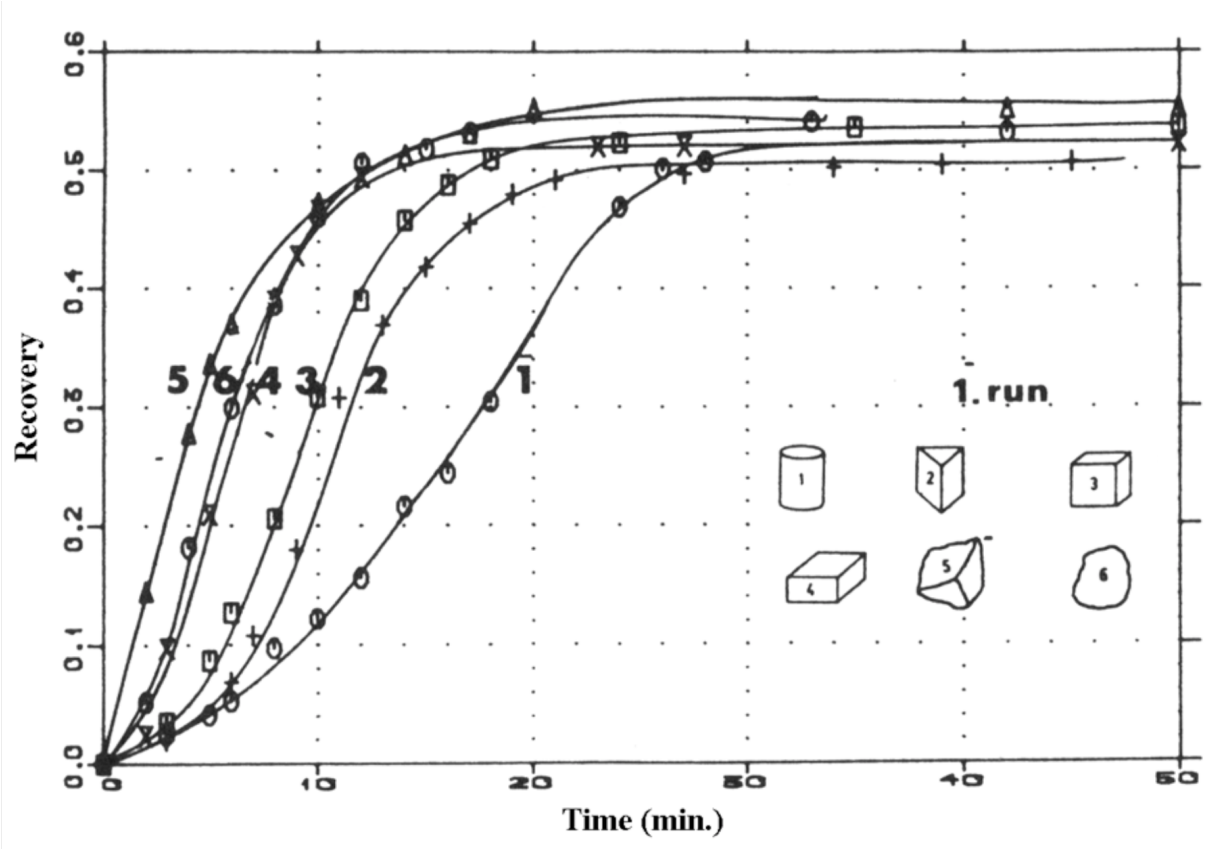

Figure 2.12: Effect of size and shape on water imbibition oil recovery. Figure from Torsaeter and Silseth (1985).

With current simulators, the shape of matrix blocks is accounted for by a sigma factor that assumes identical and paralellepiped matrix block (Kazemi et al.'s formula). There is however questions to whether this sigma factor represents the actual shape or if it is related to other processes affecting transmissibility between matrix and fracture (Lu, 2008). Regardless of this, it is natural to assume that the matrix blocks in a reservoir are not identical, but consist of varying shape and size. Torsaeter and Silseth (1985) conducted laboratory experiments investigating the effect of shape and size of different sandstone and chalk cores during water imbibition. They found that the sizes, shapes and boundary had little effect on the ultimate recovery by spontanous imbibition, but for early and intermediate times, recovery rates differed significantly (**Figure 2.12**).

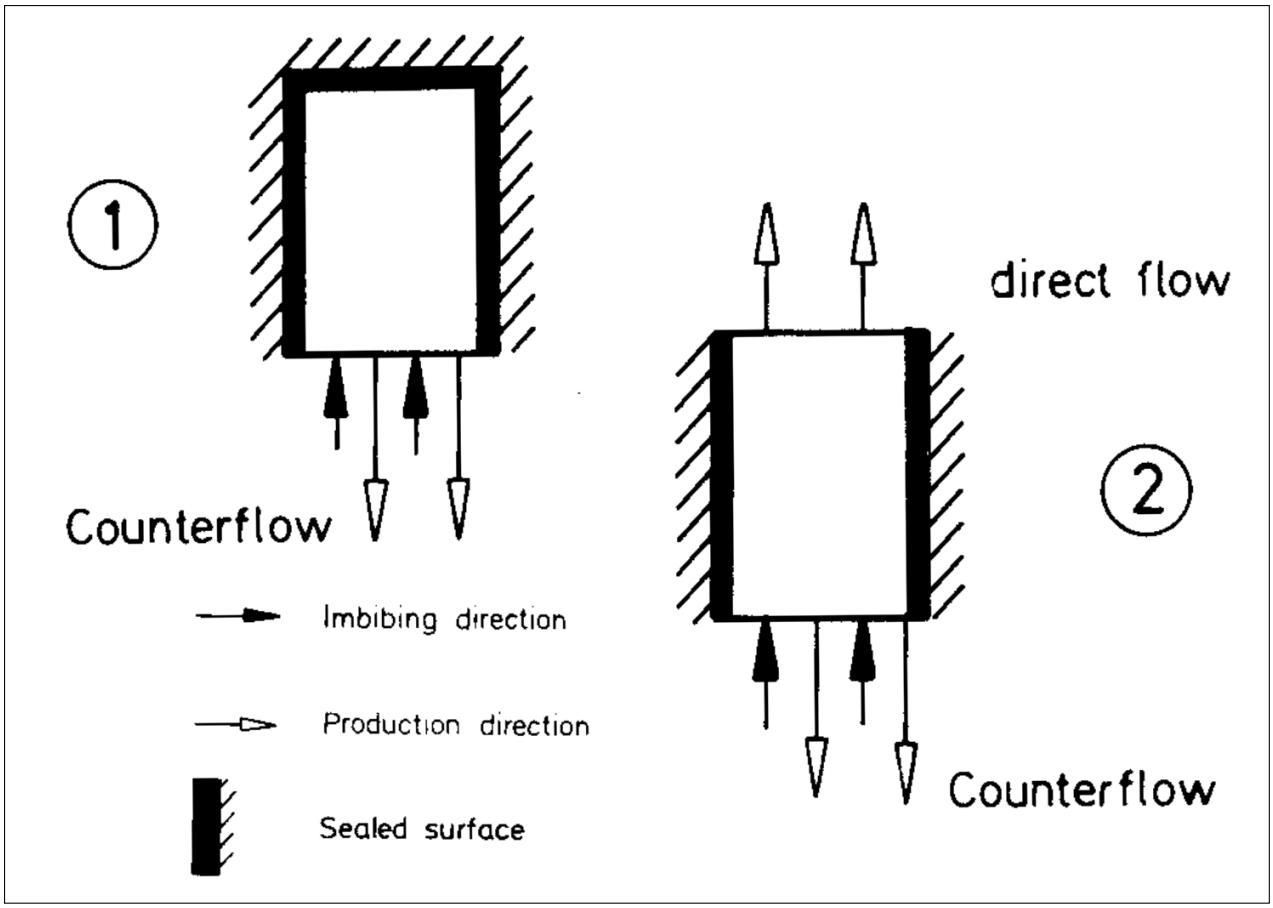

Figure 2.13: Flowing directions during water imbibition; 1) Counter-current flow, 2) counter-current at the bottom, direct/ co-current at the top of the matrix block. Figure from van Golf-Racht (1982).

2.3.3 Co-Current and Counter-Current Flow

An important issue to be addressed when imbibition mechanisms govern the recovery, is the one of the flowing direction's relationship between the displaced and the displacing fluid. Counter-current imbibition is the process where the wetting phase, usually water, enters a water-wet rock, while oil escapes by flowing in the opposite direction (no. 1 in **Figure 2.13**). This has generally been believed to be the dominant form of spontaneous imbibition in fractured reservoirs, but Hughes and Blunt (2000) found that the pattern of displacement and the rate of imbibition were very sensitive to the shape and magnitude of the capillary pressure curve. Co-current recovery or 'direct flow' has therefore been suggested to play a more dominant role (Firoozabadi et al., 2000; Pooladi-Darvish et al., 1998). Co-current flow is when the displacing fluid (wetting phase) and displaced fluid (non-wetting phase) have the same direction (top side of block 2 in Figure 2.13). Co-current is believed to be faster and more efficient than counter-current imbibition and is an expected flow direction when only parts of the matrix surface is exposed to water (Fernø, 2008). In sandstone experiments, Karpyn et al. (2006) found that counter-current flow prevailed at early and intermediate times, while both co-current and counter-current flow coexisted at late times. To improve modeling of the flow directions during imbibition, correct measurements of the saturation

functions at reservoir flow conditions is vital (Uleberg and Kleppe, 1996).

2.4 Experience from Fractured Reservoir Management

Casablanca Karst Reservoir, Spain

The Casablanca Field offshore Spain is often cited as an example of good fractured reservoir management. The reservoir is a Type 2, fractured, karstic carbonate sequence consisting primarly of limestone and dolomite (Allan et al., 2003). The original oil column was 268 meters and no gas cap exists (Orlopp et al., 1988). No secondary recovery or EOR techniques were applied for exploitation, but the production rate were carefully controlled by reducing choke size as water cuts reached only 2%. In 2003, the field had achieved an oil recovery factor of 47.5% and this is expected to rise to 50 % or greater (Allan et al., 2003; Meehan et al., 2011).

Yangling Karst Reservoir, China

The Yanling karst reservoir has rock and fluid properties similar to those at Casablaca, but reservoir management and subsequent recovery factor differ. The Yangling field is a fractured karstic carbonate oil reservoir in northeastern China, undersaturated and with dolomite as main reservoir lithology. The first two years of production, production rates were very high, which prevented matrix oil from draining into the fractures, leading to rapid pressure and production decline (Allan et al., 2003; **?**). Like the Casablanca Field, the reservoir has a strong water drive, but now water injection were also applied to maintain reservoir pressure. Water cut were not as carefully controlled, which resulted in rapid increase of water cut, subsequent shortening of the fields production life and a recovery factor of 19.5 %, which is lower than recovery from the same formation in different fields (Meehan et al., 2011).

Ekofisk Chalk Reservoir, Norway

The Ekofisk Field is a giant oil field in the North Sea, outside Stavanger, Norway. The field produces from several water-wet naturally fractured chalk reservoirs. Average matrix permeability is estimated to 1-2 mD with fracture permeability of approximately 50 mD (Sylte et al., 1999). The field was produced with solution gas drive and reservoir compaction from 1975 to 1987. As steep decline was experienced, water injection was initiated, following several pilot injection projects. Production decline was reversed and a secondary production almost as high as the primary was reached in the late 1990's. The current best estimate of recovery under waterflooding is 44 % (SPE, 2015).

Natih Diagenetic Chalk Reservoir, Oman

The Natih Field, situated in the North of Oman consists of primarly oil-wet chalky and vuggy/rudist carbonate facies with moderate to low matrix permeability (Van Dijkum et al.,

1991). Before water flooding, primary production profile of the field is almost identical to that at Ekofisk and as steep pressure and production decline were experienced, a water-injection program was initiated. At the Natih Field, production decline was however not arrested by the water injection and crestal gas injection was begun in stead. Gas injection arrested the production decline but was not able to reverse the decline, and ultimate recovery factor was 22 % (Allan et al., 2003).

Chapter 3

Dual Porosity Modeling

In conventional modeling of a fractured reservoir, the fracture and matrix properties are assigned on a grid block to grid block basis. Such fine-grid modeling is the most accurate and is commonly used on laboratory scaled simulations. For full field simulations, this approach is too computationally expensive, hence the need for dual porosity simulators. The concept of dual-porosity modeling was developed by Warren et al. (1963) and their idealized fractured reservoir representation is shown in **Figure 3.1**. In this system, flow towards the well is considered to take place only in the highly interconnected fracture network, and the numerous small matrix blocks to act as a source, supplying fluid to the fractures.

In dual porosity / dual permeability models, the fracture and matrix grid are identical and superposed. This is done by associating each geometric grid block with two simulation cells, representing the matrix and fracture volumes of the block. In other words, any matrix cell is associated to the fracture cell found at the grid location under consideration. If the dual permeability option is activated, an extra transmissibility is added to the matrix cell calculation, connecting it to both the superposed fracture as well as the neighboring matrix cell. In a given grid block, a large number of individual and identical matrix blocks exist, as illustrated in **Figure 3.2** for parallelepipedic matrix blocks.

3.1 Reservoir Simulator

Rock Flow Dynamics' (RFD) software tNavigator^{TM} is used along with the Schlumberger ECLIPSE syntax to run dual porosity simulations for this thesis. tNavigator is a software package consisting of six modules which allows building of static and dynamic reservoir models, and run dynamic simulations, among other. The simulator is built to utilize more of the modern computational resources in parallel simulations and multicore Central Processing Unit (CPU) computers and offers an interactive user control of the simulation run. In tNavigator, the simulation core and the visualizer are one joined application, which allows the user to perform operations with the model during the run, and quick visualization due to no time spent on writing and reading data from the disk.

The tNavigator simulator is able to handle input decks from exiting models such as the

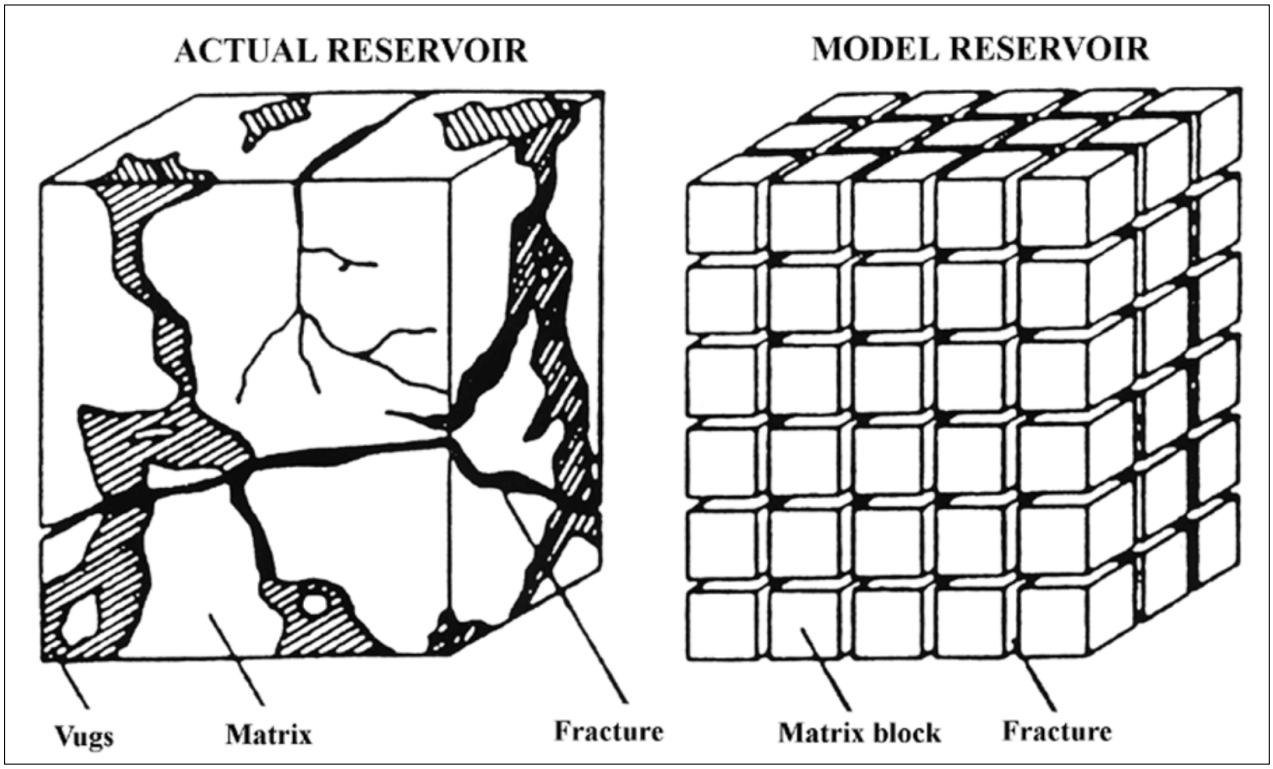

Figure 3.1: Idealization of a fractured system (Warren et al., 1963).

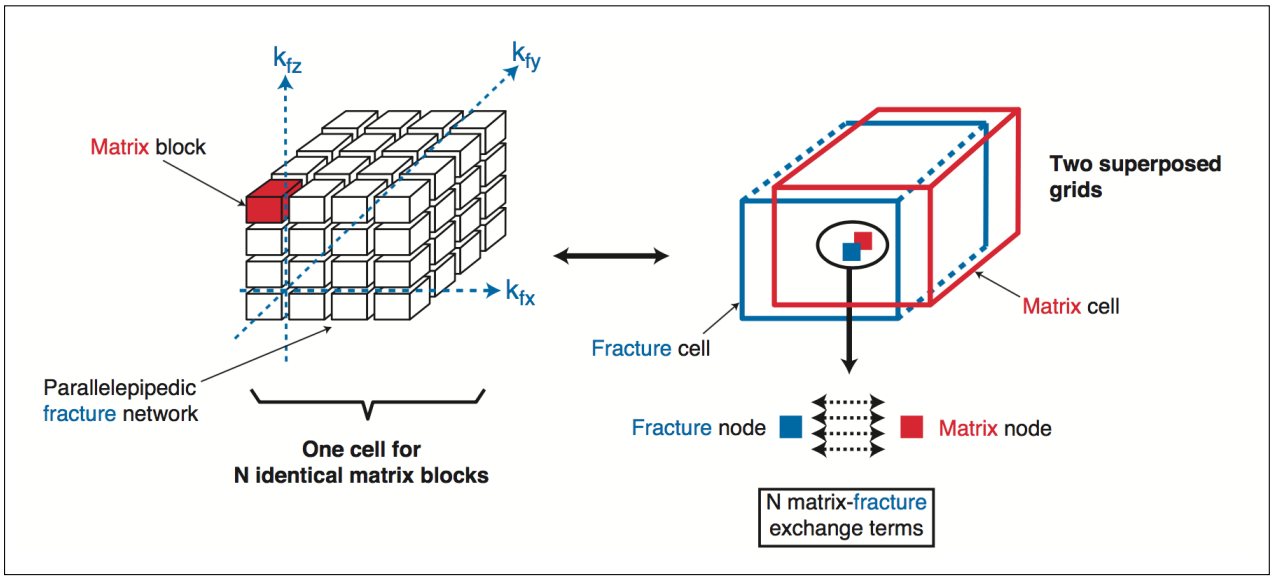

Figure 3.2: Dual porosity representation of a fractured reservoir Bourdon et al. (2004). component k in phase p between a matrix block and the surronding fractures. Bourdon et al. (2004)

Schlumberger E100 'Black Oil' syntax. Like with the ECLIPSE software, a fully implicit time scheme is used to solve systems of differential equations. The E100 'Black Oil' model assume that the hydrocarbons can be described as either gas or oil and is used in reservoirs where fluid properties can be expressed as a function of pressure and bubble-point pressure (Kleppe, 2017). Black oil reservoir simulation is widely used in the petroleum industry, as it is less CPU intensive than compositional models where the mass balance is calculated for each hydrocarbon component Ghorayeb et al. (2005).

3.2 ECLIPSE^{TM} Dual Porosity, Dual Permeability Formulation

ECLIPSE E100 has a Dual Porosity / Dual Permeability option for modeling of naturally fractured reservoirs. The main keywords associated with this simulation mode is summarized in **Table 3.1**. The ECLIPSE dual porosity model can be used to simulate all the principal recovery processes in fractured reservoirs; fluid expansion, capillary imbibition, gravity imbibition / drainage, diffusion and viscous displacement. The capillary imbibition process is modeled by specifying different saturation table numbers for the matrix and fracture cells respectively, while the three latter processes are activated by including specific keywords in the RUNSPEC section, e.g. GRAVDR, DIFFUSION and VISCD.

When the dual porosity run is specified by the keyword DUALPORO in RUNSPEC, connections are made only between the superposed matrix and fracture, as illustrated by black arrows in **Figure 3.7**. The connection is made by a matrix-fracture coupling transmissibility term (TR) given in Equation 3.1:

$$TR = CDARCY \cdot K \cdot V \cdot \sigma \tag{3.1}$$

where $CDARCY$ is Darcy's constant (a unit conversion factor), K is the X-direction matrix block permeability in mD, V is the matrix cell bulk volume in m^3 and σ is Kazemi's 'sigma factor' in m^{-2} (Equation 3.2).

Shape Factor (σ)

The sigma factor, or shape factor, σ, included in Equation 3.1, is related to the size of the matrix cells through Kazemi's equation (3.2). σ accounts for the matrix/fracture interface area per unit volume and can be specified using the keyword SIGMA in the GRID section. The relationship proposed by Kazemi et al. (1976) assumes rectangular parallelpiped and isotropic matrix block and is given by the expression:

$$\sigma = 4\left(\frac{1}{l_x^2} + \frac{1}{l_y^2}\frac{1}{l_z^2}\right) \tag{3.2}$$

Table 3.1: Dual Porosity Keyword Summary from the ECLIPSE Reference Manual (Schlumberger Ltd, 2015)

Keyword	Section	Description
DUALPORO	RUNSPEC	Two simulation cells associated with each block in the geometric grid, flow is between matrix and fracture.
DUALPERM	RUNSPEC	Extends the dual porosity option to allow flow directly between matrix cells.
SIGMAV	GRID	Modifies the matrix-fracture coupling transmissibility.
GRAVDR	RUNSPEC	Requests that gravity drainage and imbibition are modeled between the matrix and fracture cells.
GRSVDRM	RUNSPEC	Alternative gravity dranage model that can include reinfiltration of oil from fractures.
DZMTRXV	GRID	Specifies the vertical dimension of a typical block of matrix material used in GRAVDR(M), equal to l_z in Kazemi's formula. Typically much smaller than the vertical dimension of a simulation matrix cell, DZ.
MULT$_i$	GRID	Transmissibility multiplier, i = X, Y, Z.
SATOPTS	RUNSPEC	Enables the use of hysteresis through separate saturation function tables defined for drainage and imbibition.
SATNUM	REGIONS	Saturation function region numbers, taken as defining the drainage curves when the hysteresis option is activated.
IMBNUM	REGIONS	Used in runs with the hysteresis option, specifies which saturation table is to be used for each cell for imbibition processes.
EHYSTR	PROPS	Hysteresis parameters and model selection, used to define a curvature parameter for capillary pressure hysteresis which normally lies in the range 0.05 to 0.1.
SWOF	PROPS	Input tables of water relative permeability, oil-in-water relative permeability and water-oil capillary pressure as functions of the water saturation.
SGOF	PROPS	Input tables of gas relative permeability, oil-in-gas relative permeability and oil-gas capillary pressure as functions of the gas saturation.
TABDIMS	RUNSPEC	First item NTSFUN defines the number of saturation tables entered. Must be doubled for use with capillary pressure hysteresis.
FIPNUM	REGIONS	Fluid-in-place region numbers.
NODPPM	RUNSPEC	Allow input of effective fracture permeabilities (otherwise they are calculated from fracture porosity).
RSVD	SOLUTION	R_s versus depth tables for equilibration.
VISCD	RUNSPEC	Requests that the viscous displacement mechanism should be modeled in dual porosity runs.
DIFFUSE	RUNSPEC	Enables molecular diffusion.
DIFFDP	PROPS	Can be used to restrict molecular diffusion in dual porosity runs, to only calculate matrix-fracture diffusion.

TABLE 1—OVERVIEW OF SHAPE FACTORS PROPOSED IN THE LITERATURE*

1D	2D	3D	Author
$\frac{12}{L_x^2}$	$\frac{8\left(L_x+L_y\right)^2}{\left(L_xL_y\right)^2}$	$\frac{60\left(L_xL_y+L_xL_z+L_yL_z\right)^2}{9\left(L_xL_yL_z\right)^2}$	Warren and Root
$\frac{4}{L_x^2}$	$4\left(\frac{1}{L_x^2}+\frac{1}{L_y^2}\right)$	$4\left(\frac{1}{L_x^2}+\frac{1}{L_y^2}+\frac{1}{L_z^2}\right)$	Kazemi
$\frac{12}{L_x^2}$	$\left(\sum_{k,l=0}^{\infty}\left[\frac{8^2}{\alpha_k^2\alpha_l^2\left(\alpha_k^2+r\alpha_l^2\right)}\right]\right)^{-1}\frac{1}{L_x^2}$	$\left(\sum_{k,l,m=0}^{\infty}\left[\frac{8^3}{\alpha_k^2\alpha_l^2\alpha_m^2\left(\alpha_k^2+r\alpha_l^2+s\alpha_m^2\right)}\right]\right)^{-1}\frac{1}{L_x^2}$	Coats
$\frac{\pi^2}{L_x^2}$	$\pi^2\left(\frac{1}{L_x^2}+\frac{1}{L_y^2}\right)$	$\pi^2\left(\frac{1}{L_x^2}+\frac{1}{L_y^2}+\frac{1}{L_z^2}\right)$	Chang, Lim, and Aziz

*In Coats' results, the following abbreviations are used: $\alpha_k=\pi\left(2k+1\right)$; $r=\left(k_y/k_x\right)\left(L_x/L_y\right)^2$; $s=\left(k_z/k_x\right)\left(L_x/L_z\right)^2$.

Figure 3.3: Overview of shape factors proposed in literature. Figure from van Heel et al. (2008)

where l_x, l_y, l_z = X, Y and Z dimensions of the blocks material making up the matrix volume (not related to the simulation grid dimensions).

The shape factor is an important parameter in the transmissibility and hence, flow calculations, but it's physical meaning remains unclear. Several authors have proposed different expressions for the shape factor, most of which are related to the size and/ or shape of a matrix block, like the one of Kazemi et al. (**Figure 3.3**). In addition to geometry, van Heel et al. (2008) found that the shape factor is not always a constant but depends on the different processes the matrix is subjected to. From these studies it is concluded that the shape factor is better applied as a tuning factor for history matching, than to relate it to any physical process.

Capillary Imbibition

For an oil-water system, spontaneous imbibition will occur as long as the imbibition capillary pressure curve is positive. In ECLIPSE, this is modeled by specifying different saturation table numbers for the matrix and fracture cells respectively, where the fracture cells typically have zero capillary pressure (Schlumberger Ltd, 2015). The saturation tables define both relative permeabilities and capillary pressure for the different cells, where flow from matrix to fracture takes the relative permeability calculated using the matrix properties, and flow from fracture to matrix uses fracture saturation and table.

To model separate drainage and imbibition curves in ECLIPSE, the option HYSTER

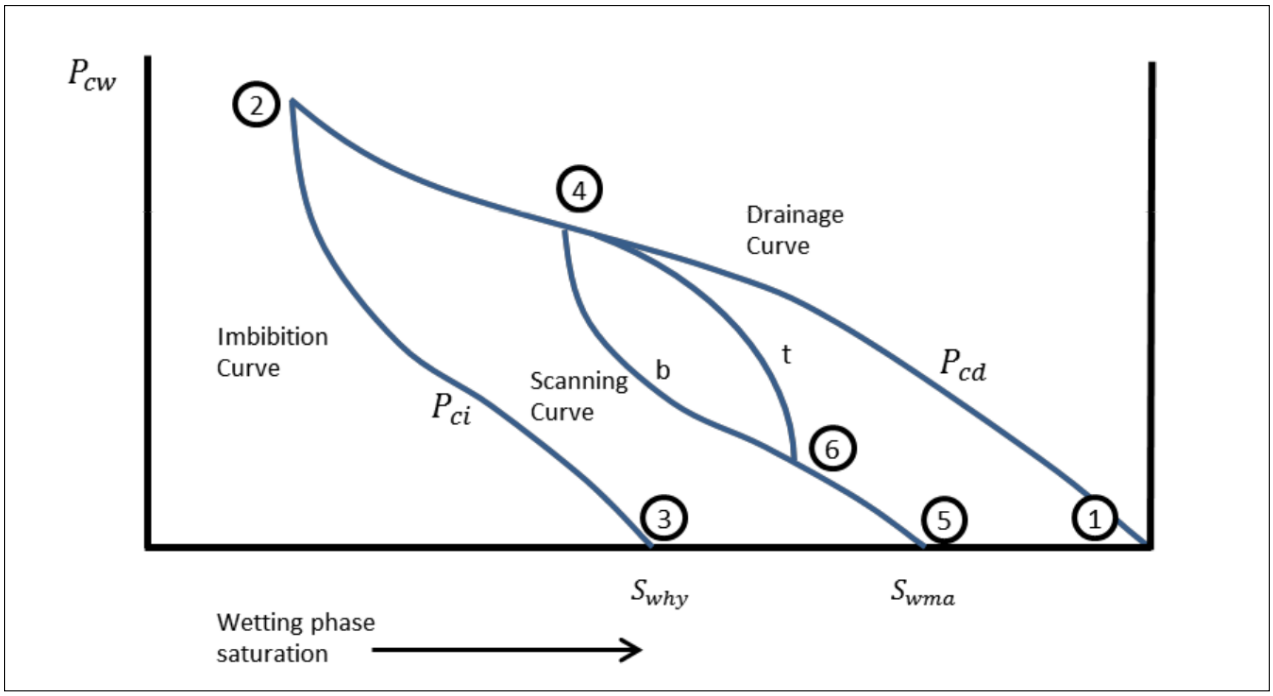

Figure 3.4: Hysteresis scanning curves in an oil-water capillary pressure case. Figure from Schlumberger Ltd (2015).

in the SATOPTS keyword is required. The default SATNUM tables are now taken as the drainage curves, and imbibition curves are identified using IMBNUM in the REGIONS section. The scanning curves are then defined by an EHYSTR value larger than zero in the PROPS section. ECLIPSE uses Killough et al.'s model (Equation 3.3) to form the scanning curves, starting with 100 % of the drainage curve at point 4 in **Figure 3.4**. The fitting parameter E in Equation 3.4 is specified by the EHYSTR keyword and should normally lie in the range of 0.05 to 0.1, where 0.05 defines a branch closer to the bounding imbibition curve (P_{ci}), and EHYSTR = 0.1 closer to the bounding drainage curve (P_{cd}). The method by Killough et al. (1976) predicts hysteresis capillary pressures by using a form for weighted average (by weighting factor F) and may be written as:

$$P_c = P_{cd} + F(P_{ci} - P_{cd}) \tag{3.3}$$

with

$$F = \frac{\frac{1}{S_w - S_{why} + E} - \frac{1}{E}}{\frac{1}{S_{wma} - S_{why} + E} - \frac{1}{E}} \tag{3.4}$$

where

S_{why} = is the water saturation at the hysteresis reversal point 4 (Figure 3.4), that is the minimum historical water saturation in the cell, and

S_{wma} = is the maximum water saturation attainable allowing for the trapped non-wetting phase saturation

The limitations of Killough et al.'s hysteresis loop logic are thoroughly discussed in

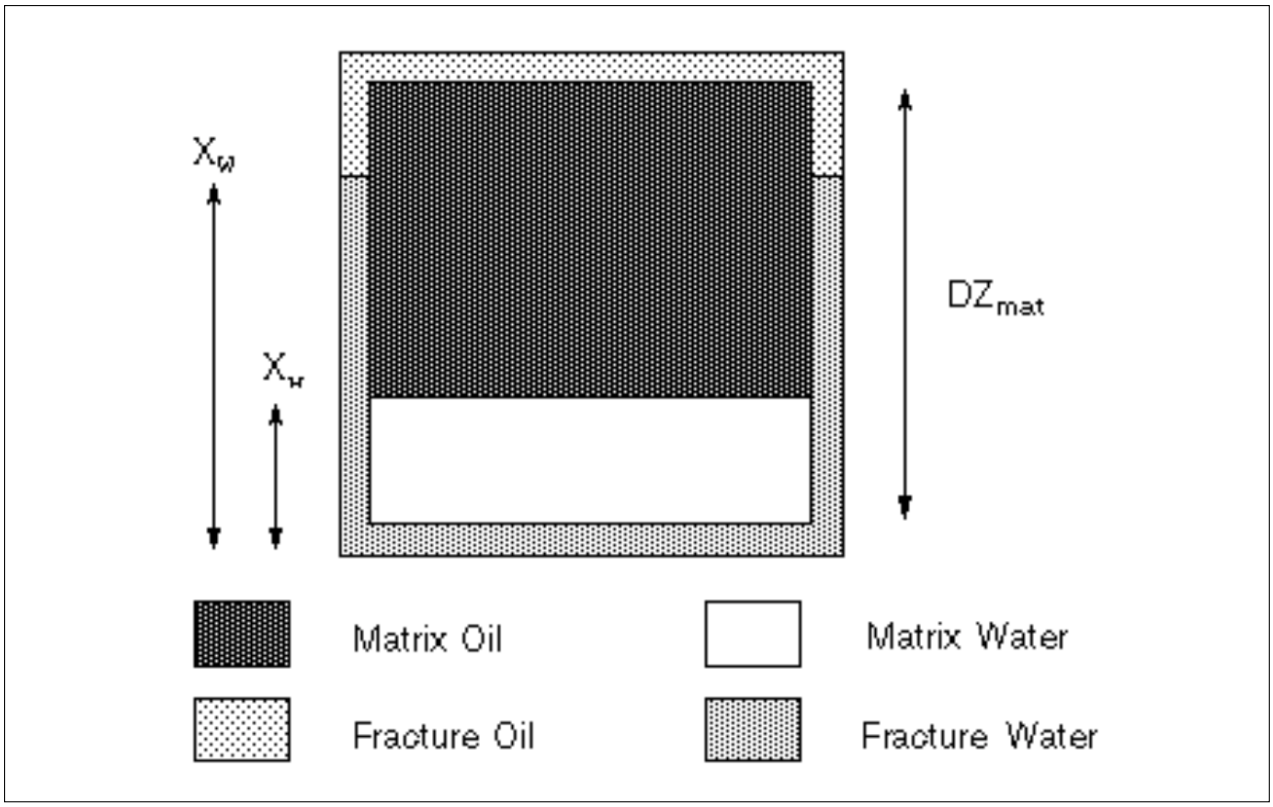

Figure 3.5: A typical block of matrix material containing oil and water. Figure from Schlumberger Ltd (2015).

literature (Kleppe et al., 1997; Skjaeveland et al., 1998; Kriebernegg and Heinemann, 1996; Tan et al., 1990). Killough's method is often inadequate since it was formulated for the case where the drainage and imbibition curves meet at the residual oil saturation. As the model does not scale the saturation ranges in question, Kleppe et al. (1997) found that it failed to match laboratory examples of the hysteresis behavior. Kleppe et al. (1997) proposed a new method for modeling of scanning curves where the curves are not interpolated but rather each depends on only one bounding curve.

Gravity Drainage -and - Imbibition

The Schlumberger ECLIPSE suite offers three methods to model fluid exchange due to gravity; GRAVDR (Sonier et al., 1988), GRAVDRM and VERTICAL. The standard gravity drainage model, GRAVDR, is used in this thesis. This method assumes that the matrix and fracture are separately in vertical equilibrium and calculates additional potential due to difference in fluid-contact heights. **Figure 3.5** illustrate a typical oil saturated single matrix block partially immersed by water, where X_W and X_w is fractional height of the water table in the fracture, and the water displacement front in the matrix block, respectively. DZ_{mat} is the vertical dimenson of a single matrix block, specified by the keyword DZMTRX in the GRID section.

The total flow F from a fracture to a matrix cell in a gas-oil system is computed as:

$$F_g = TR \cdot GMOB\left(P_{o,f} - P_{o,ma} + d_{f,ma}\rho_g g P_{cog,f} - P_{cog,ma} + \frac{DZ_{mat}(X_G - X_g)(\rho_o - \rho_g)g}{2}\right) \tag{3.5}$$

$$F_o = TR \cdot OMOB\left(P_{o,f} - P_{o,ma} + d_{f,ma}\rho_o g - \frac{DZ_{mat}(X_G - X_g)(\rho_o - \rho_g)g}{2}\right) \tag{3.6}$$

where
$GMOB, OMOB$ = gas and oil mobility in the (upstream) fracture cell,
$P_{o,ma}, P_{o,f}$ = oil phase pressure in the matrix and fracture cell,
$d_{f,ma}$ = the difference in depth between the fracture and matrix cells (usually zero), and
$P_{cog,f}, P_{cog,ma}$ = the capillary pressure of gas in the fracture cell (normally zero) and the matrix cell

The dual porosity mode (specified by DUALPORO and not DUALPERM) with no flow between matrix cells represent a reservoir where the matrix blocks are separated by horizontal fractures so that they are capillary discontinuous. The volume of oil recoverable by full gas immersion (gravity drainage) in this mode is exactly the number of matrix blocks times the recovery from one block. However, if the four blocks are capillary continous, the blocks behave essentially as one tall block and ultimate recovery is substantially more optimistic. According to Fung et al. (1991) the dual permeability model is the optimal method to account for a high degree of capillary continuity. However, effects of partial matrix continuity may be approximately accounted for if an effective matrix block height (DZMTRX) is used (Fung, 1991).

Recent research of dual porosity gravity-drainage modeling suggests that neither Kazemi's sigma factor nor the GRAVDR keyword are able to capture the full recovery behavior of a fractured reservoir (Lu, 2008). Lu (2008) developed an analytical solution for the matrix-fracture transfer function, which he validated against fine-grid simulations of a water-oil system. In comparison with the dual porosity model, his results showed that without the GRAVDR option, the conventional dual porosity model underestimates recovery at early time and at final recovery. By adjusting SIGMA and DZMTRX in a GRAVDR model ('Sonier et al. (1988) model'), either initial or final recovery could be matched, but not both. An example of fine grid-final recovery for a matrix block height of 1 m was matched by GRAVDR with DZMTRX = 3.2 m. Two sigma factors (the same and 0.13 times the original / analytical) were tested with DZMTRX = 3.2 m. Both matched final recovery but using the same sigma captured more of the late time recovery behavior. **Figure 3.6** illustrate three examples of the GRAVDR model (Sonier et al., 1988) compared to a fine grid model. Lu's studies may indicate that, for a water-oil system, the actual reservoir may have an additional upside compared to simulations done with a dual porosity simulator.

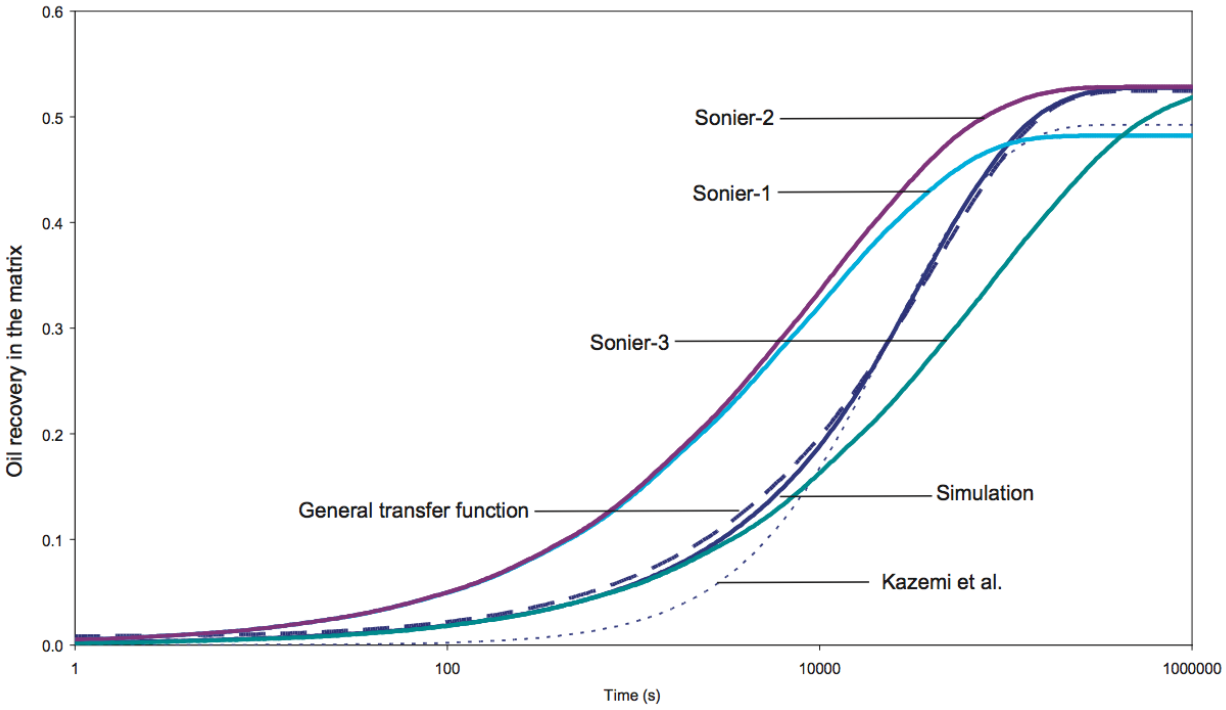

Figure 3.6: Matching of the dual porosity GRAVDR model ('Sonier') with analytical solution ('General transfer function'), and fine grid simulation ('Simulation') for a block height of 1 m. Sonier-1 is same SIGMA, same DZMTRX; Sonier-2 is same SIGMA, different DZMTRX (3.2 m); Sonier-3 is 0.13 times SIGMA, different DZMTRX (3.2 m). Figure from Lu (2008).

Block-to Block Simulation, DUALPERM

Figure 3.7 illustrates the block-to-block transmissibility term activated by the DUALPERM keyword. Fung et al. (1991) compared three fractured reservoir models which account for the gravity drainage process; the gravity segregated model, the subdomain method and the dual permeability model. His study showed, that when capillary continuity is important, the dual permeability model is the most appropriate model for handling the gas gravity drainage problem. The dual-permeability model assumes the matrix to be completely continuous and the matrix oil recovery under gravity drainage reflects the gravity/ capillary balance for the entire matrix column (not the individual matrix block height). The model does not account for the reinfiltration of oil from gridblock to gridblock, but this may be modeled by an alternative gravity drainage option in the dual porosity mode: GRAVDRM. The degree of contact between matrix cells may be altered by including a value for MULT_i between 0.0 and 1.0.

3.3 Limitations of the Dual Porosity Principle

The conventional dual porosity model being used today is an extension of Barenblatt et al. (1960) and Warren et al.'s 1963 work made by Kazemi et al. (1976). Research to improve this model is currently focused on three aspects: 1) shape factor calculation 2) physical

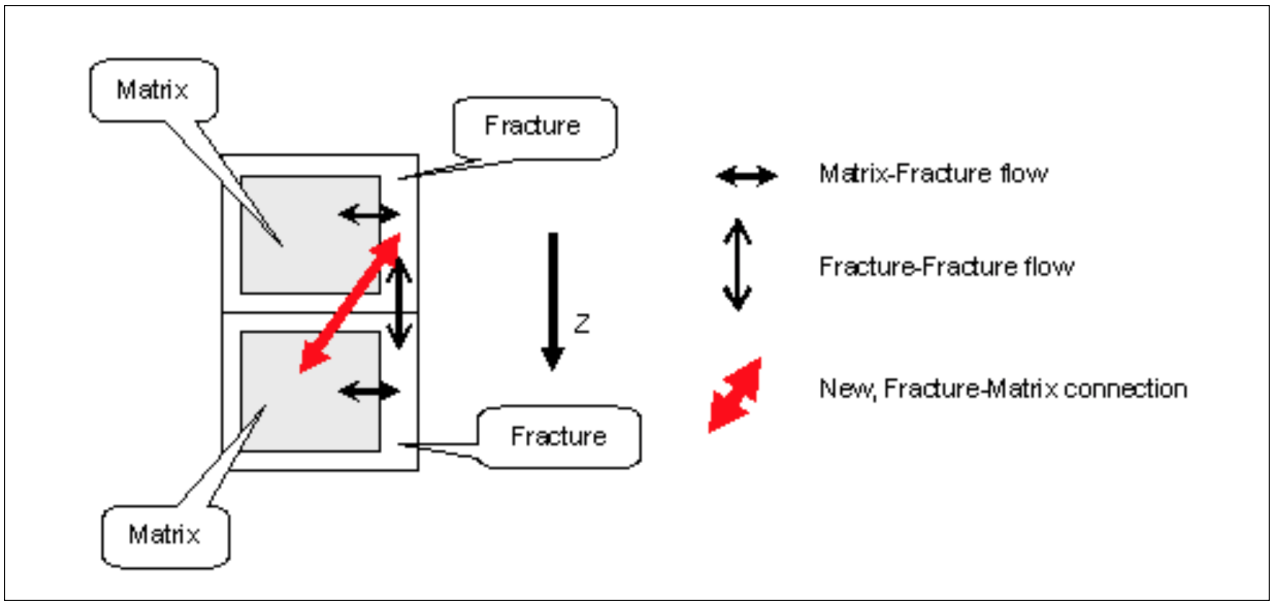

Figure 3.7: Physical view of the matrix and fracture cells for the block to block connection. This figure appears to show the lower matrix disconnected from the upper fracture by its own surrounding fracture, but this is only for presentation purposes: there will always be some contact between the upper fracture and lower matrix. Figure from Schlumberger Ltd (2015).

modelling of multi-phase flow in naturally fractured reservoirs, and 3) refining of matrix blocks / reduction of computational time (Di Donato et al., 2003; Lu, 2008). The current Kazemi-Barrenblatt approach assumes the shape factor given in Equation 3.2 and a quasi-steady state between matrix and fracture in order to calculate transfer-rate.

Attempts to improve the model also relate to the coarse grid normally used in dual porosity simulators. As the upscaled grid block consists of many matrix blocks, saturation gradients in the matrix block is not measured and the resulting saturation gradients of the grid blocks are sharper than that of conventional models. Uleberg and Kleppe (1996) presented a *multiple grid concept* where the matrix block were refined into multiple blocks of similar behavior. This would allow individual computation on one representative matrix block, which can be multiplied with the number of grid blocks present. Local grid refinement is of particular importance if the matrix block size is small (less than 1 m^3), as the representable grid block would contain several tens of thousands of matrix blocks requiring significant computational time. Attempts to reduce the run time of dual porosity simulations also include streamline-based models. Di Donato et al. (2003) demonstrated that by using streamlines run time could be orders of magnitude smaller than equivalent grid-based simulation (ECLIPSE), allowing multi-million cell models to be run using standard computing resources. Stability problems related to rapid changes in saturation (f.ex. by coning) or large differences between fracture and matrix porosity can be avoided by detailed modeling made possible by reduced run time (Lu, 2008).

Chapter 4

Model Description

The test model is a full-scale reservoir model supplied by Lundin Norway's Petroleum Technology department. The grid is generated using Schlumberger's Petrel E & P Software Platform (Schlumberger, 2016) and exported for use with Eclipse / tNavigator. To save simulation time, the pink part in **Figure 4.1** was sectioned out from the complete Alta East Flank model and is used for the cases described in this thesis. The resulting grid is divided into $i \cdot j \cdot k = 35 \cdot 18 \cdot 184$ grid blocks, where blocks with $k = 1$ - 92 reflect the matrix volume and $k =$ 93-184 the fractures. Obviously, the wells are placed in fracture grid blocks which ensure flow towards the well. All grid blocks are approximately equally sized, with dimensions of 100 x 100 x 5 m^3 in the aquifer and gas cap, and $100 \cdot 100 \cdot 1.3$ m^3 in the more fine gridded oil zone (**Figure 4.2**). If we assume cubic formed matrix blocks with sides of 1 m, this implies that inside an oil zone grid block, more than 13 000 matrix blocks exist, and for the coarser part of the grid, 50 000 matrix blocks per grid block. This will of course vary as the matrix block dimensions are changed.

Two horizontal wells are included for each test system, one producer and one injector. The locations of the wells change in accordance with the secondary recovery method chosen, gas injector in gas zone and water injector in the aquifer. The production well is constrained to the same limits in both test systems, given in **Table 4.1** and **4.2** . This may be a weakness of the model, as constraints on liquid production would give more realistic results especially for the water injector case. Fluid and rock properties of the reservoir model is given in **Table 4.3**.

Table 4.1: Production Well ('OP') Limits

Well Control Data					Economic Limits	
Oil Rate	BHP	Gas Rate	Water Rate	Liquid Rate	Min. Oil Rate	Water Cut*
Sm^3	*barsa*	Sm^3/day	Sm^3/day	Sm^3/day	Sm^3/day	%
1500	175	825 000	No Limit	No Limit	10	95

**Shuts in the worst offending perforation and below*
BHP = Bottom Hole Pressure

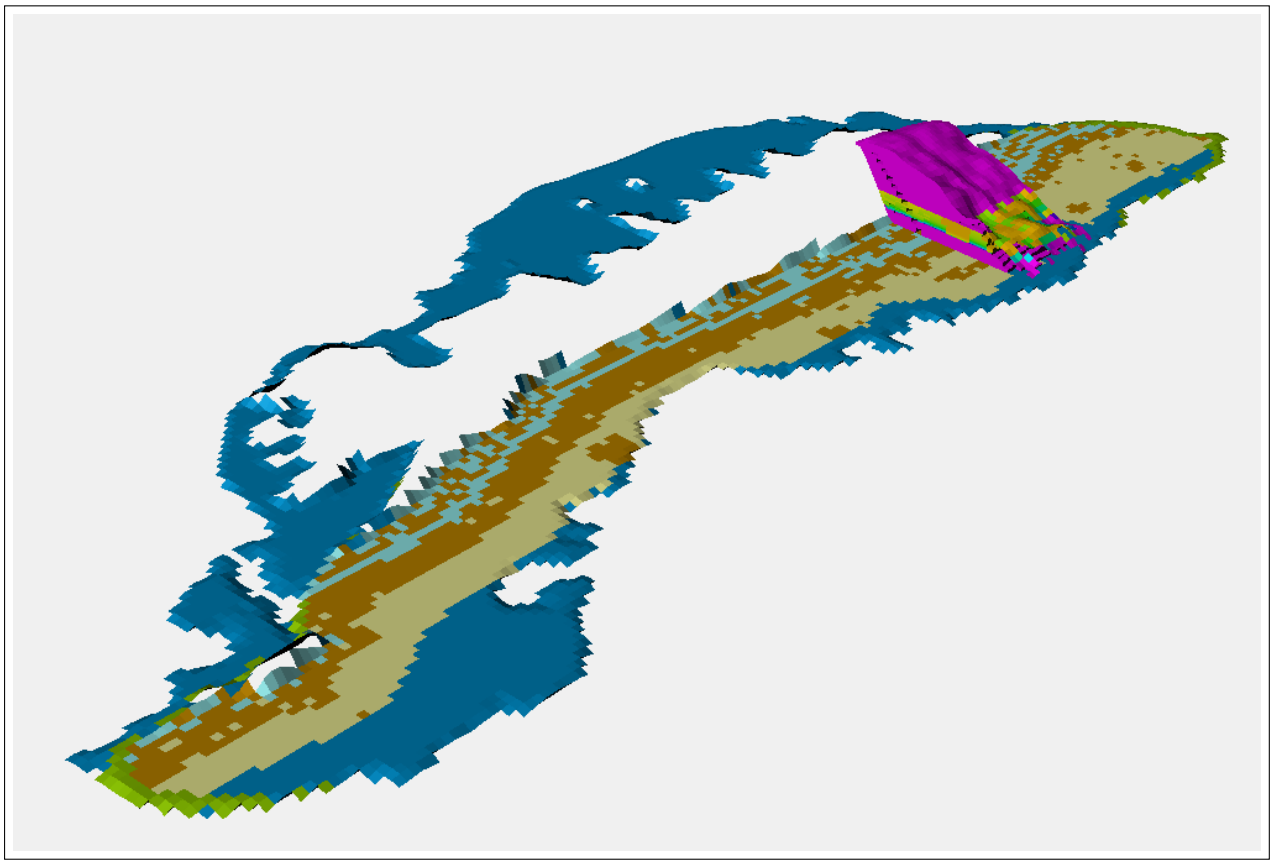

Figure 4.1: The complete Alta East Flank grid, illustrating the location of the studied section. Courtesy of Lundin Norway AS.

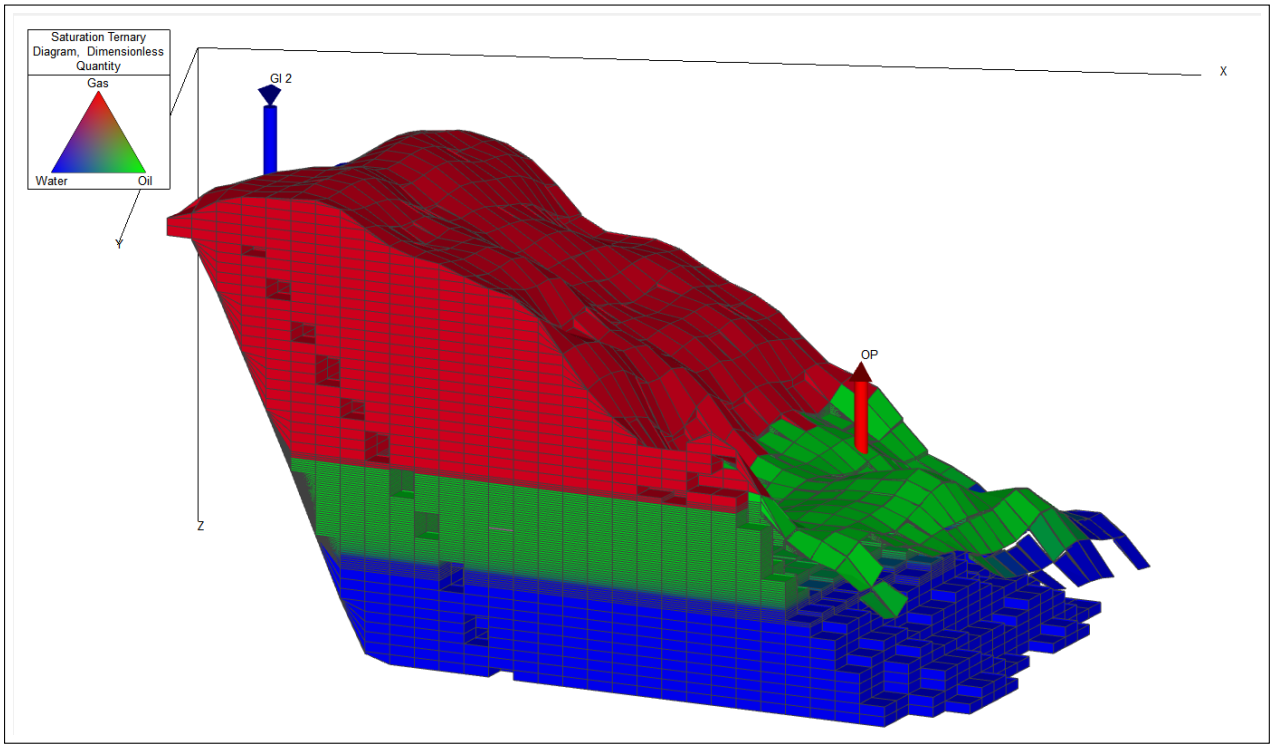

Figure 4.2: Saturation ternary diagram of reservoir model, shown with one oil producer ('OP') and one gas injector ('GI 2'). Saturation is shown at initial time and the figure's Z dimension is scaled up times eight. Red = mostly gas, green = mostly oil, blue = mostly water.

Table 4.2: Injector Well ('GI 2' and 'WI') Limits

Well Control Data	
Bottom Hole Pressure *barsa* 300	Voidage Rate* *fraction* 1*

* *The fields reservoir volume injection rate is controlled so that it equals the fields production voidage rate*

Table 4.3: Fluid & Rock Properties

Values given at P_{ref}		
P_{ref} *@ GOC*	196,6	*barsa*
μ_w	0,68636	cP
μ_o	0,444	cP
μ_g	0,020246	cP
ρ_w	1168,7	kg/m^3
ρ_o	826,3	kg/m^3
ρ_g	0,93884	kg/m^3
B_w	1,0184	$rm^3/Sm3$
B_{oi}	1,3524	$rm^3/Sm3$
B_g	0,005511	$rm^3/Sm3$
R_{si}	114,24	$Sm^3/Sm3$
C_w	3,36E-05	$1/bars$
C_{rm}=C_{rf}	5,79E-05	$1/bars$
S_{wir}	0,12	fraction
$S_{or,ow}$	0,28	fraction
$S_{or,og}$	0,4	fraction
$k_{ro}@S_{wir}$	1	fraction
$k_{rw}@S_{or,ow}$	0,18	fraction
$k_{rg}@S_{or,og}$	0,84	fraction
$S_{or,ow}$	$= S_{or}$ at $k_{row}= 0$	
$S_{or,og}$	$= S_{or}$ at $k_{rog}= 0$	

Facies Sectioning

The model has a complex geometry reflecting the actual Alta East reservoir. **Figure 4.3** describe the reservoir zonation for which porosity and permeability parameters are assigned. Reservoir properties as well as OOIP values of each Fluid-In-Place region (FIPNUM) is given in Table **??**, and permeability is the same in all directions of the matrix / fracture block ; $k_x = k_y = k_z$.

Base Case Saturation Functions

All cases in this thesis is simulated with linear fracture relative permeability for both oil-gas and oil-water, as plotted in **Figure 4.4** for oil and gas. The matrix relative permeabilities, $k_{r,m}$, are shown in **Figure 4.5** and **4.6** for oil-water and oil-gas, respectively. Matrix relative permeabilities are also constant for all examples in this thesis. Endpoint relative permeabil-

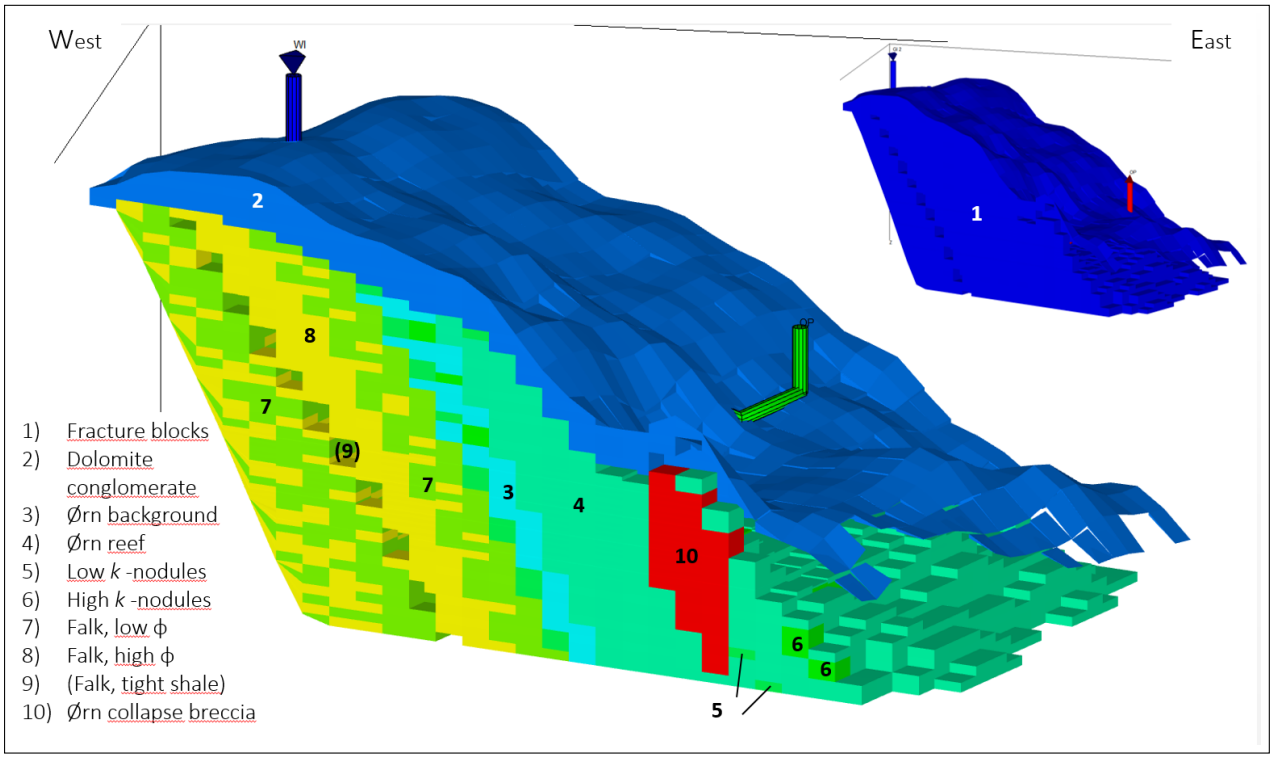

Figure 4.3: Schematic figure illustrating the facies modeling through Fluid-In-Place regions (FIPNUM). OOIP as well as approximate porosity and permeability values for each FIPNUM zone is given in Table **??**. The model's Z dimension is scaled up times eight.

Table 4.4: Facies Reservoir Property Modeling

FIPNUM	Model Zone	ϕ	k	*OOIP*	
-	-	%	mD	MSm^3	*% of total*
1	Fracture blocks	0-3	880-10000	1.64	17
2	Dolomite conglomerate	15	1000	1.45	15
3	Ørn background	5	60	0.38	4
4	Ørn reef	12	100	3.00	32
5	Low k nodules	7	10	0.16	2
6	High k nodules	5.0	100	0.50	5
7	Falk, low ϕ	2.5	0.1	0.50	5
8	Falk, high ϕ	10.0	100	2.10	22
9	Falk, tight shale	0.0	0	0.00	0
10	Ørn collapse breccia	6.0	10	0.19	2
Total OOIP / Total Matrix Block OOIP Fraction:				9.51	83

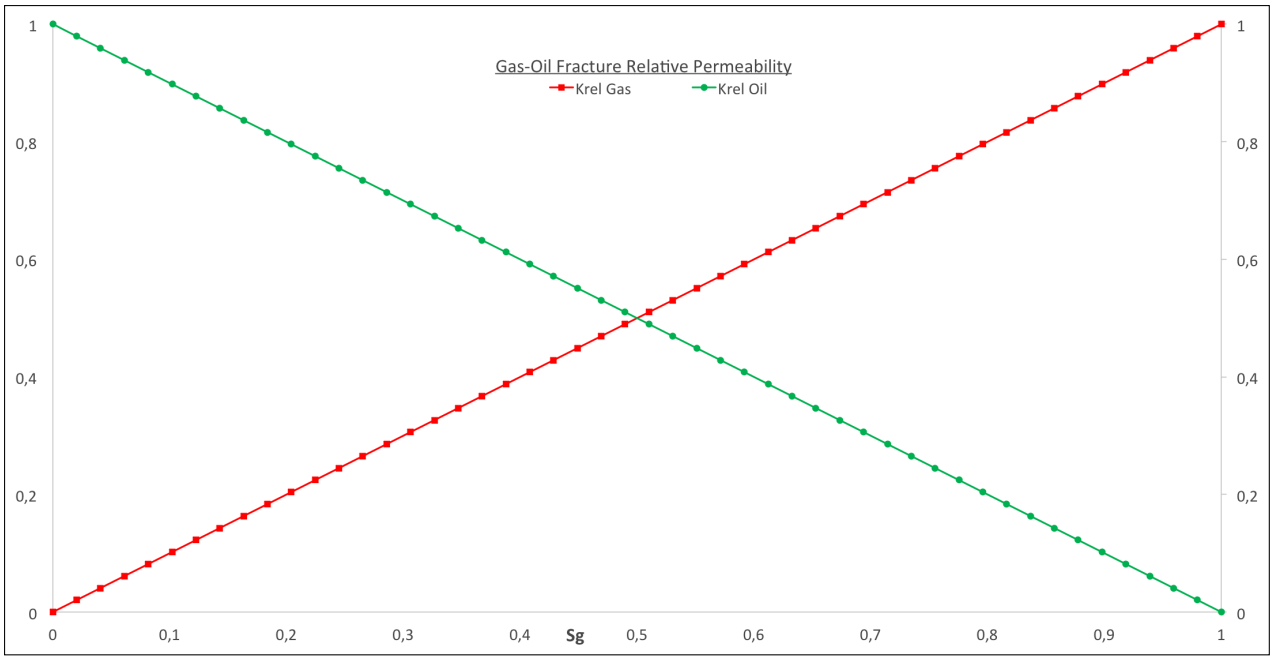

Figure 4.4: Fracture oil-gas relative permeabilty vs gas saturation. Oil-water relative permeabilities are also modeled as linear.

ities are given in Table 4.3. Crossover saturation along with S_{wi} and endpoint water relative permeability ($k_{rw}@S_{or}$) imply that the matrix have quite neutral wetting preferences, slightly more oil-wet.

Matrix capillary pressure is an important subject of this thesis. The Base Case gas-oil capillary pressure in the matrix, P_{cog}, is zero, and matrix oil-water capillary pressure, P_{cow} is given in **Figure 4.7**. The fracture capillary pressures are zero and kept constant in all simulations, while capillary pressure for the matrix is varied. In the Base Case P_{cow}, hysteresis is not modeled, meaning that drainage and imbibition processes follow the same path of saturation change. Thus $P_{cow,Base}$ approaches 100% water saturation at zero capillary pressure (indicates very strong water-wetting), or that $S_{or} = 0$. This is an unlikely situation and represent a crude simplification of the capillary pressure curve. Residual phase saturations are however limited to the relative permeability curve where endpoint values of k_{rw} and k_{ro} indicate S_{wi} of 0.12 and S_{or} of 0.27.

4.1 Gas Injection System

The horizontal gas injector is perforated in the top dolomitic conglomerate layer (FIPNUM zone 2). The wellhead is located in grid block i, j = 2, 13 and the well's trajectory runs through i, j, k = 2-5, 13-6, 98 (sixth fracture grid cell from the top). For this system, the oil producer is placed east of the injector, with perforations in the 'Ørn reef' facie; i, j, k = 22-21, 5-15, 159. Figure 4.2 shows the gas-oil system with production wellhead in grid block i, j = 22, 5.

In addition to the Base Case with $P_{cog} = 0$, four different non-zero matrix rock gas-oil

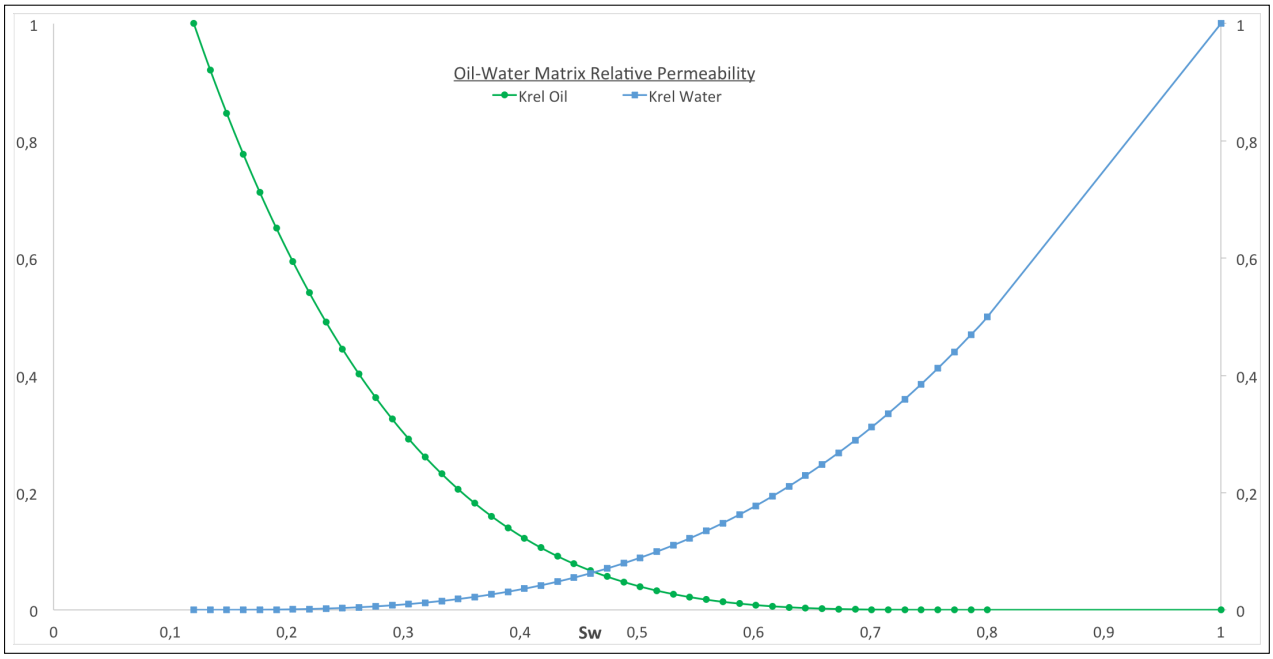

Figure 4.5: Matrix oil-water relative permeabilty vs water saturation.

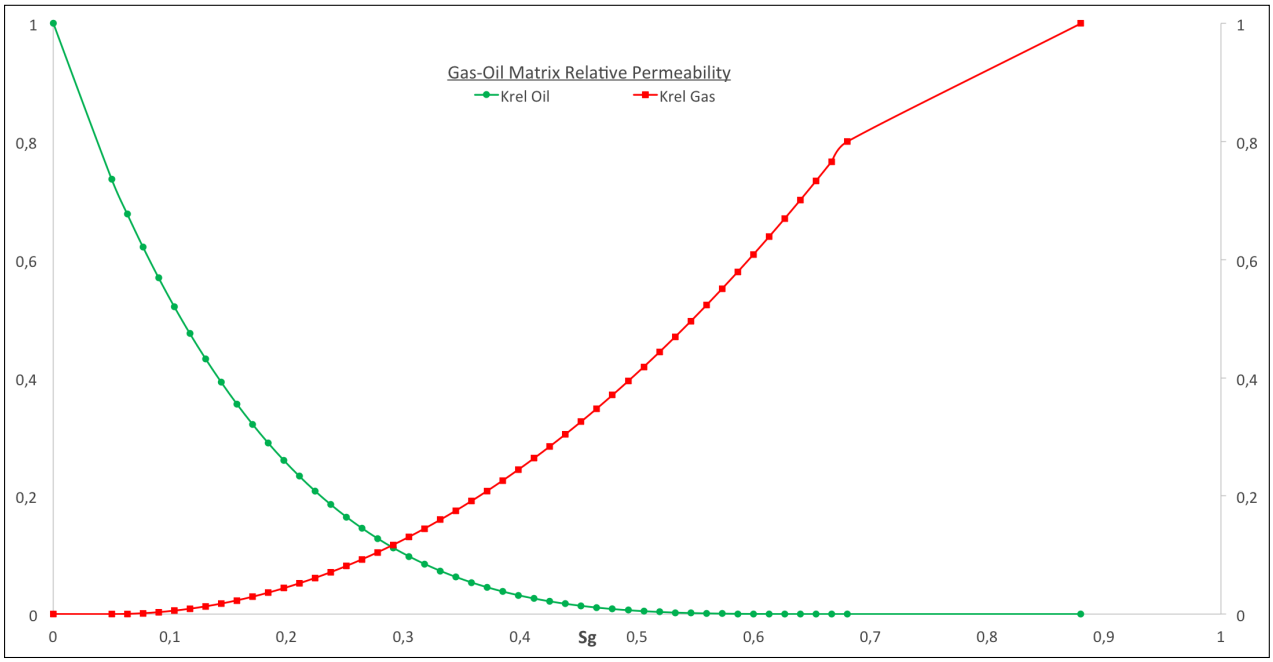

Figure 4.6: Matrix oil-gas relative permeability vs gas saturation.

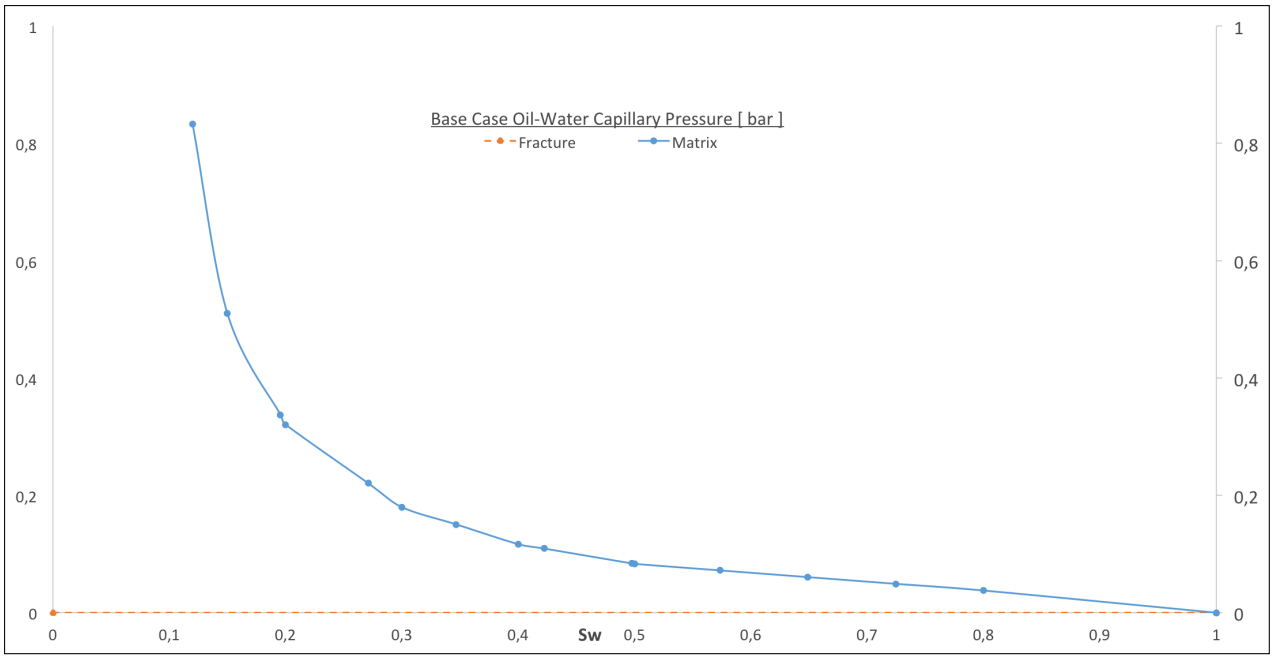

Figure 4.7: Base Case matrix oil-gas capillary pressure vs water saturation.

capillary pressure curves were used in the simulations. The curves are adapted from Kossack et al. (2006) who simulate vuggy carbonate matrix properties using capillary pressure curves generated from a numerical procedure that is built on input of the vug fraction, distribution, and the approximate ratio of viscous and gravity forces. Results from the very fine grid grid single porosity simulations are then matched to fit a dual porosity model. The curves adapted from Kossack et al. (2006) are shown in **Figure 4.8**, these have maximum values of 0.119 (P_{cog} = 'Normal') and 0.689 (P_{cog} = 'High') bar and zero capillary threshold pressure. In addition, two curves *with* threshold pressure is simulated (**Figure 4.9**). These curves have the same maximum values as the original, and threshold pressure of 0.034 (P_{TH} = 'Normal') and 0.07 (P_{TH} = 'High'), corresponding to P_{cog} = 'Normal' and P_{cog} = 'High', respectively. Kossack et al. (2006) argued that an entry pressure of 0.14 bar is unlikely high in the real world, which is why lower values have been chosen for this thesis. The cases with zero threshold pressure simulate reservoirs with large vugs that are instantly filled with injected gas, which has also been reported by Sylta (2010).

4.2 Water Injection System

One challenge in the Alta East reservoir is to place the wells strategically with respect to the sealing Falk shale (region 9, Figure **??**). To account for this layer, empty grid blocks are included in both the matrix and fracture volumes. Several well patterns were tested for the water injection system, and the run that showed highest oil recovery were used for further simulations. The resulting system has a water injector in the aquifer, lateraly close to where the producer is placed in the gas injection cases, and a producer in the 'Ørn reef' region to the west. The injector well head is in grid i, j = 24, 5 and trajectory in i, j, k = 24-23, 5-15,

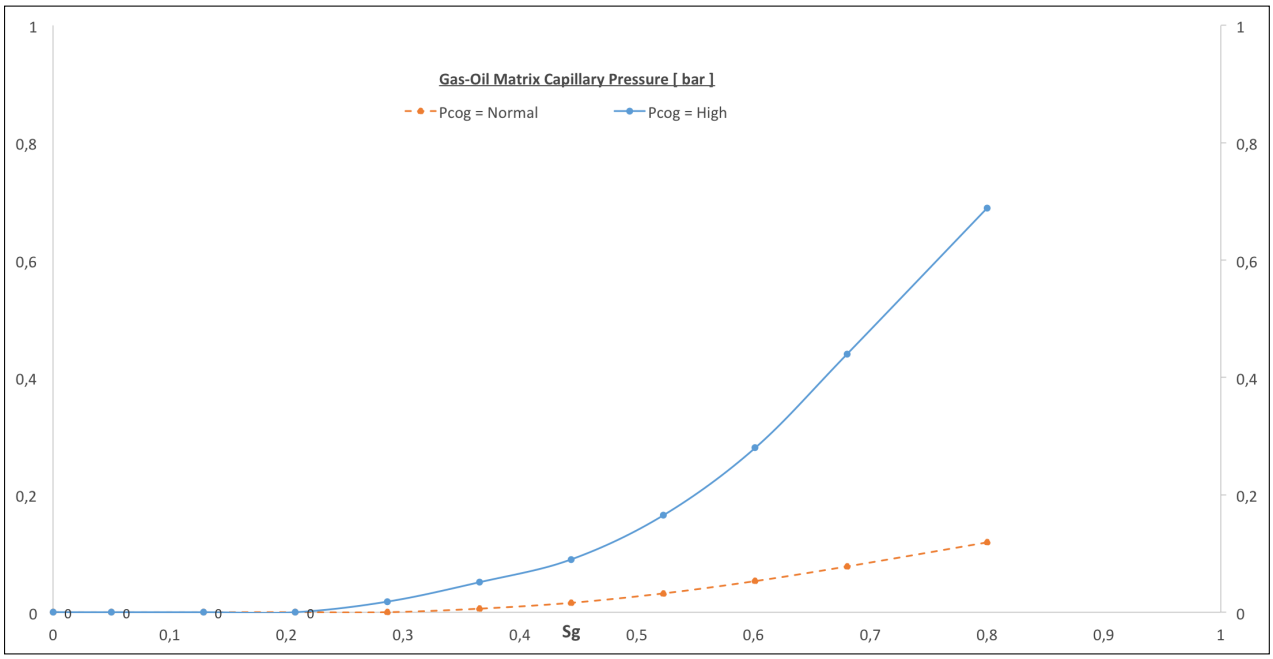

Figure 4.8: Matrix rock capillary pressure curves adapted from Kossack et al. (2006), P_{cog} = 'Normal' have a maximum pressure of 0.119 bars, and P_{cog} = 'High' of 0.689.

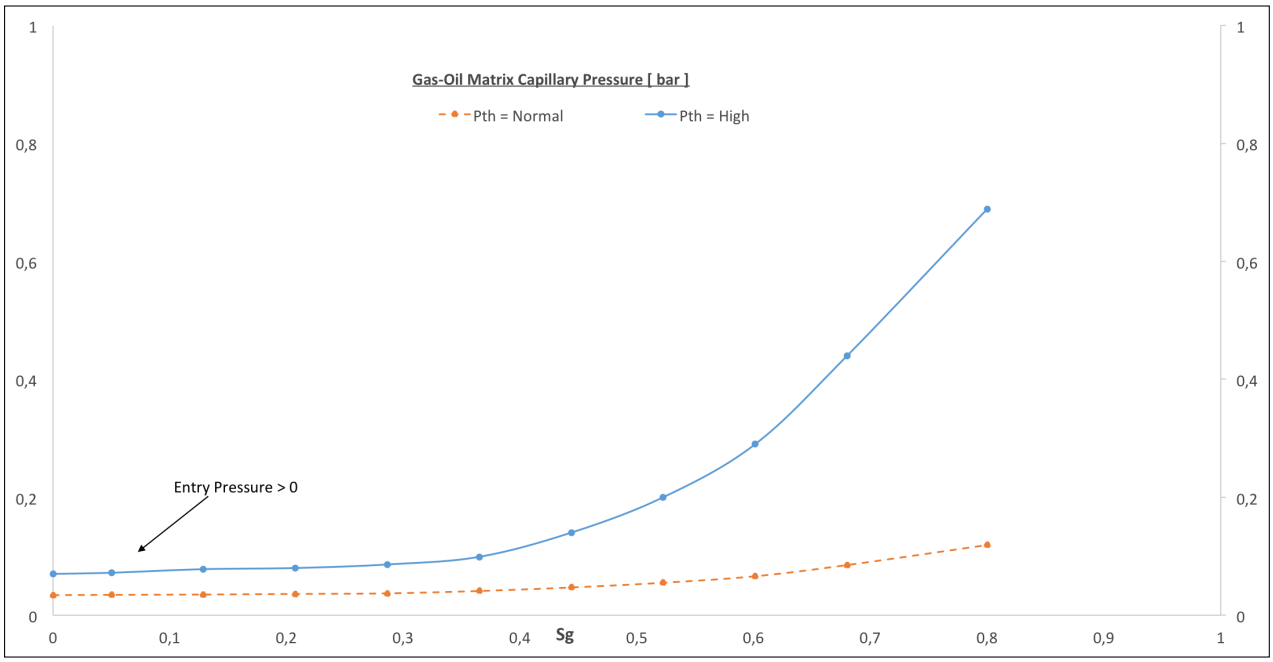

Figure 4.9: Matrix rock capillary pressure curves with $P_{TH} > 0$. P_{cog} = 'Normal' have an entry pressure of 0.034 bars, and P_{TH} = 'High' of 0.07.

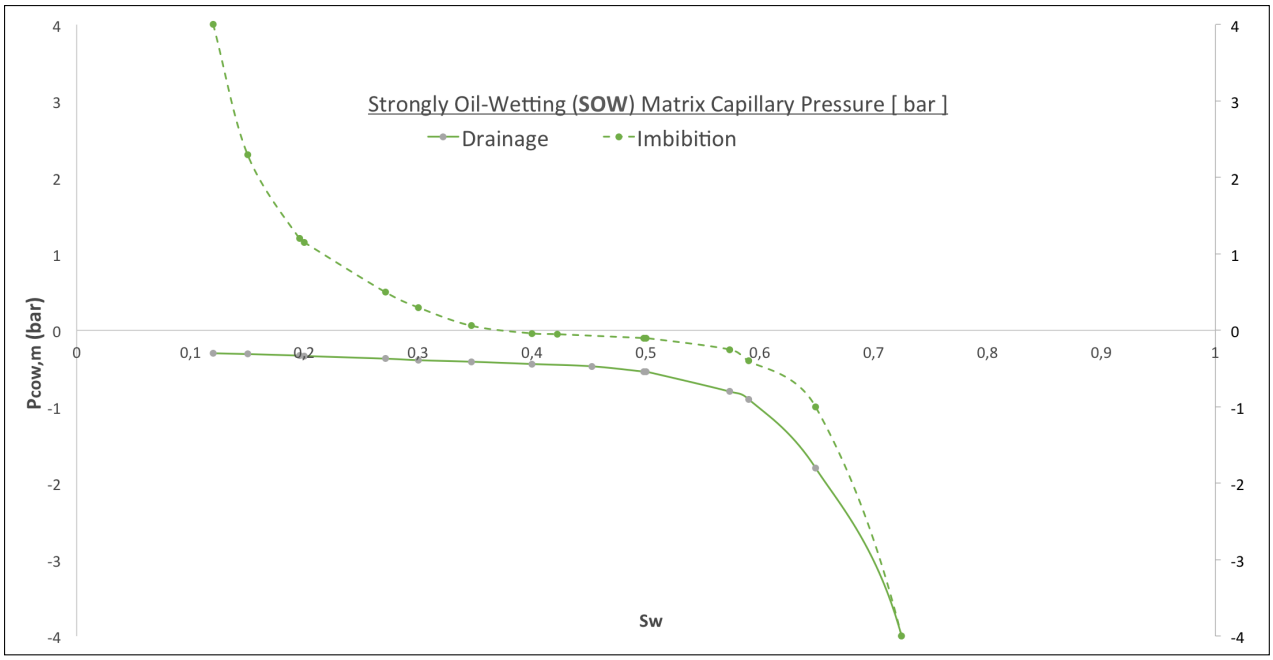

Figure 4.10: Strongly oil-wet matrix capillary pressure (SOW) for the oil-water system.

177. The producer trajectory is i, j, k = 13-16, 13-6, 133 with well head in i, j = 13, 13.

Matrix wettability is one of the main parameters for successful water flooding. Wetting preferences are modeled with capillary pressure tables and ECLIPSE's hysteresis option (note that matrix relative permeability is always equal to the Base Case showed in Figure 4.5). Four different capillary curves are implemented to analyze the effect of wetting: 'Strongly Oil-Wet' / SOW (**Figure 4.10**), 'Oil-Wet' / OW (**Figure 4.11**), 'Mixed Wet' / MW (**Figure 4.12**) and 'Strongly Water-Wet' / SWW (**Figure 4.13**). The physical principles controlling wettability measurements by capillary pressure are explained in Section 2.1.2. For oil-wet matrices, recovery is ultimately controlled by the drainage curve (solid line) and for water-wet, both forced and spontaneous imbibition (dotted line) describe the recovery behavior. More neutral wetting is indicated by a reduced transition zone and area under drainage capillary pressure. A less oil-wet rock is also indicated by a higher non-wetting residual saturation (S_w at imbibition-curve = 0), while a less water-wet rock shows the opposite trend compared to strong water-wet (reduced S_w at drainage-P_{cow} = 0). This is because less work is necessary for displacement during imbibition as the preference of the rock surface for the wetting phase decreases.

4.3 WAG System

A simplified water-alternating-gas (WAG) scheme is simulated with the given water-oil capillary pressures (Figures 4.10 through 4.13). WAG is implemented with cycles of 60 days the first two years of production (until November 2025), starting with water, then 6 months in which the first period also is water injection. The same, conventional hysteresis is modeled for the WAG scheme as the two-phase water injector cases. The work on WAG is conducted

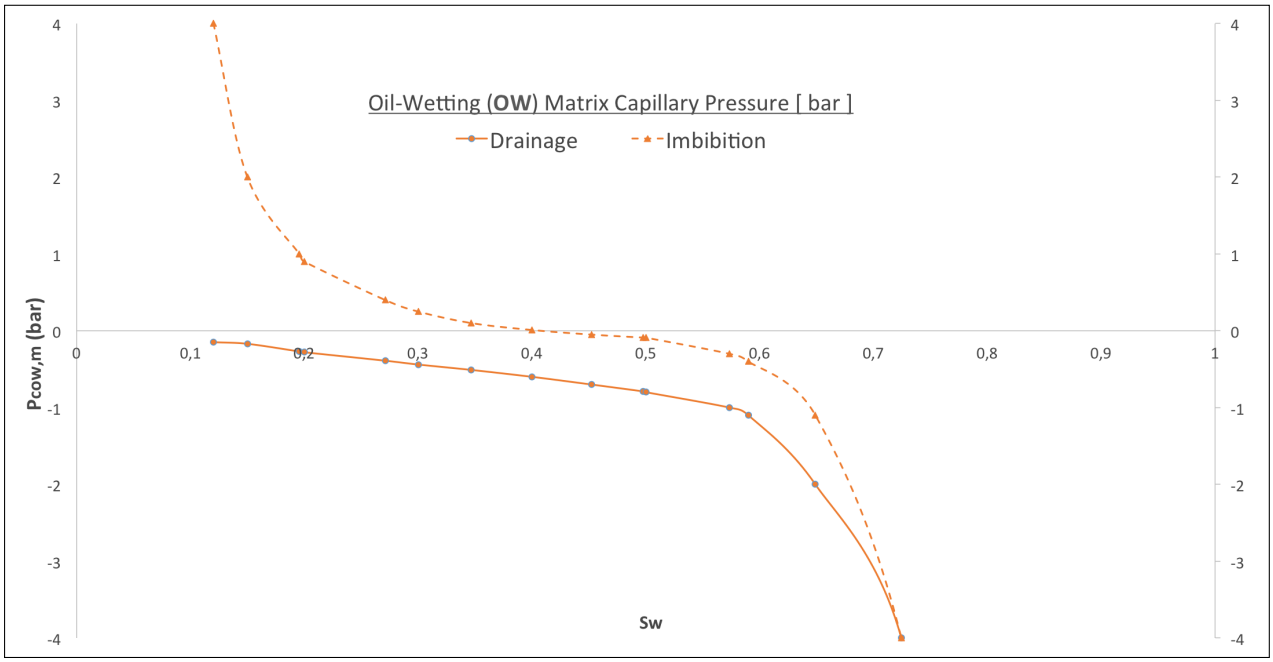

Figure 4.11: Oil-wet matrix capillary pressure (OW). S_w as the imbibition-curve reaches zero is slightly higher than in the SOW-case and area under the drainage curve is smaller.

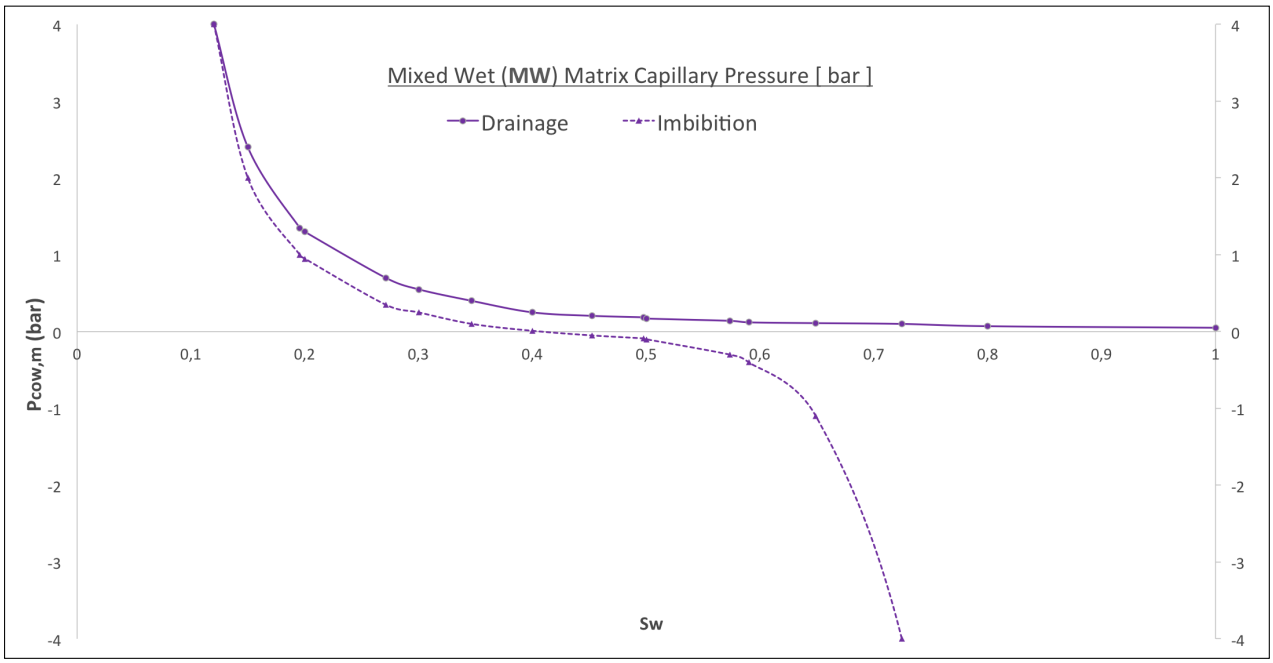

Figure 4.12: Mixed wetting matrix capillary pressure (MW). The recovery-controlling curve (imbibition) is positive, allowing spontaneous imbibition until water saturation is about 40 %. Additional water can be forced into the matrix, but this requires more work.

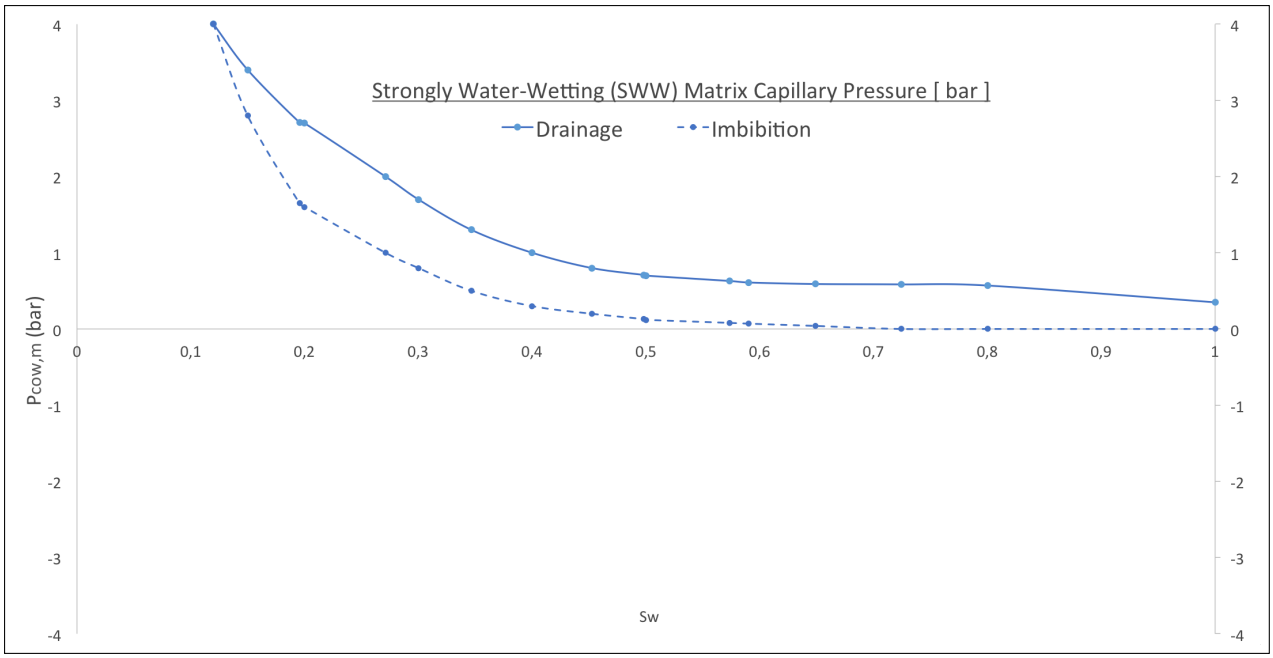

Figure 4.13: Strongly water-wet matrix capillary pressure (SWW). A great deal of water imbibes back spontaneously and the residual oil saturation is approached at zero capillary pressure.

for comparative purposes, and future work on a WAG injection concept should include three phase hysteresis and further consideration of cycle lengths, rates etc.

Water and gas are injected through the same well as the water injector in Section 4.2, i.e. in the aquifer. Same perforations as the water injector case are also applied for the producer well.

4.4 Simulation Overview

Studies have been performed on fractured reservoir recovery mechanism in combination with two secondary recovery methods: Gas and water injection. The gas cases look mainly into gas-oil gravity drainage with respect to matrix capillary pressure, size/shape and height of matrix blocks, and capillary continuity. The water cases have a mix of spontaneous imbibition and gravity drainage, and effects of matrix wettability as well as matrix block height, size/ shape, and capillary continuity are analyzed. Short description of all test runs are given in **Table 4.5** and **4.6**.

Table 4.5: Description of test runs with gas injector (G-)

Case	Models	Short description
1A	dporo	no P_{cog}, no gravity drainage / imbibition, $\sigma = 1$
1AA	dporo	no P_{cog}, GRAVDR w/ DZMTRXV = 0.01 m, $\sigma = 1$
1B	dporo	no P_{cog}, GRAVDR w/ DZMTRXV = 1 m, $\sigma = 1$
1C	dporo	no P_{cog}, GRAVDR w/ DZMTRXV = 5 m, $\sigma = 1$
1D	dporo	no P_{cog}, GRAVDR w/ DZMTRXV = 10 m, $\sigma = 1$
2A	dperm	no P_{cog}, no gravity drainage / imbibition
2B	dperm	no P_{cog}, GRAVDR w/ DZMTRXV = 1 m
2D	dperm	no P_{cog}, GRAVDR w/ DZMTRXV = 10 m
3A	dporo	$P_{TH} = 0$, P_{cog} = 'Normal', DZMTRXV = 1 m
3B	dporo	$P_{TH} = 0$, P_{cog}= 'Normal', DZMTRXV = 5 m
3C	dporo	$P_{TH} = 0$, P_{cog} = 'High', DZMTRXV = 1 m
3D	dporo	$P_{TH} = 0$, P_{cog}= 'High', DZMTRXV = 5 m
4A	dporo	P_{TH} & P_{cog} = 'Normal', DZMTRXV = 1 m
4B	dporo	P_{TH} & P_{cog} = 'Normal', DZMTRXV = 5 m
4C	dporo	P_{TH} & P_{cog} = 'High', DZMTRXV = 1 m
4D	dporo	P_{TH} & P_{cog}= 'High', DZMTRXV = 5 m
5A	dperm	$P_{TH} = 0$, & P_{cog}=N) 10 % matrix contact
5B	dperm	P_{TH}=0 & P_{cog}=H, 10 % matrix contact
5C	dperm	P_{TH}=N & P_{cog} = N, 10 % matrix contact
5D	dperm	P_{TH}=H & P_{cog} = H, 10 % matrix contact
6A	dperm	P_{TH} & P_{cog}, 5 % matrix contact
6B	dperm	P_{TH} & P_{cog}, 10 % matrix contact
6C	dperm	P_{TH} & P_{cog}, 25 % matrix contact
6C	dperm	P_{TH} & P_{cog}, 45 % matrix contact
7A	dporo	$\sigma = 0.1$, DZ = 1 m
7B	dporo	$\sigma = 0.1$, DZ = 5 m
7C	dporo	$\sigma = 0.0001$, DZ = 1 m
7D	dporo	$\sigma = 0.0001$, DZ = 5 m

dporo	*= dual porosity*
dperm	*= dual permeability*
P_{cog}	*= matrix capillary pressure*
$_{o,g,w}$	*= subscript for oil, gas, water*
P_{TH}	*= matrix capillary entry pressure, oil-gas system*
σ	*= Kazemi's shape factor for transmissibility calculations*

Table 4.6: Description of test runs with water injector (W-)

Case	Models	Short description
1A	dporo	Base Case P_{cow}, no gravity drainage / imbibition, $\sigma = 1$
1B	dporo	Base Case P_{cow}, GRAVDR w/ DZMTRXV = 1 m, $\sigma = 1$
1C	dporo	Base Case P_{cow}, GRAVDR w/ DZMTRXV = 5 m, $\sigma = 1$
1D	dporo	Base Case P_{cow}, GRAVDR w/ DZMTRXV = 10 m, $\sigma = 1$
2A	dperm	Base Case P_{cow}, GRAVDR w/ DZMTRXV = 1 m
2B	dperm	Base Case P_{cow}, GRAVDR w/ DZMTRXV = 5 m
3A	dporo	P_{cow} = SOW, GRAVDR w/ DZMTRXV = 1 m
3AA	dporo	P_{cow} = SOW, GRAVDR w/ DZMTRXV = 5 m
3B	dporo	P_{cow} = OW, GRAVDR w/ DZMTRXV = 1 m
3BB	dporo	P_{cow} = OW, GRAVDR w/ DZMTRXV = 5 m
3C	dporo	P_{cow} = MW, GRAVDR w/ DZMTRXV = 1 m
3CC	dporo	P_{cow} = MW, GRAVDR w/ DZMTRXV = 5 m
3D	dporo	P_{cow} = SWW, GRAVDR w/ DZMTRXV = 1 m
3DD	dporo	P_{cow} = SWW, GRAVDR w/ DZMTRXV = 5 m
4A	dporo	$\sigma = 0.1$, DZ = 1 m
4B	dporo	$\sigma = 0.1$, DZ = 1 m
4C	dporo	$\sigma = 0.1$, DZ = 1 m
4D	dporo	$\sigma = 0.1$, DZ = 1 m

SOW	= *Strongly Oil-Wet*
OW	= *Oil-Wet*
MW	= *Mixed Wet*
SWW	= *Strongly Water-Wet*

Chapter 5

Results & Prelimenary Discussion

In this chapter results from the simulations are presented, and a short discussion concerning the oil recovery process is given for all cases. A summary and overall discussion is given in Chapter 6, in which implications on production and field development also are reviewed.

Due to a lack of liquid constraints on the producer well, an overall observation with all the cases in this thesis, is that the oil rate typically declines more gradually when gas is the injected fluid, versus when water is used. This is because the upper gas constraint (0.825 MSm^3) limits the fluid production of the well, but water production is not limited until the water-cut exceeds 95%, at which point the well is shut in. Oil rate and water-cut versus time for one gas and one water injection case is included in **Figure 5.1** for the reader to better understand overall production pattern in the following cases. In the presentation of produced water and gas, some cases are excluded from the figures below. These include cases where DZMTRX ≤ 0.1 m as it is assumed these are not representable of any actual reservoir. For oil recovery these cases are included to gain a better understanding of the prevailing process(es).

5.1 Produced Water & Gas

In **Figure 5.2** and **5.3** gas production rates for the cases with a gas injector and with a water injector respectively, are presented. For the water injection case, the rise in gas rate corresponds to a high water cut in the producer, ultimately shutting in the well. For the gas injection cases, which generally have less water production, oil rate is limited by the gas rate constraint (825 000 Sm^3/day) but the well is not shut in until minimum oil rate is reached (10 Sm^3/day), indicated by the drop in gas rate in Figure 5.2. Figure 5.2 illustrates the range of gas-breakthrough dates. With mentioned cases excluded, gas breakthrough varies from four to nine years (end 2027 to end 2032) after production is commenced. The cases that have a low SIGMA value or high P_{cog} have an earlier gas breakthrough than cases with zero P_{cog} and/ or a large degree of capillary continuity, which correspond to amount of oil produced as injection is controlled by the production voidage rate equal to one (volume in = volume out).

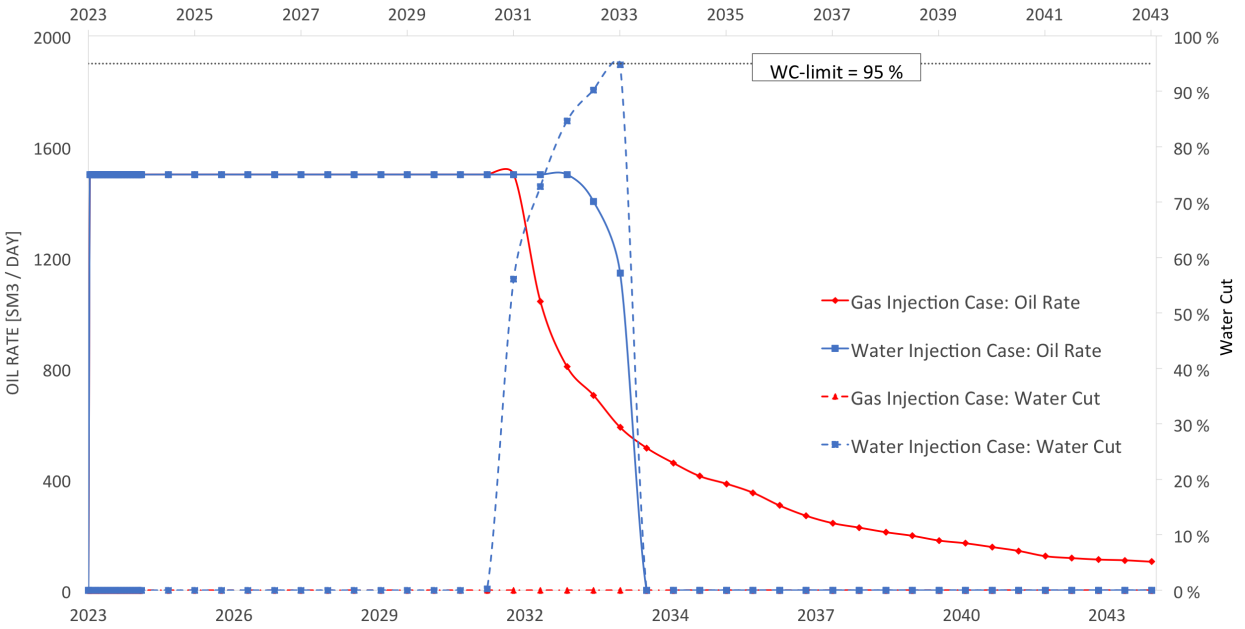

Figure 5.1: Oil rate and water cut (WC) vs time illustrates the typical decline after plateau for water compared to gas injection cases.

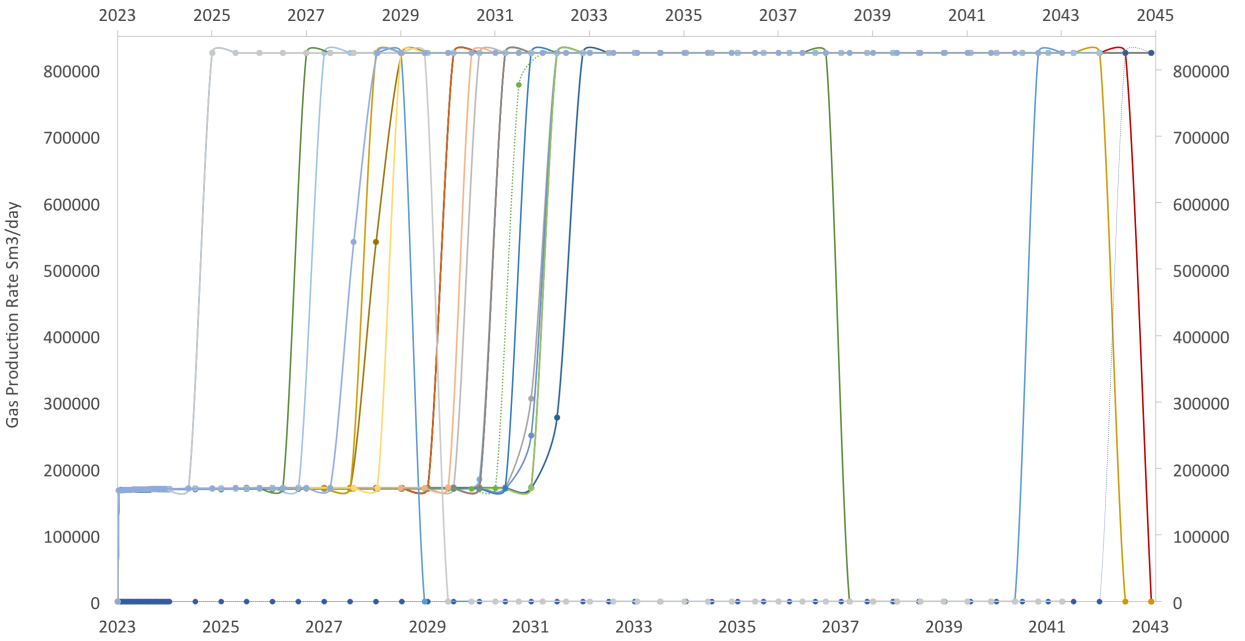

Figure 5.2: Produced gas rate for all gas injection cases, the well has a maximum gas rate limit of 825 000 Sm^3/day. The figure is included to show a general trend, and more details on gas production is included as the individual runs are discussed. Generally, the cases that have a low SIGMA value or high P_{cog} have an earlier gas breakthrough than cases with zero P_{cog} and/ or a large degree of capillary continuity.

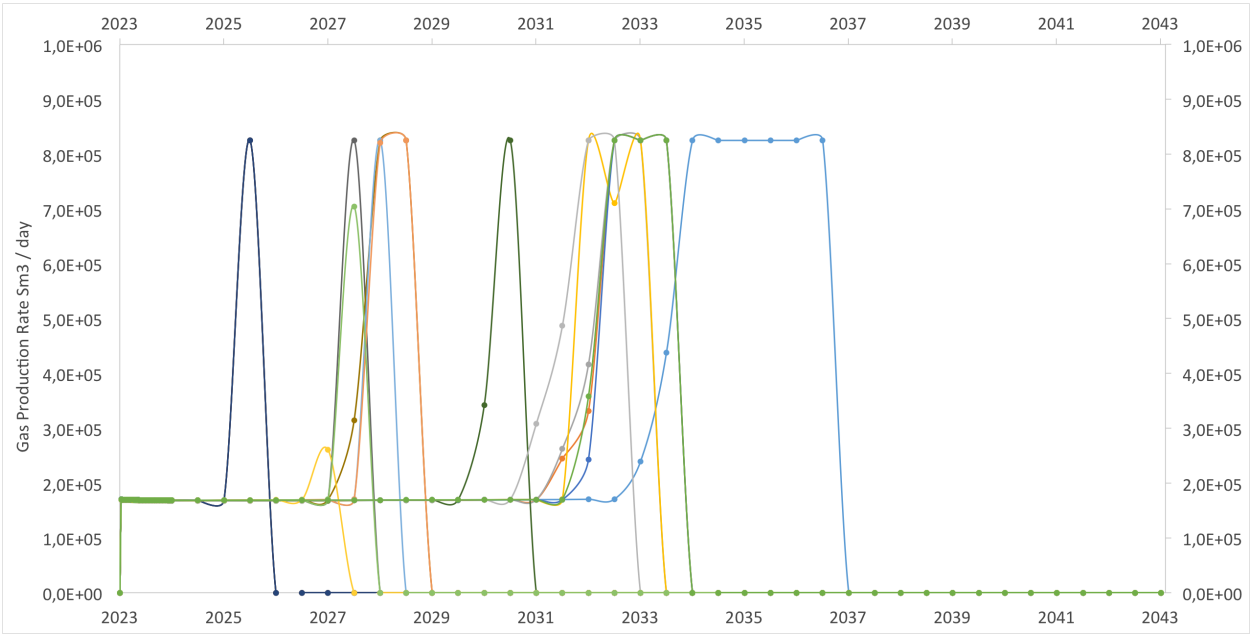

Figure 5.3: Produced gas rate for all water injection cases, the well has a maximum gas rate limit of 825 000 Sm^3/day. The figure is included to show a general trend, and more details on gas production is included as the individual runs are discussed. For the water injection cases, gas breakthrough mostly correlates with water breakthrough and the well is shut-in at 95% water cut.

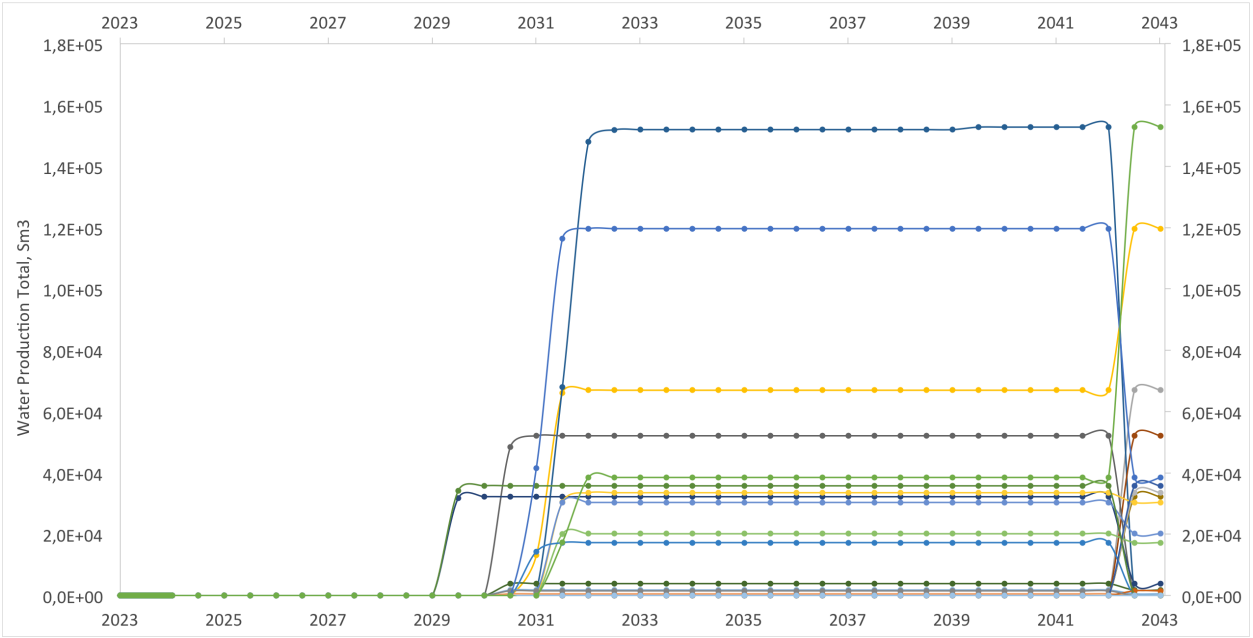

Figure 5.4: Total water production for all gas injection cases, notice that the vertical axis is different than for the water injection cases, here maximum produced water volume is lower, and close to 0.15 MSm^3.

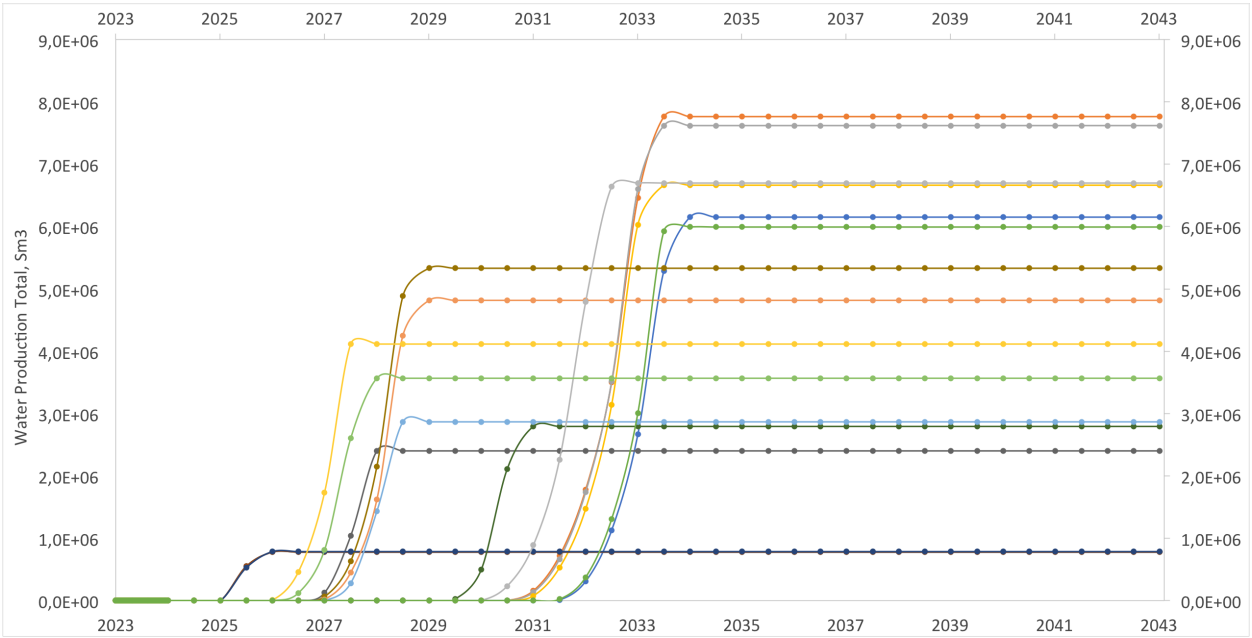

Figure 5.5: Total water production for all water injection cases, notice that the vertical axis is different than for the gas injection cases, here maximum produced water volume is close to 9 MSm^3.

In **Figure** 5.4 and 5.5 total water production for the cases with a gas injector and with a water injector respectively, are presented. Naturally, the water production is higher when water is injected than gas. In the gas injection case water cut does not exceed 40%, with maximum rates of 900 Sm^3/day and total produced water volumes ranging from zero to 150 000 Sm^3. For the water injection cases, the volumes produced are large (from 0.8 to 7.6 M Sm^3) and the time of water breakthrough is more sensitive to reservoir parameters. Production rates differ from 9000 to 21 000 Sm^3/day and more than 80 % of the presented water injection cases are shut in due to 95 % water cut. Time of water breakthrough ranges from 3.5 to 9 years after production is commenced. The earliest cases are seen with capillary hysteresis and low sigma, and the latest with Base Case capillary pressure and small matrix height. Injection volume is controlled by same parameter as for gas injection, and for most water injection cases produced water correlates to injected volume.

5.2 Oil Recovery by Gas Injection

5.2.1 Vertical Matrix Block Size

Cases 1A - 1D are modeled as discontinuous blocks with the dual porosity model and assume zero gas-oil matrix capillary pressure, P_{cog}. Oil recovery factor (RF) for five different values of DZMTRXV vs time is plotted in **Figure** 5.6; 0, 0.01, 1, 5 and 10 m. With DZMTRXV = 0, almost all oil produced is from the fractures (97%), with only 3% of the total oil corresponding to drained matrix volume (this has been measured from current oil in place in the respective FIPNUM regions). 73% of the original oil in the fractures is produced

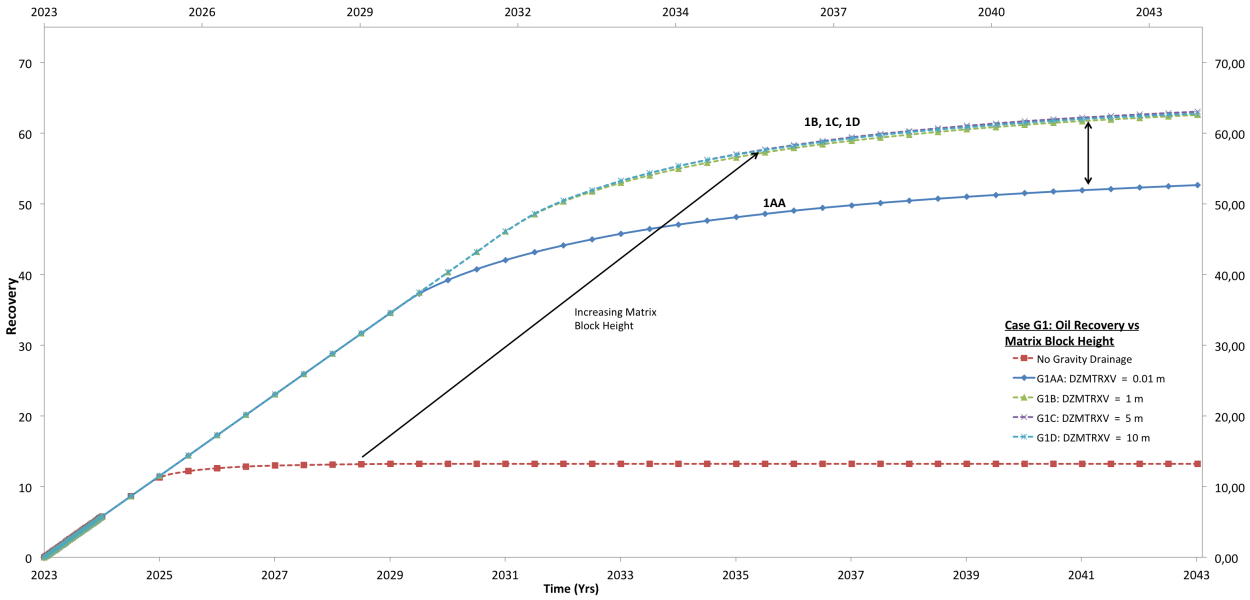

Figure 5.6: Case 1: Effect of gravity drainage strength / vertical matrix block size on oil recovery factor. DZMTRXV = 0, 0.01, 1, 5 & 10 m. Maximum recovery from gas-gravity drainage is achieved with 0.01 m blocks and additional recovery is due to coning of the natural aquifer.

(RF_f) with this case. With a vertical matrix size of 0.01 m, total recovery increases to 53 %, corresponding to an oil recovery factor in the matrix, RF_{ma} of 48%. Case B, C and D have approximate total recoveries of 63% and RF_{ma} equal to 60%. All cases maintain plateau production until maximum gas rates are reached, which is after nine years for all cases where gas gravity drainage is modeled, and two years when it is not.

DZMTRXV = 0 corresponds to a theoretical system with no gravitational pressure. For a gas - oil system, oil is the wetting phase, meaning that no gas enters the matrix due to capillary imbibition. Thus the matrix oil produced in Case 1A corresponds to fluid expansion/ pressure equilibration alone. As the fractures are highly permeable, in the range of 10 Darcy, very little drawdown (less than 1 bar) is necessary for oil to start flowing towards the well and matrix pressure will then equilibrate with the pressure in the drained fractures. For zero matrix capillary pressure, even 0.01 m matrix height (DZMTRXV) is sufficient to yield ultimate recovery from gas-oil gravity drainage, and additional recovery when DZMTRXV is increased is a result of an accelerating water-front. It should be mentioned that discontinuous matrix blocks with 0.01 m vertical height is also used for illustrative purposes and is unlikely in an actual fractured reservoir.

The maximum theoretical recovery factors from the matrix, $(RF_{ma})_{max}$ can be approximated from S_{wi} and S_{or} corresponding to the relative permeability curves of oil-gas and oil-water systems, respectively. Recall that the Base Case relative permeability curves were given in Chapter 4, Figure 4.5 and 4.5. For an oil-gas system the oil is for practical purposes immobile at $S_g = 60\%$ ($k_{rog} = 0.017\%$), corresponding to $S_{or} = 40\%$. In an oil-water system the oil is more mobile, corresponding to an S_{or} of 28% at $k_{row} = 0.015\%$. The resulting $(RF_{ma})_{max}$ is given by Equation 5.1;

$$
\begin{aligned}
(RF)_{max} &= \frac{1 - S_{wi} - S_{or}}{1 - S_{wi}} \\
\text{For the oil-gas system: } \Rightarrow (RF_{ma})_{max} &= \frac{1 - 0.12 - 0.40}{1 - 0.12} \approx \underline{\underline{55\%}} \\
\text{For the oil-water system: } \Rightarrow (RF_{ma})_{max} &= \frac{1 - 0.12 - 0.28}{1 - 0.12} \approx \underline{\underline{70\%}}
\end{aligned}
\tag{5.1}
$$

Thus, at $(RF_{ma})_{max} \approx 55$ %, maximum recovery from gas drainage is achieved, while water imbibition represents additional potential. It should be mentioned that measured relative permeability for oil commonly is higher in a gas-oil system than a water-oil system, and in this sense the presented curves are somewhat special. The relative permeability curves given for the model has not been a focus of this thesis, and therefore further action has not been taken to investigate the applicability of these curves to the actual reservoir and they are assumed representable of the reservoir.

Figure 5.7 shows the saturation ternary diagrams of Case G1AA and Case G1B after 3 years of production (end 2026) and after 8.5 years of production (mid 2032). Matrix water saturation in the near-wellbore area (matrix cell 21-10-70) is more than 70% for the 1 m case and 22% for the 0.1 m case (lower left and right insert). For a matrix cell further away from the well in the lateral plane, 12-10-70, water saturation is still 22% at this point, and $S_w > 70\%$ occurs six cells lower in the vertical plane, 12-10-76. As DZMTRXV is increased to 5 and 10 m, the time to reach $S_{w,max}$ = 1 - $S_{or} \approx 70$ % in the matrix close to the well is further reduced to 5.5 years at DZMTRXV = 5 m and 5 years at DZMTRXV = 10 m. Maximum recovery for the oil-water system is achieved at DZMTRXV = 1 m, which is why the curves G1B, G1C and G1D overlap.

The advancing water front proportional to DZMTRXV ultimately causes an earlier water breakthrough, but for these cases the produced water rate is not significant, as the water rate does not exceed 400 Sm^3/day for any of the cases in question. However, the total amount of produced water is doubled with DZMTRXV = 10 m, compared to DZMTRXV = 5 m, suggesting that if these results represent the actual reservoir behavior, net profit is reduced by higher costs related to water handling. As mentioned, gas injection is controlled so that total reservoir volume injection rate of the well/field equals its production voidage rate. **Figure 5.8** shows that the total injected gas volumes for DZMTRXV = 1, 5 and 10 m (Case 1B, C, D) overlap, and it has already been established that the oil production rates and recovery are equal. Still, more water is produced when DZMTRXV = 5 and 10 m (**Figure 5.9**), compared to lower DZMTRXV. As the volumes are relatively small (120 000 and 65 000 Sm^3 total) it is assumed this is due to small differences in the aquifer pressure making the water expand more and flow towards the well, as DZMTRXV is increased. Unfortunately, the simulations were run without a specified output for overall/ aquifer pressure, so this were not evaluated. Depending on the aquifer volume vs the volume of the fractures, variations in the aquifer pressure could result in significant coning. The drop in hydrocarbon pore-volume

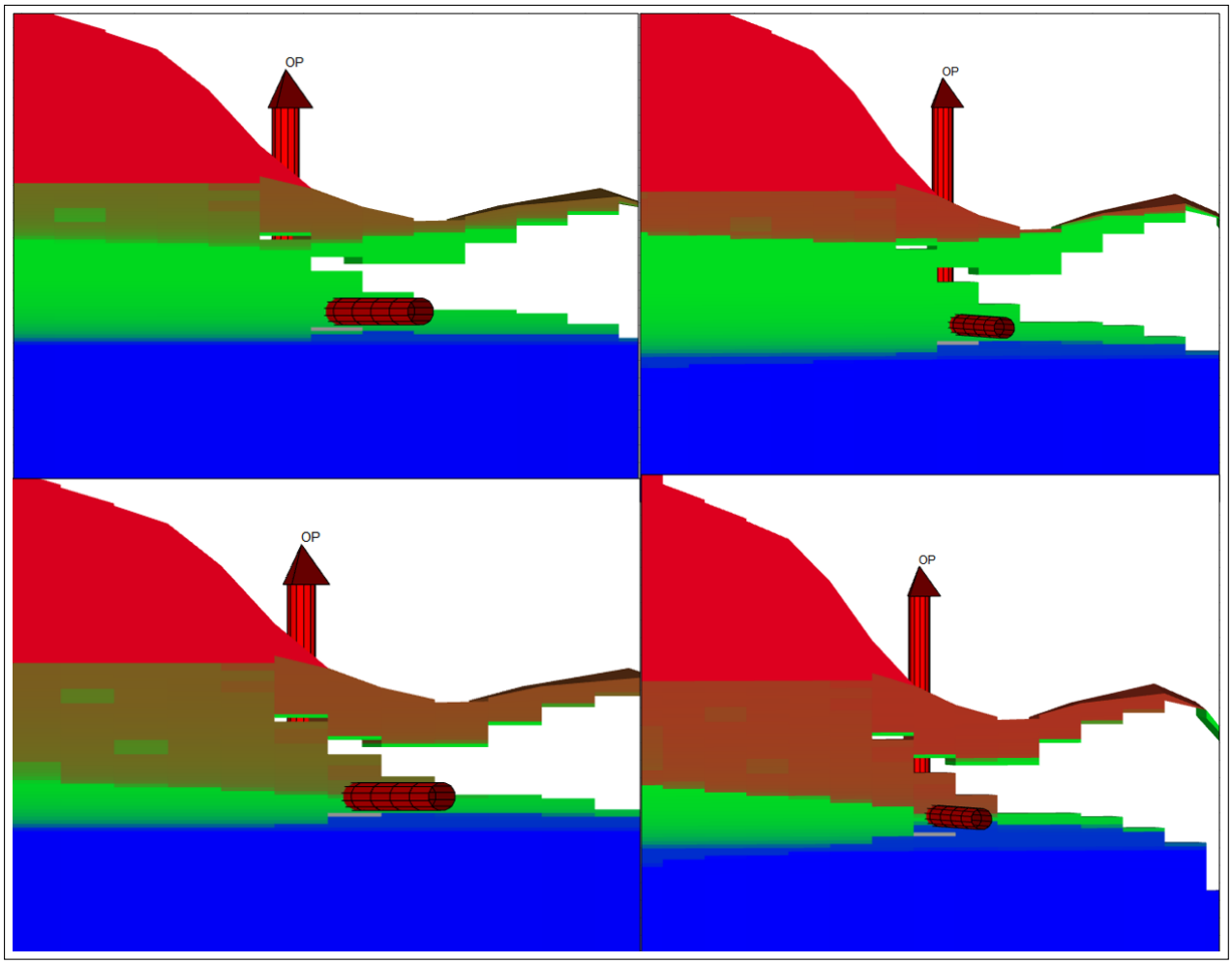

Figure 5.7: Case 1: More water production is experienced when DZMTRXV is increased, here illustrated with 0.01 vs 1 m matrix block height. Upper left: Case 1GAA (0.01 m) after 3 years of production, $S_w = 22$ %. Upper right: Case 1GB (1 m) after 3 years of production, $S_w = 22$ %. Lower left: Case 1GAA after 8.5 years of production, $S_w = 22$ %. Lower right: Case 1GB after 8.5 years of production, $S_w = 75$ %. Blue is water, green is oil, red is gas.

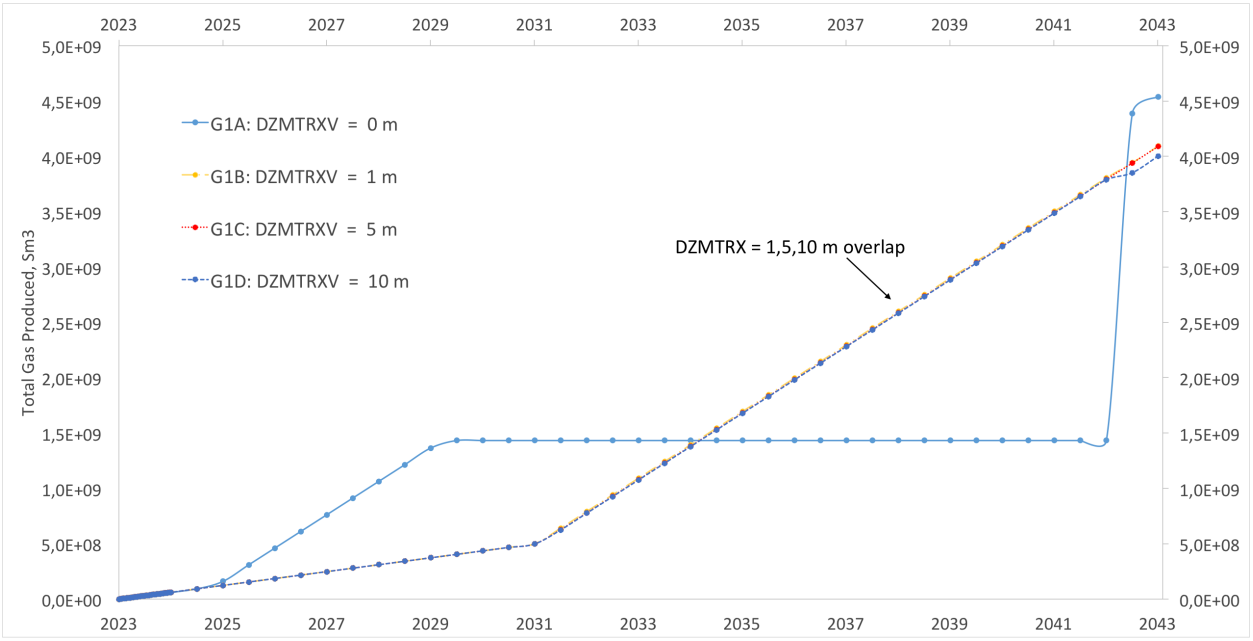

Figure 5.8: Case 1: Total gas injection volumes for Case 1A, 1B, 1C, 1D / DZMTRXV = 0,1, 5, 10 m. As injection is controlled by production volumes, the injected volumes for Case 1 B, C and D overlap.

weighted-average pressure (ECLIPSE's "FPR") is less than one bar during the course of the simulation. Small effects might also be due to computational inaccuracy, as fewer blocks occupy the vertical grid cell dimension as DZMTRXV is increased, which results in more abrupt saturation changes for the vertical coarser grid.

5.2.2 Matrix-Matrix Flow

In **Figure 5.10** the dual porosity cases from last section are compared to the same cases in dual permeability mode, where DZMTRXV equals 0, 1 and 10 m. The effect of dual permeability is clearly illustrated with DZMTRXV = 0, which indicates that the dual porosity GRAVDR option is inactive. Without gravity drainage, recovery is increased by 47 points when modeling with dual permeability, i.e. flow between matrices, vs discontinuous blocks in the dual porosity mode. Two additional comparisons show interesting results; 1) As long as GRAVDR is included, early time recovery is higher for the dual porosity cases than dual permeability, but at late time the curves meet. 2) Changing DZMTRXV from 0 to 1 gives an increased recovery also in the dual permeability mode (ΔRF = 2.5 %). All of the dual permeability cases go off plateau after nine years of production (mid 2032), due to maximum gas production rates reached.

The cases shown in Figure 5.10 model capillary continuity in two ways; Case 1 may simulate inter-block contact by assigning an effective matrix height (DZMTRXV) higher than the actual block height, meaning that parts or intervals up until 5 or 10 m of the total vertical matrix column are in contact (i.e. 'height'). With dual permeability, *all* matrix blocks making up the column have equal and full contact between them. Both methods

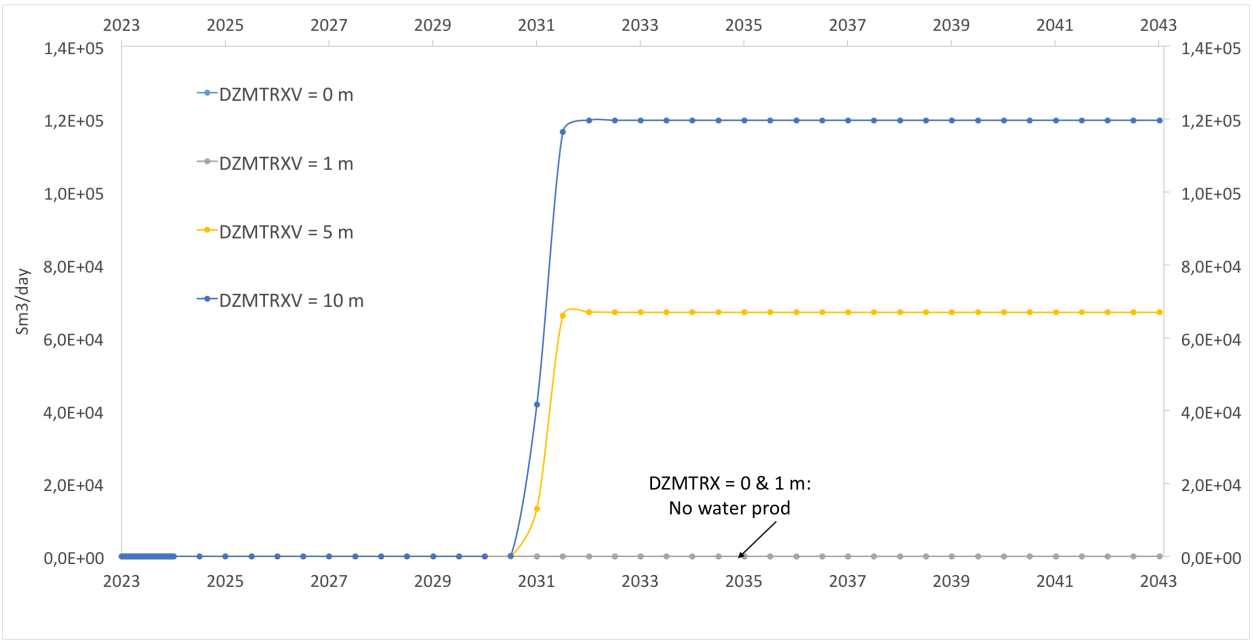

Figure 5.9: Case 1: Total water volumes produced for Case 1A, 1B, 1C, 1D / DZMTRXV = 0,1, 5, 10 m. Even though produced oil and injected gas volumes are similar, the cases with highest DZMTRXV produce some water, while the 0 and 1 m cases have zero water production.

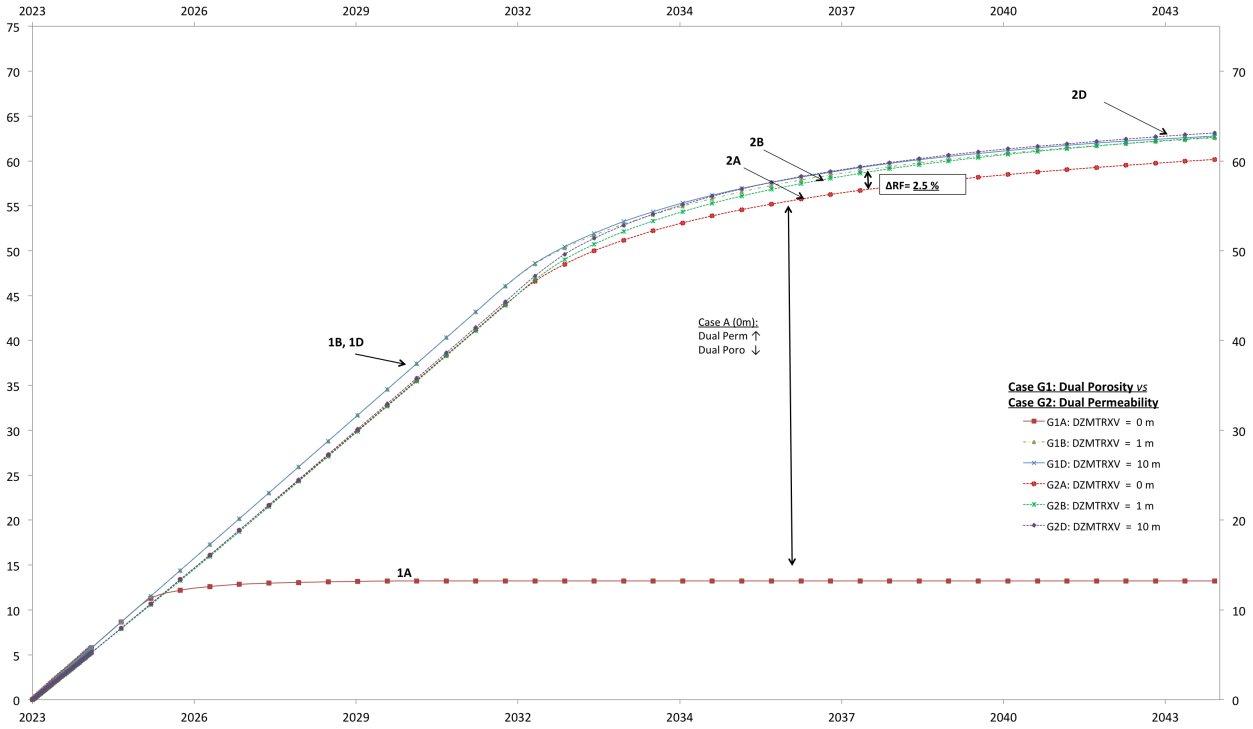

Figure 5.10: Case 2: Comparison between 100 % capillary continuity in parts of matrix block column (Case 1 - capillary continuity modeled as effective matrix height DZMTRX) vs all of the matrix block column (Case 2 - DUALPERM). Illustrated with DZMTRX = 0, 1 & 10 m.

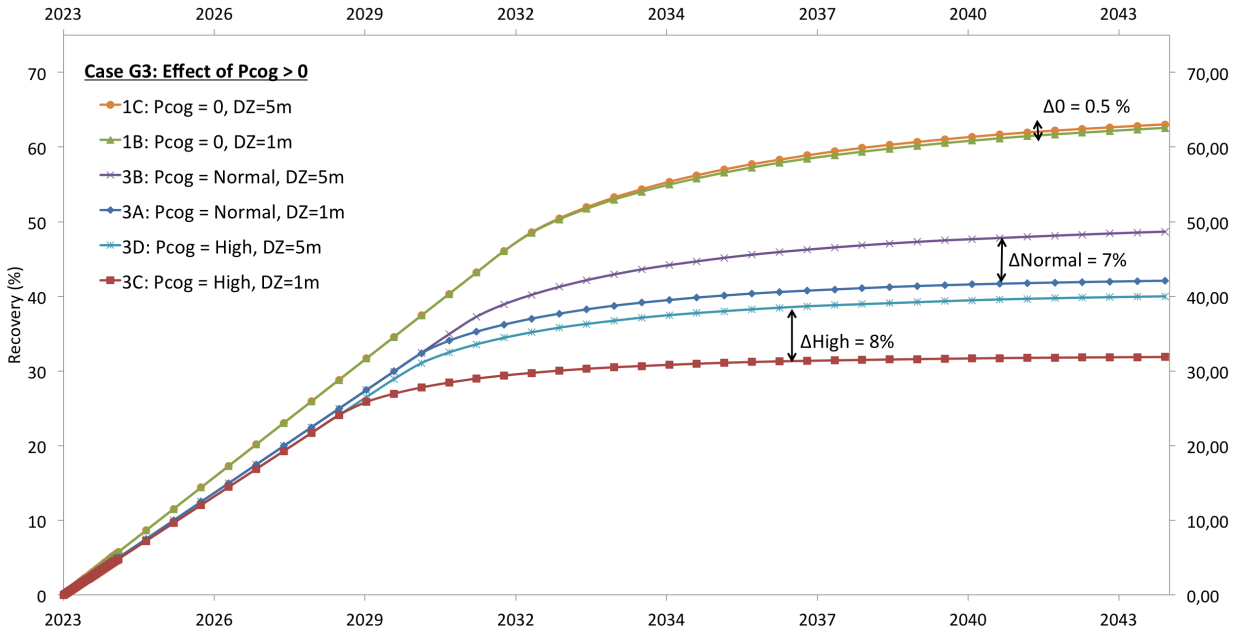

Figure 5.11: Case G3: Effect of $P_{cog} > 0$. Comparison of 1 and 5 m effective matrix height. 'Normal' P_{cog} is equivalent to a maximum gas-oil matrix capillary pressure of 0.12 bar, and 'High' to 0.69 bar. $P_{TH} = 0$, corresponding to values given by Kossack et al. (2006).

model 100% contact between blocks, if any contact. Thus, the different recovery seen in these cases at early time, is mainly a function of the *portion* of the matrix column that have 100 % capillary contact. As reimbibition is a slow process compared to matrix-fracture transfer where the oil reaches the fracture within a short distance, matrix-matrix flow has a retarding effect on recovery, which is why Case 2B (DUALPERM) has a lower recovery than Case 1B (DUALPORO) initially, while ultimate recovery is the same.

Due to capillary continuity, the water front in the connected matrices also move more gradually than it does in the dual porosity case. For the water saturation in the matrix, DZMTRXV does not have a notable effect, but within the fractures, water coning is more significant for 2B (1 m) than 2A (0 m). Ultimately this gives a higher degree of water imbibition into the matrices and an oil recovery from the matrix that is higher than in the 2A case, but also more water produced. Maximum water rates for the 0, 1 and 10 m cases are 0, 520 and 895 Sm^3/day.

5.2.3 Matrix Gas-Oil Capillary Pressure

Figure 5.11 shows recovery vs time for three different values of P_{cog}; Zero, Normal ('N') and High ('H') in addition to the effect of gravity forces through DZMTRXV = 1 and 5 m. With matrix capillary pressure, the behavior of the previously discussed runs are quite different. While an effective matrix height DZMTRXV of 1 m is sufficient to yield ultimate recovery in Case 1 ($P_{cog} = 0$), Case 3 show a significant enhancement when DZMTRXV = 5 m. Case 3 has no capillary threshold pressure, and the largest effect of DZMTRXV is observed when $P_{TH} > 0$, which is illustrated by Case 4 in **Figure 5.12**.

As the gas is non-wetting, capillary forces act in the opposite direction of gravity drainage,

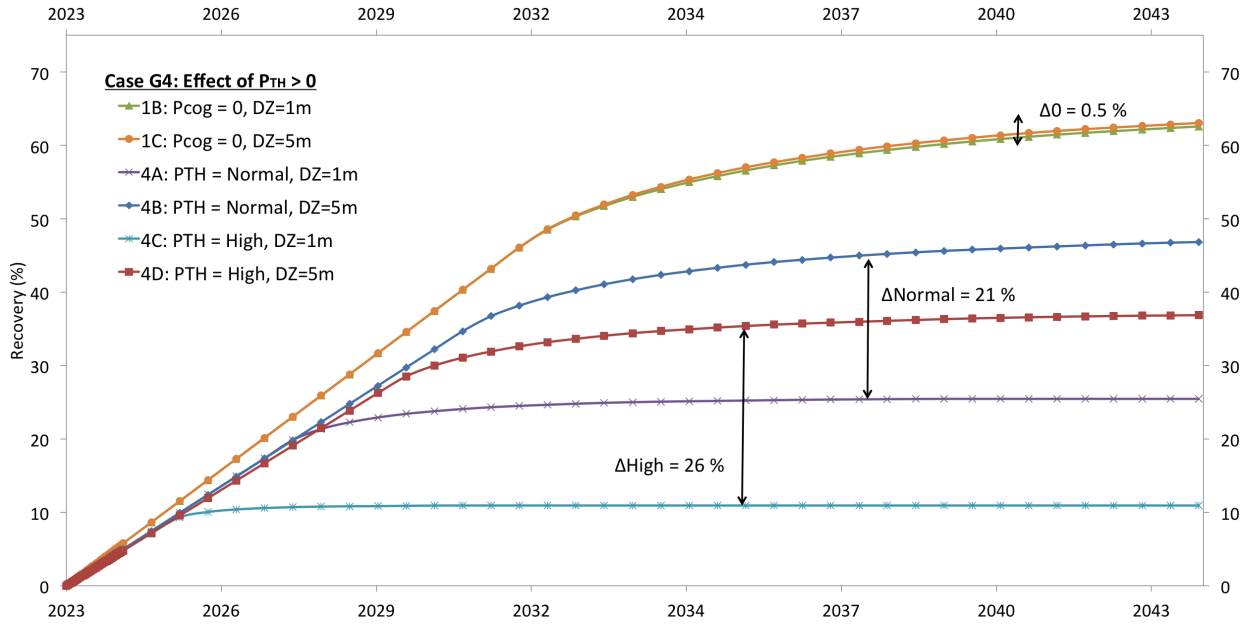

Figure 5.12: Case 4: Effect of $P_{TH} > 0$. Comparison of 1 and 5 m effective matrix height. "Normal" P_{TH} is equivalent to a threshold pressure of 0.034 bar, and "High" to 0.07 bar. Maximum P_{cog} is equal to Case 3. The difference in recovery (Δ) between 1 and 5 m is given for all cases.

and transfer from the matrix occurs only if the gravity potential exceeds the capillary threshold, and lasts until these two forces are in equilibrium. In this situation, the existence of the matrix-matrix contact is crucial to maintain capillary continuity within the matrix column. With large vugs, indicated by zero threshold pressure in the 'Normal' Case (ref. Kossack et al. (2006)), 27% of the pores will fill instantly. To recover additional oil, pressure difference of 0.0292 and 0.0887 bars are applied by the 1 and 5 m fluid columns, respectively. Maximum recovery is reached at $P_{cog,max}$ =0.12 ('N') and 0.69 ('H') bars capillary pressure, corresponding to 1.5 and 8.5 m of inter-block contact (at reservoir conditionS). Thus full recovery is achieved only in case 3B ('N') where effective matrix height = 5 $m > h_c = 1.5$ m.

Figure 5.12 show recovery for the same P_{cog} as discussed with Case 3, but now a threshold pressure > zero is added. The threshold pressure indicate a distribution of smaller pore size, and significantly reduces recovery if the amount of capillary contact in the reservoir is low, as is seen from Case 4C and 4D ('High' in Figure 5.12). As the displacement front advances, $H - Z \leq h_{TH}$, and gas-oil drainage is no longer possible. For threshold of 0.034 and 0.07 bar this corresponds to $H - Z \leq 0.4$ and 0.9 m respectively. For a higher matrix continuity, the displacement front Z can travel longer before gas drainage ceases. For Case 4A and 4B where the threshold pressure is lower, ultimate recovery is close to that of Case 3, but for threshold height of 0.9 m, it is severely reduced both for DZMTRXV = 1 and 5 m. With 1 m matrix height, no oil is recovered from the matrices, for 5 m, $RF_{ma} = 30$ %. For higher capillary or threshold pressure, less gas enters the matrix and thus the injected gas travels faster towards the producer, which ultimately shortens the length of plateau oil production.

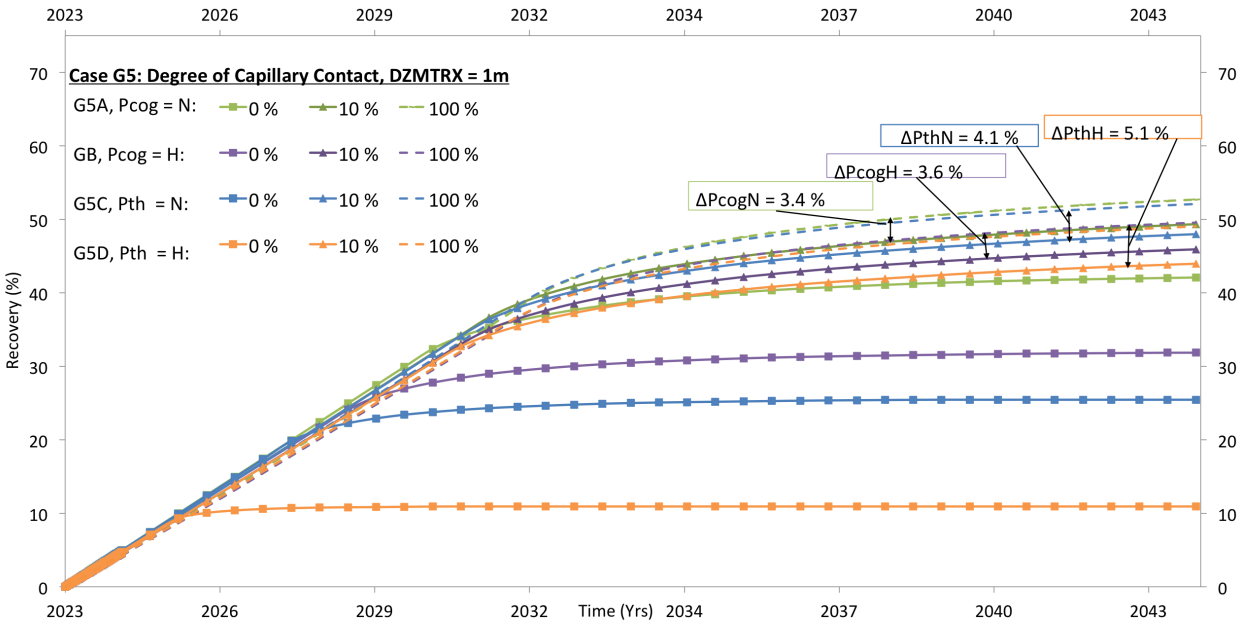

Figure 5.13: Recovery vs time for the four cases where $P_{cog} > 0$: $P_{cog}N$, $P_{cog}H$, $P_{TH}N$, and $P_{TH}H$. Comparison between completely discontinous (dual porosity), partially continous (10 % contact, dual permeability) and completely continuous (100 % contact, dual permeability). The difference in recovery (ΔP_c) between 10 and 100 % is given for all cases.

5.2.4 Degree of Capillary Contact

Figure 5.13 shows the result of Case 5 where Case 3 and 4 have been simulated with 0, 10 and 100 % contact. The runs with zero contact correspond to Case 3 and 4 with DZMTRXv = 1 m and dual porosity mode. All the examples in Case 5 are simulated with the dual permeability model and transmissibility multipliers, MULT_k (k = X, Y, Z) of 0, 0.1 and 1. The method is validated by comparing results with the dual porosity run (0 % contact), and dual permeability without MULT_k (100 %), and found consistent. In Figure 5.13 the difference between 10 and 100 % transmissibility is highlighted, showing a maximum at 5.1 % when P_{TH} = 'High'. Tabulated values show that with $\text{MULT}_k = 0.1$, ultimate recovery for all four cases are between 70-90 % of the recovery at $\text{MULT}_k = 1$ (100%).

The effects of capillary continuity between matrix blocks have been analyzed for 0 and 100 % contact area between portions of the matrix stack (DZMTRX / Case G1) as well as the full length of the matrix stack (DUALPERM / Case G2). However, if horizontal fractures exist, the contact area will neither be 0.0 nor 100 %, but more likely somewhere in between. The effect of 10 % contact is proportional to the strength of the negative matrix capillary pressure (given in Figure 4.9), and therefore higher when threshold and ultimate capillary pressure are large.

As the results of Case 5 showed that the effect of partial inter-block contact were largest for the highest capillary pressure, this case is studied further in Case 6. The results are shown in **Figure 5.14** where oil recovery vs time is plotted for 0, 5, 10, 25 and 100 % contact. Even with 5% contact, recovery is significantly higher than with completely discontinuous blocks (0 %). When the contact is at 10 %, Figure 5.13 showed that recovery was only 5 %

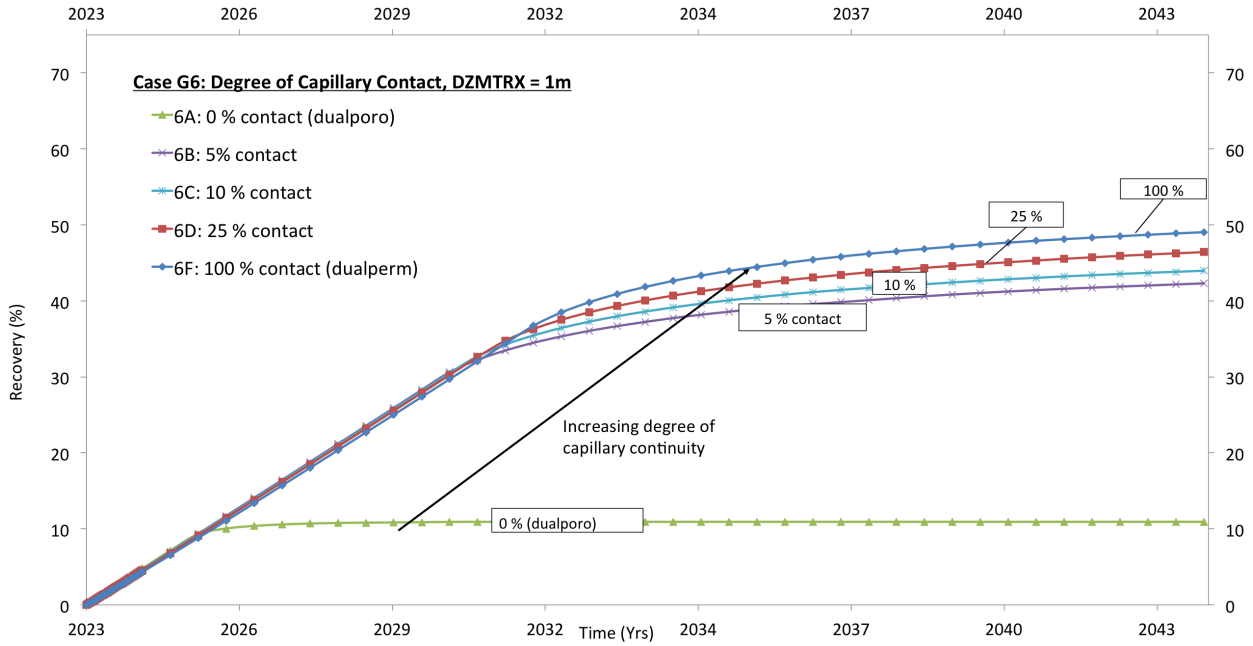

Figure 5.14: Case G6: Degree of capillary contact vs oil recovery; 0, 5, 10, 25 & 100 % contact between matrix blocks is modeled using DUALPERM mode and MULTk.

less than for 100 % contact, and with 25 % matrix-matrix contact, the difference is further reduced to 2.5 %. Recovery from the matrix , RF_{ma} range from 36% with MULT$_k$ = 0.05 and 44% with MULT$_k$ = 1.

Case 6 illustrate the effect of a "tortuous continuous matrix" (concept introduced by Festoy and van Golf-Racht (1989)). The examples show that amount of contact between matrix blocks has a significant effect on recovery as long as the contact area is small, i.e. between 0 and 25% of the matrix block surface. Even for 5 % contact area, oil recovery is closer to that of the completely continuous matrix stack than the discontinuous. At MULT$_k$ = 0.25, ultimate recovery approaches that of 100 % contact, and further enlarged inter-matrix contact has a maximum total recovery potential of 2.5 %. At MULT$_k$ > 25%, the effect of a larger contact area is for practical purposes negligible, and recovery rises with less than 1% per 10 % contact area added (verified through additional simulations of MULTk = 0.45, 0.55, 0.65, 0.75, 0.85, 0.95 that are not included in the figure).

Figure 5.13 and 5.14 illustrate the same effects of capillary continuity as described before; Matrix- to -matrix contact reduces the static capillary holdup zone that is left in discontinuous blocks. For a reservoir to have completely discontinuous matrix blocks, each matrix block need to be cut by numerous fractures for each dimension. Observations on surface outcrop suggests that even in heavily fractured formations, the matrix rock may still be connected (Festoy and van Golf-Racht, 1989). The results of Case 6 show that even 5% contact between matrix blocks yield a dramatic increase in final recovery, and is of great significance in defining a reservoirs potential as contact fractions within all fractures in an actual reservoir is practically impossible to characterize exact.

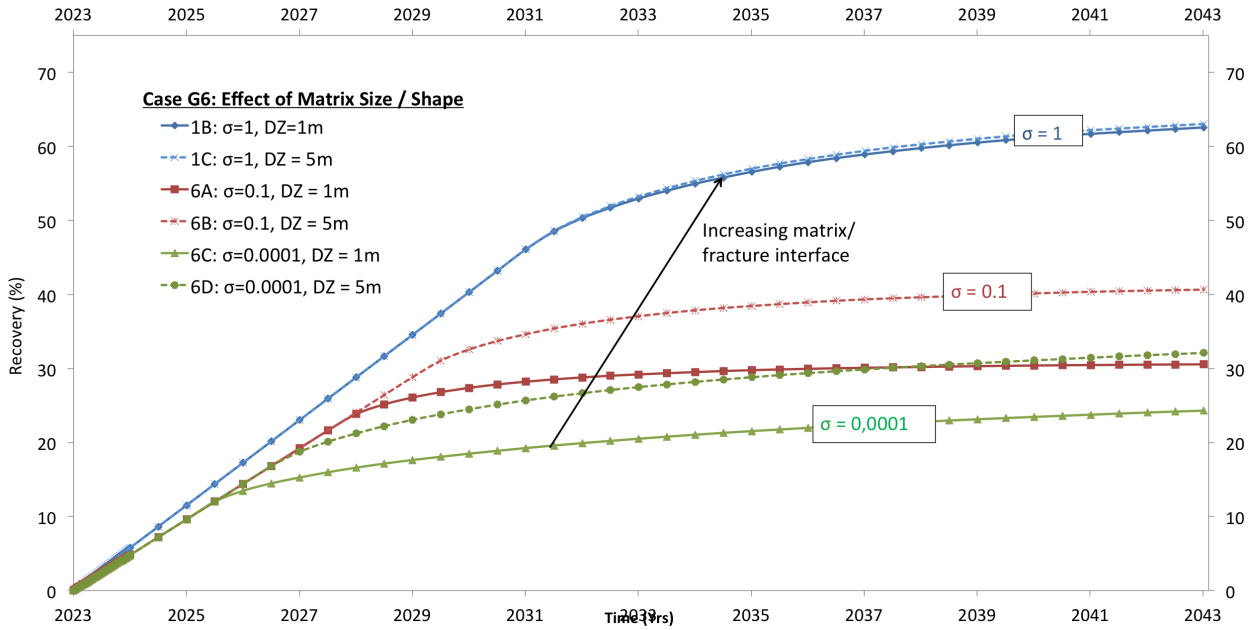

Figure 5.15: Case 7: Effect of Kazemi's shape factor SIGMA with matrix height = 1 and 5 m. The cases are simulated with SIGMA = 1 (Base Case), 0.1 and 0.0001 $1/m^2$.

5.2.5 Matrix Block Shape / Size

Figure 5.15 show the results of Case 7, where different values of SIGMA - Kazemi's shape or size factor, are tested. SIGMA is tested with Base Case fluid and rock properties (P_{cog} = 0) and DZMTRXV = 1 and 5 m. The Base Case sigma factor that has been used in all previously discussed cases is 1 m^{-2}, this factor is multiplied by 0.1 and 0.0001 in case 6A / 6B and 6C / 6D respectively. The results show that the shape factor has significant impact on recovery, as ultimate recovery is reduced by almost 40 points in the maximum (σ=1) vs minimum (σ=0.0001) cases.

The sigma factor is an important parameter in the transmissibility calculations determining matrix-fracture flow. However, as it's physical meaning still is debated, the factor is better applied as a tuning factor for history matching than as an actual representation of the matrix' dimensions. An important result is the dependency on DZMTRX, implying that for a large σ the effect of matrix block height is negligible, but for a smaller sigma factor, correct matrix height is essential to estimate final recovery. Reducing sigma reduces the total transfer rate due to gravity drainage, F_g, proportionally (ref. Equation 3.6), so that the oil recovery from matrix is retarded. This causes a retardation of gas flow from the fracture to matrix, thus more gas flows directly to the well.

5.3 Oil Recovery by Water Injection

5.3.1 Vertical Matrix Block Size

Figure 5.16 shows the recovery for DZMTRXV = 0, 0.1, 1 and 10 m with P_{cow} as described for the Base Case (water-wetting). Compared to the gas-oil system, the recovery behavior

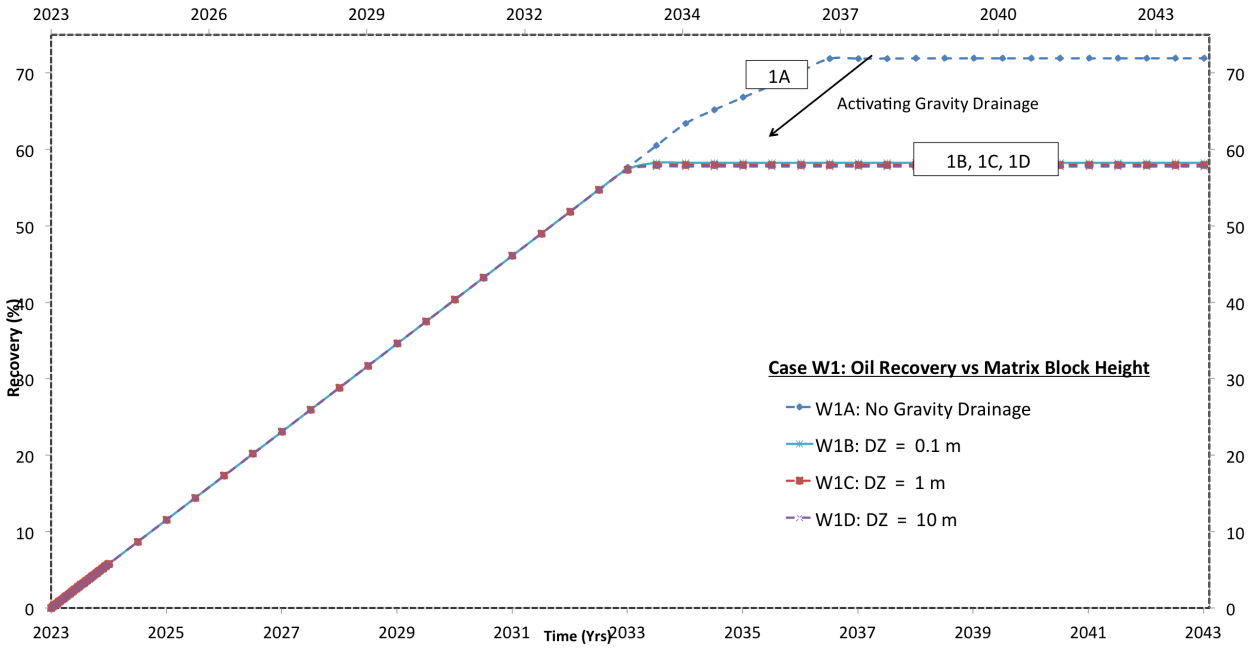

Figure 5.16: Case W1: Oil recovery vs time for DZMTRXV = 0, 0.1, 1 and 10 m with P_{cow} as described for the Base Case (water-wetting).

is different, in particular the recovery at DZMTRXV = 0. For DZMTRXV = 0, indicating no gravity drainage acting on the matrix block, recovery is higher than in case B, C, D where DZMTRXV > 0. Changes in recovery when GRAVDR is activated and DZMTRXV is between 0.1 and 10 m is negligible, and ultimate recovery is close to 58%, 14% lower than the no gravity drainage case. Matrix recoveries RF_{ma} are 73% for DZMTRXV = 0 and close to 55% for the other cases.

Maximum recovery in the oil water system was shown with Equation 5.1 and is approximately 70%, which is consistent with RF_{ma} for case W1A. As the capillary curve is always above zero, full imbibition potential is obtained with the water injection cases, only limited by flow properties (k_{ro}). This means that recovery by spontaneous water imbibition is reduced as the GRAVDR option is introduced in cases B through D.

The strength of the gravity imbibition effect is directly proportional to DZMTRXV. DZMTRXV = 0 is an unphysical situation, but allows us to analyze the different recovery mechanisms in more separate forms. When gravity drainage is activated, the produced water rate rise more rapidly than when DZMTRXV = 0 (**Figure 5.17**). It is hard to tell exactly why this occurs, as a system with no gravity drainage is unrealistic. As a result of the higher water production, the maximum water cut allowed in the well is reached several years earlier in Case B, C and D, compared to the no gravity Case A. **Figure 5.18** illustrates this for Case 1A and 1C, where the producing well is shut in 3.5 years earlier in case 1C due to water cut limitations. Note however that the presented reservoir simulation does not include any limitations on the liquid production rate, which is an unlikely situation taking rig facilities into consideration. Had proper limitations on liquid handling limits been applied, e.g. twice the maximum oil production rate = 2 ·1500 Sm^3/day = 3000 Sm^3/day, all simulations shown in Figure 5.16 would shut in the well at an earlier time of production, and at the

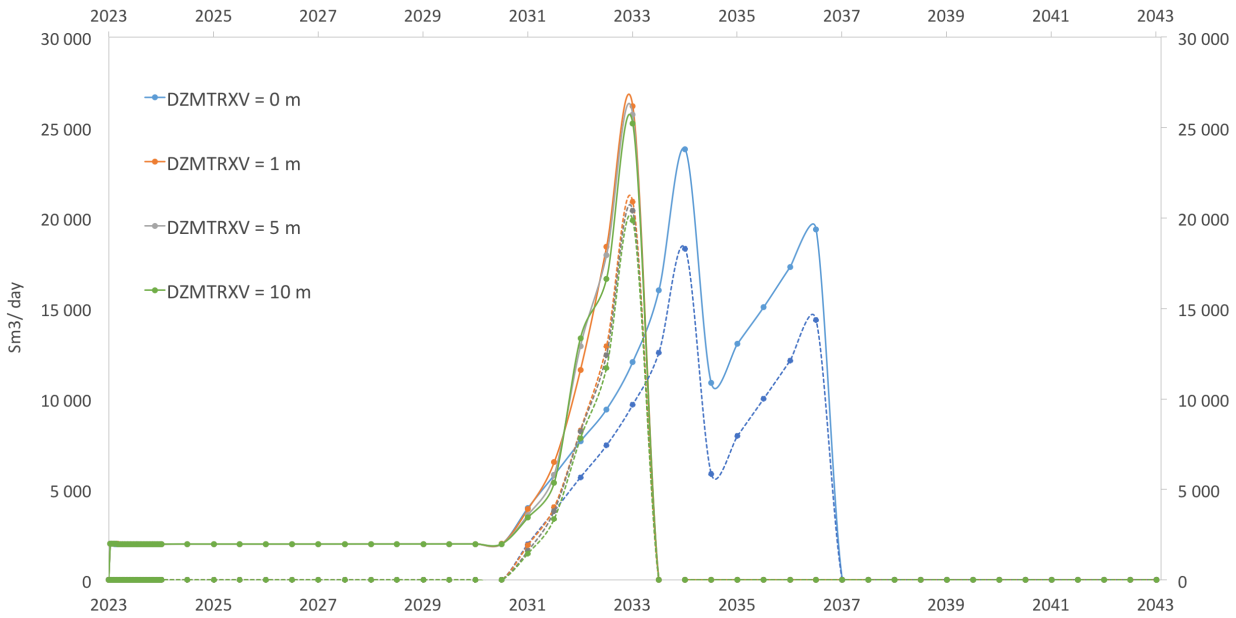

Figure 5.17: Case W1: Water injection (solid lines) and water production (dashed lines) rates. Water production correlates with injection.

same time (year 2031).

5.3.2 Matrix-Matrix Flow

In **Figure 5.19** the dual porosity cases from last section are compared to the dual permeability mode, with DZMTRXV equal to 0 and 1 m. Compared to the dual porosity model, contact between blocks in the full length of the column shows a decrease in recovery for DZMTRXV = 0 (2A), and a slight increase for DZMTRXV = 1 m (2B).

The 11% decrease between dualporo and dualperm (0 and 100% matrix contact) is due to the high water-cut explained in Section 5.3.1. For the dual permeability cases, water production is further delayed which is why the resulting recovery factor is 2.5% higher than with discontinuous blocks. The water front moves more gradually when it travels through matrix blocks in addition to the fracture continuum, as was also observed for the flow of oil in Case G2. Tabulated values confirm that the WC-limit is violated one output step (= 6 months) before in the dualporo case than in the dualperm (1 m), which causes the 2.5% higher recovery. This difference is for practical purposes small and probably largely affected by the size of the time steps in the simulator.

5.3.3 Matrix Block Shape / Size

In the water injection Base Case, nearly all oil is produced by spontaneous water imbibition, so effect of gravity forces can be neglected between all cases where GRAVDR is included. In the gas injection case (Figure 5.6) there is a crossover at SIGMA = 0.1 / DZMTRX = 1 m and SIGMA = 0.0001/ DZMTRX = 5 m. This crossover does not exist in the water injection case (**Figure 5.20**), signifying the larger effect of gravity drainage in the gas injection case

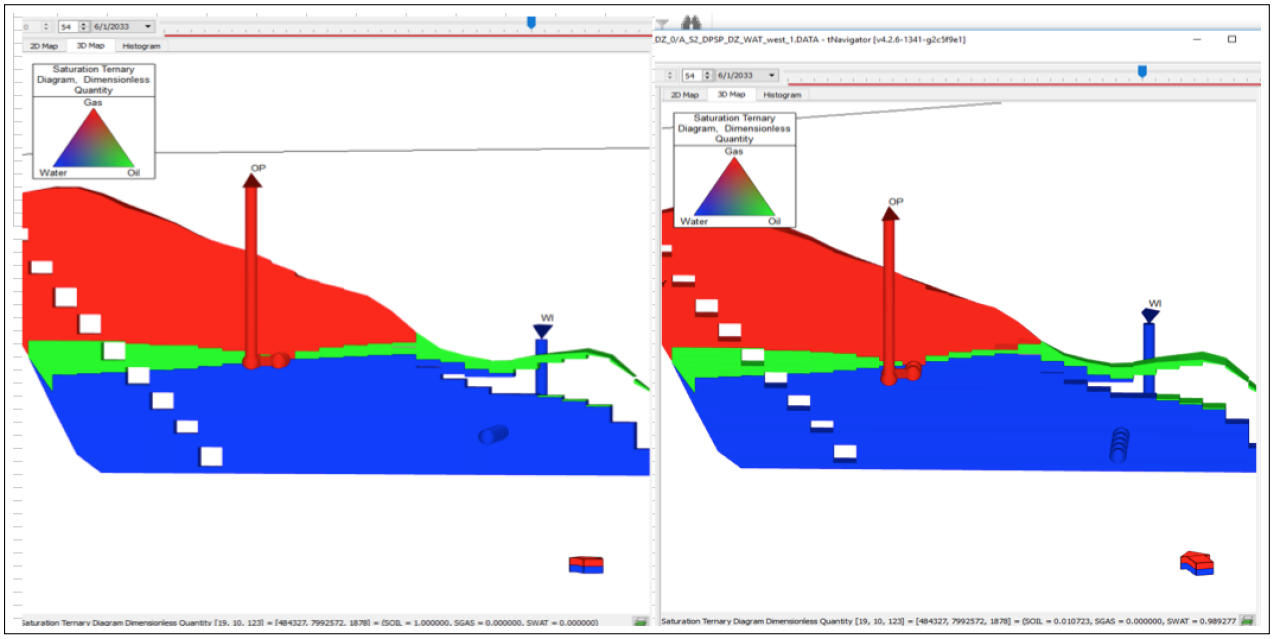

Figure 5.18: Fracture saturation ternary diagram for Case W1A / DZMTRXV = 0 m (left) and Case W1C / DZMTRXV = 1 m (right). In the 1 m -case, water production is higher and the well is shut-in 3.5 years earlier than the 0 m case, due to a high water cut. Blue is water, green is oil, red is gas.

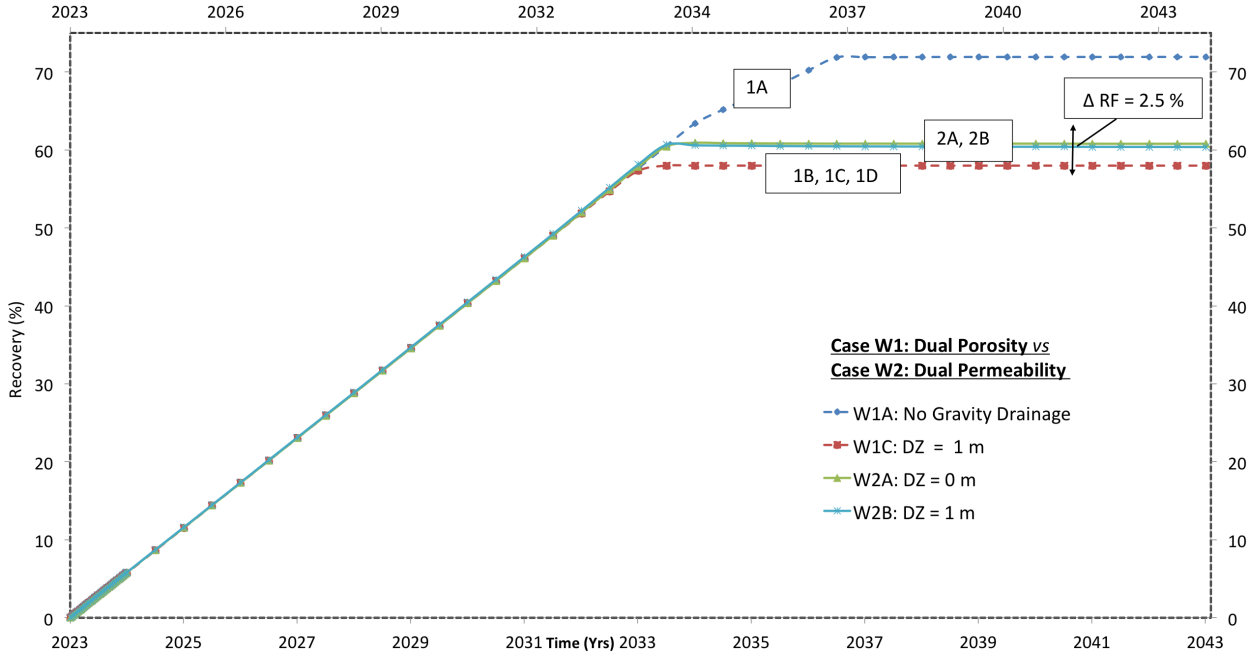

Figure 5.19: Case W2: Comparison of oil recovery vs time between the dual porosity and the dual permeability model with DZMTRXV = 0 and 1 m.

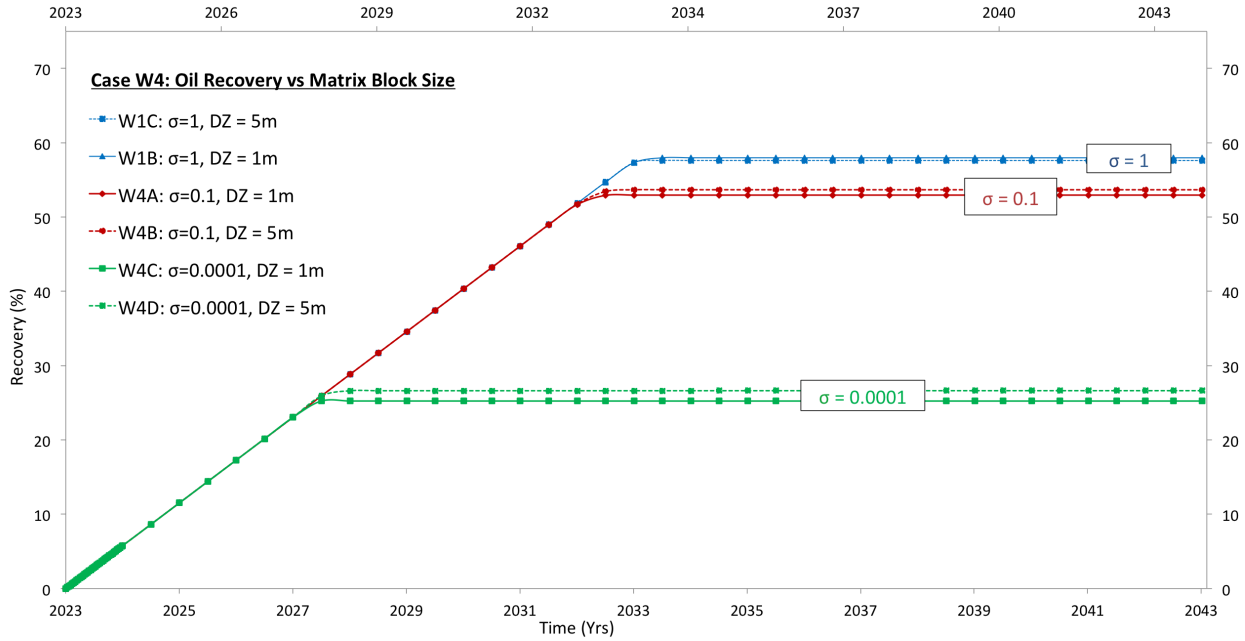

Figure 5.20: Case W4: Oil recovery vs time for three values of the sigma ('shape') factor: 1, 0.1, 0.0001 and gravity effects through DZMTRXV= 1 and 5 m. Solid lines indicate DZMTRXV = 1 m, and dashed line 5 m.

(G7).

SIGMA accounts for the matrix/fracture interface area per unit volume. With spontaneous imbibition of water, lowering the SIGMA factor has a more deteriorating effect on recovery than it does with gas-oil gravity drainage. This is because imbibition occurs through all surfaces of the matrix block, while gravity drainage pushes oil only through the top or bottom face. Thus the matrix/fracture interface area per unit volume for parallelepiped blocks is six times larger in a spontaneous imbibition process than with gravity drainage. Thus when SIGMA is applied in history matching, it is important to consider the recovery process to be matched, as correct SIGMA is essential for correct matching of matrix height and overall recovery potential.

5.3.4 Wettability

Figure 5.21 illustrate the effect of wettability on oil recovery. Wettability is altered by including different sets of matrix primary drainage and imbibition capillary pressure tables (given in Chapter 4), while relative permeability (which is also a common indicator of wettability) is kept constant. Four cases of P_{cow}-hysteresis have been simulated: Strongly oil wet (SOW), oil wet (OW), mixed wet (MW) and strongly water wet (SWW). The effect of changing matrix capillary pressure is illustrated by the early phase recovery, ultimate recovery, as well as ΔRF resulting from changing DZMTRXV (1 or 5 m). More water wet preferences show a higher early phase as well as final recovery, and a weaker dependency on gravity forces given by DZMTRXV (smaller ΔRF).

Previously, recovery of the Base Case has been discussed, this case does not include

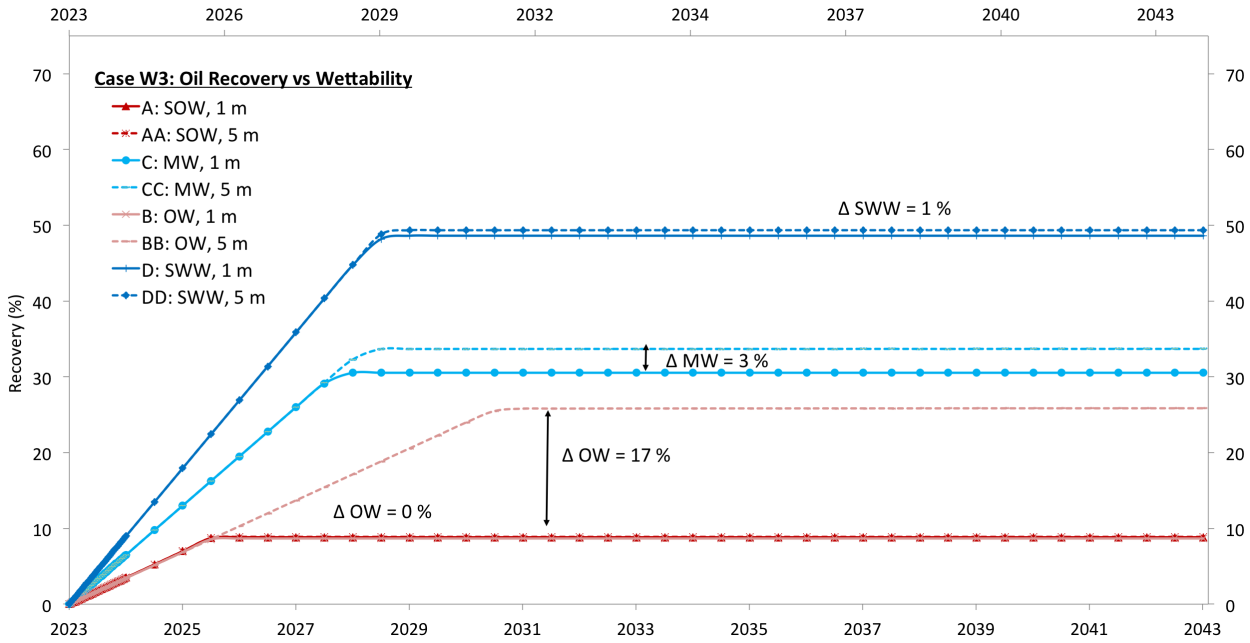

Figure 5.21: Case W6: Oil recovery vs time for different sets of drainage and imbibition curves, P_{cow}. SOW: Strongly Oil Wet, OW: Oil Wet, MW: Mixed Wet, SWW: Strongly Water Wet. Solid lines indicate DZMTRX = 1 m and dashed lines indicate 5 m.

hysteresis, and has water-wetting capillary pressure (Figure 5.16). Figure 5.21 shows that the deviation between recovery in the DZMTRXV = 1 vs DZMTRXV = 5 m cases is much larger than in Figure 5.16 and that the effect of DZMTRXV is more significant when the negative part of the capillary pressure curve is large.

When wettability of the matrix blocks are changed through different capillary curves, it affects the saturation processes in the pore volume. The resulting Original Oil in Place (OOIP) is given in **Table 5.1**. Generally, a more oil wet reservoir will have a higher initial oil saturation, as matrix capillary forces 'pull' at the oil during migration (imbibition), but typically a lower RF because the oil then sticks more to the rock during production also (drainage).

Table 5.1: Original Oil in Place (OOIP) vs P_{cow} $[MSm^3]$

	Base Case	SOW	OW	MW	SWW
Fracture	1,64	1,64	1,64	1,64	1,64
Matrix	7,87	14,1	14,4	6,8	4,5
Fraction fracture	17 %	10 %	10 %	20 %	27 %
Total	9,51	15,7	16	8,4	6,11

SOW: Strongly Oil-Wet, OW: Oil-Wet, MW: Mixed Wet, SWW: Strongly Water-Wet

The Base Case capillary pressure with no hysteresis corresponds to theoretical values not likely in the actual reservoir, and it has been shown that this case recovers all mobile oil due to spontaneous imbibition, as $S_{or} \rightarrow 0$ when $P_{cow} \rightarrow 0$. The OW and MW P_{cow}-cases are more complex and thus show a larger dependency on DZMTRXV.

The SOW and OW capillary curves have zero positive values, i.e. no spontaneous imbi-

bition is possible. Total recovery for these cases when DZMTRXV = 1 m is 9%, of which all oil volume were originally stored in fracture cells. As the wetting phase for these systems is oil, the displacement of oil in the matrix by water is a drainage process, and the gravity force must overcome capillary resistance for drainage to occur. The negative capillary pressure is larger for the SOW case than the OW case, which is why OW shows increased recovery as function of DZMTRXV, but SOW does not. 5 m does not yield large enough gravity force G to overcome the SOW-matrix' entry pressure of (minus) 0.292 bar. For a matrix block totally immersed in water and with fluid densities at reservoir conditions;

$$\begin{aligned} G &= H(\rho_w - \rho_o)g \\ &= 5m(1168,7kg/m^3 - 826,3kg/m^3)9,81m/s^2 \\ &\Rightarrow \underline{\underline{0,168bar}} \end{aligned} \tag{5.2}$$

Water enters the matrix block of SOW capillary pressure when $G = P_c$, thus the matrix height required is;

$$\begin{aligned} G &= P_c \\ H &= \frac{P_c}{(\rho_w - \rho_o)g} \\ H &= \frac{0.292 \cdot 10^5 Pa}{(1168,7kg/m^3 - 826,3kg/m^3)9,81m/s^2} \\ &\Rightarrow \underline{\underline{8.69m}} \end{aligned} \tag{5.3}$$

In the more water wet simulations, recovery of oil by water is an imbibition process and the amount of water spontaneously imbibed into the matrix is proportional to the positive area under the matrix capillary *imbibition* curve (given in Figure 4.11, 4.12 and 4.13). Spontaneous imbibition is a much faster process than gravity-controlled displacement, which is why the early phase behavior in Figure 5.21 is the same for DZMTRXV = 1 and 5 m. When the capillary pressure reaches its equilibrium between matrix and fracture, gravity dominated recovery is indicated by a more gentle slope. Gravitational effects are more significant when the potential for spontaneous imbibition is less, which is why DZMTRXV = 5 m yields 17% increase in recovery for the OW case, 3 % for MW and 1 % for SWW.

5.3.5 Water Alternating Gas Injection vs Wettability

In the initial work of this thesis, it was considered to include a thorough study of Water-Alternating-Gas (WAG) injection with the dual porosity model. This was eventually discarded, but one simulation-case is included with **Figure 5.22** to illustrate the potential of combined water and gas injection. The WAG-cases were run with reservoir properties corresponding to Case W3 (Figure 5.21). WAG is implemented with cycles of 60 days until November 2025 (the first two years of production), starting with water, then 6 months in which the first period also is water injection. The figure shows that WAG injection gives

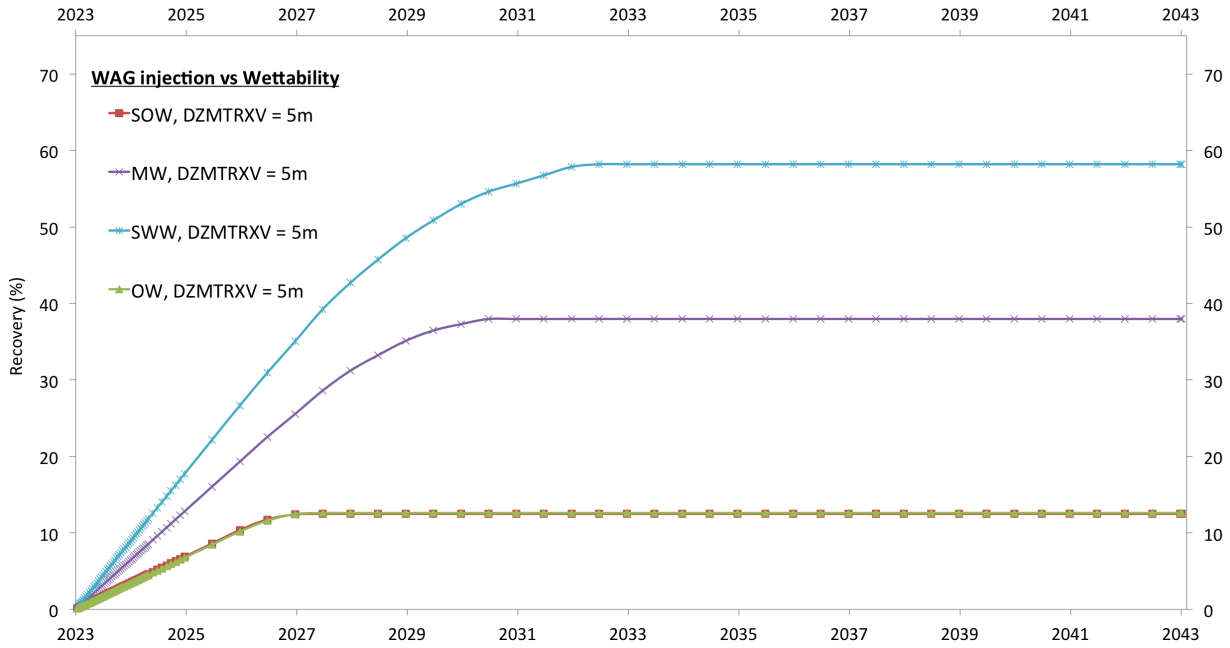

Figure 5.22: WAG has higher recovery than water injection

an ultimate recovery higher than the water injection scenario not only for oil-wet cases, but also for the strongly water-wet (SWW) case. Final recovery is increased by approximately 4% for the SOW and OW Case, 7% for the mixed wet case and almost 10 % in the strongly water-wet case which has an ultimate recovery close to 60 %.

The results are somewhat surprising, as it could be expected that the introduction of gas would have a higher effect in oil-wet scenarios than for water-wetting. However, the matrix height in this system is 1 m, so gravitational pressure is limited even though density differences are periodically higher than with single phase water injection. The cyclic form of the water injection delay water breakthrough, so more oil can be transferred from the matrix to the fracture system before the well is shut in. It is possible the same effect would be obtained without any gas injection, i.e. cyclic water injection. Typically, relative permeability of oil is higher in a gas-oil system than in a water-oil system. This is not the case in the presented simulations, and means that WAG injection could represents additional potential if the relative permeability curves are changed.

Chapter 6

Main Discussion

In the following chapter, results are discussed and compared to some of the work done by other parties. First of all, we are interested in seeing whether the results we have obtained are in line with what has been done earlier, or if there are new findings for this specific model. Secondly, we want to have results that can provide a better understanding of the reservoir behavior, e.g. through history matching. Thirdly, we want to assess the effects that the studied reservoir characteristics have for a feasible field development.

As the subjected field development project is in a concept study phase, a longer production test during 2018 is being prepared (Lundin, 2017). To be able to identify reservoir characteristics from the well test, it is important to have simulation studies to guide the history matching of the test. Well tests along with other data and measurements form the foundation to make an investment decision for a bigger development, and by history matching the results to recovery-sensitive parameters such as those studied in this thesis, an optimal recovery strategy can be selected. Simulated field performance can be compared to historical field performance by adjusting parameters of the reservoir and try to match oil production, water production and water cut for example. A summary of the main findings from the presented simulations is given below.

6.1 Summary of Main Observations

Gas Injection Scenario

1. When the matrix height is increased, more water coning is observed, which for the given Base Case saturation functions (without hysteresis) enhance recovery compared to gas flooding alone. If the matrices are less water wet, maximum recovery would be approached by gas-gravity drainage and water coning would in this case reduce ultimate recovery due to limitations of the well.

2. For zero gas-oil capillary pressure, maximum gas-oil drainage is achieved with discontinuous matrix blocks of small height. For single matrix blocks of sufficient height, a continuous matrix stack (DUALPERM mode) reduces the early phase recovery due to

a longer travel time through matrices vs. fractures.

3. Gas-oil capillary pressure of vuggy carbonates have been studied in literature (Kossack et al., 2006), and examples illustrate the crucial dependency on matrix height or capillary continuity for oil recovery. For the 'Normal' case 1.5 m of inter-block contact is necessary to achieve full recovery, and for the 'High' case, 8.5 m. With capillary threshold pressure recovery is further reduced, and discontinuous 1 m blocks yield zero oil transfer from the matrix.

4. As less gas enters the matrix blocks due to high P_{cog} and/ or high degree of discontinuous matrices, the well goes off plateau production earlier due to high gas production rates and effects of water coning (positive/negative) are not experienced. This is the more likely situation in an actual reservoir (compared to zero P_{cog}), suggesting that gas and not water -handling should be the main priority of the production facility when gas injection is implemented.

5. The effect of capillary continuity has been studied both for completely and tortuously continuous matrices. For matrix blocks of 1 m, a matrix-matrix contact of only 10 % severly enhances recovery for all examples of P_{cog}. These results further confirm the work of Festoy and van Golf-Racht (1989), where degree of contact area were tested with a fine-gridded, single porosity model.

6. For the 'High' case, where differences between complete and tortuous contact area are largest, more than 80 % of the maximum (100 % contact) recovery is achieved with matrix-matrix transmissibility corresponding to 5 % contact area. When matrix contact area exceed 25 %, the additional recovery due to capillary contact is negligible. No water production is experienced with a contact area of $\leq$ 25 %, but some is experienced with 100 % contact.

Water Injection Scenario

1. When spontaneous imbibition of water is the dominating recovery mechanism, lowering the SIGMA factor has a more deteriorating effect on recovery than it does with gas-oil gravity drainage. This is because imbibition occurs through all surfaces of the matrix block, while gravity drainage pushes oil only through the top or bottom face. This means that the matrix/fracture interface area per unit volume for parallelepiped blocks is six times larger in a spontaneous imbibition process than with gravity drainage. The recovery mechanism(s) should therefore be considered if SIGMA is used as a tuning factor for history matching.

2. The simulation results showed that when the reservoir rock went from water-wet to oil-wet (modeled by P_{cow}), both the early phase and the late phase recovery went down. The shape of the capillary drainage curve in an oil-wet resevoir is important for a drainage recovery process with water (or WAG) injection.

3. Water-Alternating Gas (WAG) injection is simulated for the given wettability - alternatives. WAG represent an upside compared to water injection alone, for both strongly oil-wet and strongly water-wet reservoirs. It can be assumed that additional recovery due to WAG will be more significant in oil-wet reservoirs as matrix height and/or capillary continuity increases. Relative permeability curves as well as hysteresis for both saturation functions should be carefully considered for further work on WAG simulations.

It has been demonstrated that when the reservoir rock is strongly oil-wet, poor recovery is achieved with water injection, as entry of water into the matrix becomes a drainage process. In drainage processes, gas-oil systems has the advantage of a much larger density difference. It has also been shown that gas-gravity drainage depends a lot upon matrix height when the matrix blocks are completely discontinuous. However, literature suggests that 0.0 % contact between matrix blocks are unlikely (Fung et al., 1991), and the work of this thesis demonstrate that only 5 % contact gives recovery corresponding to more than 80 % of the maximum recovery (completely continuous stack). In addition, simulations show that with a 'high' gas-oil capillary pressure and threshold, the matrix stack may be completely discontinuous (i.e. that contact points are impermeable) every 5 m and still gain a recovery factor higher than 35 % (Figure 5.12). The work on gas-injection simulations is conducted with water-wet capillary pressure, as the the strong water drive from the natural aquifer was not properly anticipated. Depending on the existing pipeline infrastructure and availability of gas, gas injection could be a more comprehensive concept solution compared to water, suggesting a water injection scheme is preferred as long as recovery characteristics does not imply otherwise, i.e. oil-wetting properties. Thus, an oil-wet scenario could have been more realistic with the gas injector system. However, the effect of gas-gravity drainage is demonstrated clearly in all cases where water coning is not significant (which includes those of 'high' capillary pressure), and is highlighted in Chapter 5. These results are also applicable for the initial consideration of a WAG-injection concept, as the upside to WAG vs gas-injection would require some degree of water-wetting formation. This has been demonstrated for matrix blocks of 1 m, 60/60 days followed by 6 months cycle periods and with two-phase hysteresis.

In the water injection scenario, high recovery is achieved both for the water-wet Base Case and for the one where hysteresis is modeled. With strong water-wetting, full recovery is achieved with spontaneous imbibition, and matrix block height is insignificant for the entry of water in to the matrix. When the matrix is less water-wet, gravity forces become important to push more of the oil out of the matrix. It has been shown that the shape of the capillary curve is of crucial importance, as the 'oil-wetting' case but not the 'strongly oil wetting' show significant increase in recovery as matrix height is 5 m vs 1 m. This implies that for some degree of oil-wettability, high recovery could be achieved with water injection if the matrix blocks are high or potentially if capillary continuity is prominent. Litterature (Uleberg and Kleppe, 1996) has shown that capillary continuity has a significant effect on recovery in intermediately wetted reservoirs, and the effect should be studied further as a

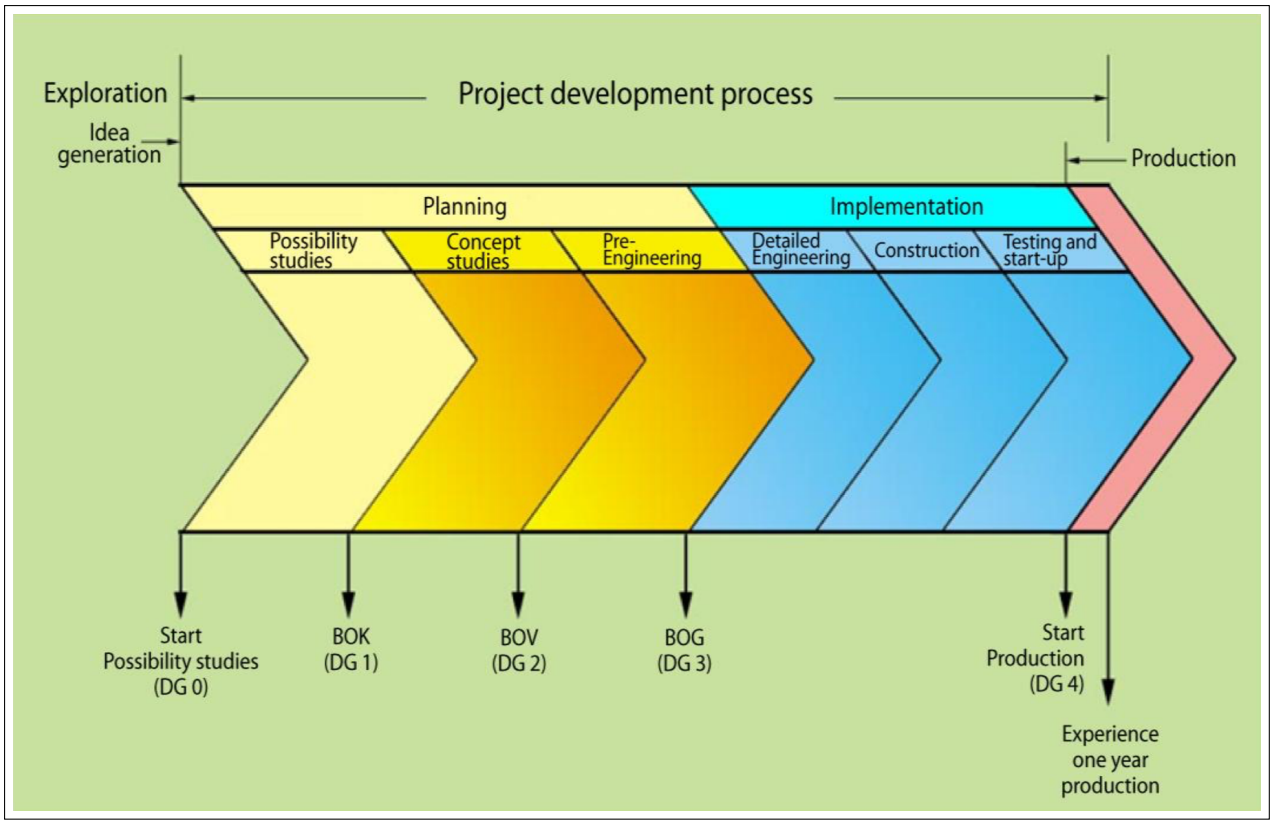

Figure 6.1: General project development model illustrating the different phases of a field development leading up to the production phase. Figure from NPD (2010).

range of likely wetting degrees for the Alta reservoir has been established.

The overall result of the presented simulations show the following; If the reservoir is strongly oil-wet, water injection does not drain any oil from the matrix materiale, and experience from similar reservoirs imply that a runner-up gas-injection strategy may not be able to reverse damages due to prior water flooding (ref. section 2.4 - the Natih Field). In this case, gas injection is the obvious strategy for oil recovery. For given relative permeability curves, any tendency towards water-wet capillary pressure represents a potential upside if gas injection is implemented, as coning of the natural aquifer will give additional recovery by spontaneous imbibition.

6.2 Field Development

In the previous section main focus were given to the effect on oil recovery due to varying parameters of the fractured reservoir. However, for the Alta discovery to have economical viability, other aspects of the production must be considered as well. In this section, focus is given to handling of water and gas that is produced along with oil, and implications this might have for the chosen concept strategy or other aspects of the field development process.

In the reservoir that has been evaluated many of the typical production characteristics for a fractured reservoir are observed: The drop in reservoir pressure is less than one bar corresponding to one bar drawdown pressure. Therefore, production is mainly constrained

to platform and flow assurance facilities including pipe dimensions, materials, multiphase separators and discharge handling. It is important to include the full lifetime-behavior of a reservoir in the early phase of field development, as initial investments impact profitability in the mature phase of the production.

At present time, the work on Alta is related to decision gate 2 (DG2) of a field development, meaning concept and feasibility studies are being conducted and the project is moving towards a decision to continue, i.e. concept selection (**Figure 6.1**). In this phase the project team looks at the development options available and determines which production and treatment plants would generally be suitable and how the oil or gas could be transported once it has been produced.

Coning

The Alta reservoir has a relatively small oil column, surrounded by a free gas cap and an underlying aquifer. The thin oil column means the reservoir is likely to experience coning, which has been confirmed for both gas and water injection scenarios described in this thesis. Usually, coning is related to viscous forces, limiting the gravity segregation in a reservoir. Highly permeable pore networks such as the fractures usually promote gravity segregation so that unwanted fluid is not produced. Common strategies to minimize coning include optimal placement of the well(s), partial perforation, or an optimized production rate. Inflow control devices (ICD) can be implemented to shut perforations as gas or water cut reaches a given limit. In cases with a gas injector, the producer is placed close to the initial water-oil contact (WOC), to allow for maximum oil displacement from the top down, and to minimize gas production. If coning of the natural aquifer is expected, the producer should be placed further away from the initial WOC. However, in reservoirs with a thin oil zone and free gas, it could be possible to reduce water production by inducing coning of the gas cap in stead. This strategy is implemented on the Troll field, a giant oil and gas field off the coast of western Norway (Mikkelsen et al., 2005). The oil zone at Troll West is thinner than the Alta discovery, between 4-27 m vs Alta's 45 m column. The field includes a giant gas cap which was the main production target initially, and a connecting aquifer. A successful strategy here has been to use horizontal wells with open hole branches and screens with inflow control devices along the entire reservoir section. The horizontal well sections were gradually increased and multi-lateral wells were used to gain a higher drainage area per invested capital.

To induce gas coning by purpose of reducing water cut when producing from a thin oil reservoir, the following strategy is implemented (Mikkelsen et al., 2005): The well is placed very close to the initial oil-water contact (OWC), at Troll 0.5 m above is normal. Thus, the initial water cut is usually very high, typically higher than 50%. The water cut will decrease when the oil is coned into the water. In this thesis the producer is placed 9.5 m above the OWC, so this scenario has not been tested. As the gas cap expands, the GOC is deepened and eventually comes in contact with the wellbore. As contact is established, the well will cone down free gas from the gas cap. This solution would be particularly interesting for an

oil-wetting fractured reservoir, as we would want as little water as possible to immerse the oil saturated matrix block in order to optimize gas-oil gravity drainage. However, the concept would have to be tested for the twice as high Alta oil column. If successful, a challenge is now to optimize oil versus gas rate.

For a water injection concept it would be natural to place the well close to the gas cap, this time to maximize oil displacement from the bottom and up. Minimization of coning should be studied closely with respect to injection and production rates and the effects controlled by zonal control, partial perforation and IDC's to maximize profit.

Water Handling

For the discussion of fluid handling some of the presented cases are excluded. These include cases where DZMTRX $\leq 0.1\ m$ as it is assumed these are not representable of a actual reservoir.

For the water injection case, water handling is a significant part of the investment decision. In the demonstrated cases, water injection is controlled so that the total reservoir volume injection rate equals the production rate, so naturally a higher oil production yields a higher water production eventually. The volumes produced are large and the time of water breakthrough is sensitive to reservoir parameters. Production rates differ from 9000 to 21 000 Sm^3/day and more than 80 % of the presented water injection cases are shut in due to 95 % water cut. These numbers represent production that is only subject to an upper WC-limit and not total production of liquids. It is more realistic that the oil rate would be limited to water rates of 3-4000 Sm^3/day, suggesting both oil and water production are reduced. Time of water breakthrough ranges from 3.5 to 9 years after production is commenced. The earliest cases are seen with capillary hysteresis and low SIGMA, and the latest with Base Case capillary pressure and small matrix height (Figure 5.5).

The water produced with the gas injection case is less significant. Water cut does not exceed 40 %, with maximum rates of 900 Sm^3/day and total produced water volumes ranging from zero to 160 000 Sm^3. Thus, the impact on flow line capacity is small and water does not affect plateau production if a capacity of 3-4000 Sm^3/day is assumed. Water breakthrough in the gas injection cases range from mid 2029 to mid 2032, meaning that proper water handling equipment, if any, must be installed between 5.5 and 8 years after production is started. The earliest water breakthrough is when capillary continuity is high, matrix height is large and matrix capillary pressure is low (zero in the Base Case). With higher P_{cog}, less oil is produced, and water production is reduced to a maximum of 300 Sm^3/day. One interesting observation is found in Case 5 - where contact area between blocks vary. Even though 25 % contact area resulted in an ultimate oil recovery factor close to the one of full contact (with a maximum ΔRF of 2.5%), water production correlation differs. No water production is experienced for MULT$_k \leq 0.25$, but with 100 % contact a small period of 120 $Sm^3\ water/day$ is experienced. Considering that this example is for a high P_c ($P_{cog} = P_{TH} =$ 'High') and that for the Base Case with lower P_{cog} but same DZMTRX and capillary contact, the water production is timed with a factor 4.3, this could signify that there is a critical

amount of contact area at which oil recovery is optimized and water production minimized for given P_{cog}. This would need to be studied further to gain a better understanding of the pressure behavior and subsequent water expansion in the aquifer. As both the contact between, and height of matrix blocks is a difficult property to quantify, it is important that flexible water handling is accounted for also if gas injection is the implemented strategy.

These results show that for a fractured reservoir where water injection is a successful recovery method, water treatment is essential for the detailed pre-engineering and concept selection and need to be planned with a great deal of flexibility. A viable oil production depends on both the timing and the rates of produced water. In the mature period, down-payment and available facilities might allow very high water cuts. Gullfaks is an example of this. The Gullfaks field has segments producing with up to 84 and 97 % water cut, and oil rates down to 250 Sm^3/day. Gullfaks is not a dual porosity reservoir, but extreme permeability contrasts characterizes the typical sand reservoirs (Tarbert and Cook). Like at Alta, oil can therefore be produced at very low drawdown.

Means to reduce water cut and / or improve oil production include selective perforation and zone isolation. Mechanical zone isolation of high water producing intervals by mechanical plugs (straddles) can be very useful to drain more oil from less-drained intervals. The injector well may also be controlled by zone isolation, to effectively change the injection pattern and thereby improve overall efficiency. This could also allow the water in given fractures additional soak time and thus a higher oil recovery (Hill et al., 1985). Production Logging Tools (PLT's) can be implemented to identify worst offended intervals in the producer. Water diversion by gel or silicate might also be applicable to reduce permeability of the fractures in one zone, e.g. zones vertically close to the producer, to improve recovery from zones were coning towards the producer is less prominent.

Other modern efforts to improve water management and water treatment include electrostatic coalescing inside the first stage separator (e.g. VIEC) or last stage Compact Flotation Unit separator (e.g. Epcon CFU Technology). The latter has a smaller volume and shorter retention time than traditional flotation units, and can treat higher water rates per operational volume (Madsen et al., 2005; Atarah, 2011).

Gas Handling

Handling of produced gas is mainly an issue when gas is injected. Discharge of gas is obviously more laborious than water, which may be unloaded to the ocean. Produced gas must either be transported through pipelines to shore, where it can be sold, or it must be injected in a new reservoir, or re-injected into the producing reservoir. Surrounding gas resources such as the Skalle discovery represents potential, near-by volumes for a gas injection scheme and may also be used for re-injection of the produced gas. If transported to shore, the produced gas may represent potential income, but this depends on infrastructure, e.g. via the Snøhvit Field. Either way, the gas processing capacity of the production facilities must also be considered.

For the cases studied, gas breakthrough varies from four to nine years, meaning that

operational costs and investments related to gas handling can be postponed by five years for a given reservoir. The cases that have a low SIGMA value or high P_{cog} have an earlier gas breakthrough than cases with zero P_{cog} and/ or a large degree of capillary continuity, as less of the gas is able to enter the matrix blocks (Figure 5.2). This indicates that the gas breakthrough is largely related to the matrix recovery attainable, in a way that either strengthens a reservoir with good recovery (late gas breakthrough) or further reduces the value of a reservoir where less oil is recovered by gas injection. The effect of injection/ production rates should be studied further to optimize the oil versus gas production, in particularly for a low sigma factor where the flow rate between matrix and fracture is slower.

6.3 Reservoir Assumptions

To simulate a reservoir with available tools and in time span of practical purposes, it is necessary for the engineers to make several assumptions. The assumptions that relate mostly to recovery mechanisms studied in this thesis include zero capillary pressure and linear relative permeability in the fractures, as well as negligible recovery by viscous forces or diffusion. The assumptions concerning saturations functions and viscous displacement are acceptable as long as the fracture width is large (for capillary pressure, a width of 100 microns is estimated by de la Porte et al. (2005)) and gravity forces prevail Kjøsnes (2012). Although diffusion is known to be accelerated by the presence of high-permeable fractures, the overall effect on recovery is usually small and can for most systems be neglected for practical purposes (Uleberg and Kleppe, 1996). Other assumptions made to simplify the study, is that saturations functions are the same in the entire reservoir, when it could have been inputed for individual zones or facies. For the case of wettability, it is natural that the shape of the relative permeability curve also changes as the capillary curve changes due to different wetting.

6.4 Validity of the Presented Data Related to Reservoir Modeling

Some remarks can be summarized with respect to the validity of the dual porosity examples discussed in this and the previous chapter. Dual porosity models have a coarse grid, somewhat depending on the matrix block size. For smaller matrices, more upscaling of the representative properties such as saturation functions are necessary and a larger error can be expected. Lu (2008) found that oil recovery when matrix blocks were 1 m tall in the analytic model corresponded to 3.2 m blocks in the dual porosity GRAVDR model. This means that for given matrix block height, oil recovery may be underestimated and there may be a potential upside in the actual reservoir compared to presented simulations. These results were when same SIGMA were used in the analytical and the dual porosity model. None of the modeling functions presented in this thesis account for the reinfiltration phe-

nomen, which could be another source of error. Finally, the method for modeling of capillary hysteresis may have implications as recovery from a fractured reservoir is more dependent upon capillary forces than a conventional reservoir.

6.5 Recommendations for Further Work

Several suggestions for improvements of the work in this thesis have been presented in the evaluation chapters. This section will be a quick summary of suggested improvements to the study of recovery mechanisms in fractured carbonate reservoirs during gas or water injection:

- First, liquid rate limits should be added to the well control, so results are more representative of actual production facilities
- The aquifer-behavior should be studied closer, as potential water drive could improve recovery from reservoirs with water-wetting properties, or potentially reduce ultimate recovery due to a high water cut
- Investigate degrees of pressure maintenance and the effect of different injection / production rates on recovery as well as water -or -gas -coning
- Investigate minimization of -or induced coning by well placement
- Investigate the effects of heterogeneous reservoir properties, e.g. assignment of matrix block height, size, relative permeability and capillary pressure per facie or other defined zones of the reservoir model
- Wettability variations should be considered through relative permeability curves in addition to capillary pressure

Other use of the work conducted in this thesis include research on alternative recovery strategies such as:

- Further WAG studies including three phase relative permeability, water/ gas cycles ratio, cycle intervals and injection / production rates
- Cyclic water injection
- EOR studies such as wettability alteration (e.g. low salinity water injection)

Chapter 7

Conclusions

Key characteristics of a fractured reservoir have been studied in literature and tested with dual porosity / dual permeability simulations in ECLIPSE. Primary focus is given to the matrix-fracture transport process and resulting oil recovery, as well as produced water and gas. The main findings of this work is as follows:

- Gas-oil gravity drainage is studied for vuggy carbonate gas-oil capillary pressure given in literature. For a stack of discontinuous matrix blocks, a large matrix block height is required to approach maximum recovery of oil.
- For a stack where matrix-matrix flow is induced by a limited contact area, recovery is dramatically increased. For small matrix height, contact corresponding to 5% of the cross-sectional area result in recovery equal to 80% of the recovery from the completely continuous matrix stack. For a contact area exceeding 25%, additional recovery due to capillary contact is negligible.
- For a water-wet reservoir during gas injection, coning of the natural aquifer is observed as height of the matrix blocks is increased. This could ultimately affect the net income of a field and should be studied further.
- When oil-wetting capillary pressure curves are introduced, both the early phase and the late phase recovery during water injection is reduced, compared to more water-wetting curves. Two strongly oil-wetting examples are tested and illustrate clearly the dependency of a highly connected matrix stack to recover oil by water-gravity drainage.
- A simplified WAG-simulation were run and shows potential for both strongly water-wetting and strongly oil-wetting cases.
- Consideration of the prevailing recovery mechanism in a reservoir is crucial for correct history matching as the shape factor has a larger effect in reservoirs where capillary forces dominate.
- From the presented simulations, gas injection emerges as the safest choice of field development strategy, as long as as necessary gas resources and discharge opportunities are

available. Gas-gravity drainage represents more flexibility with respect to characterization of uncertain reservoir properties such as matrix height, capillary pressure and wettability, and additional costs could be somewhat balanced by less water production.

Appendix A

Nomenclature

A cross sectional area , L^2, m^2

B formation volume factor, $rm^3/Sm3$

C compressibility, $Lt^2/m, 1/bars$

C_{et} total compressibility, $Lt^2/m, 1/bars$

C_r rock compressibility, $Lt^2/m, 1/bars$

g acceleration due to gravity, Lt^{-2}, m^2s^{-1}

G gravitational pressure m/Lt^2, bar

h_c height of capillary rise, L, m

H vertical block height, L, m

k permeability, mD

k_r relative permeability, *dimensionless*

l matrix block dimension, m

P pressure, m/Lt^2, bar

P_c capillary pressure, m/Lt^2, bar

P_{ref} reference pressure, m/Lt^2, bar

P_{TH} treshold pressure, m/Lt^2, bar

q rate, L^3t^{-1}, m^3s^{-1}

r radius of curvature, L, m

R_{si} dissolved gas-oil ratio, $Sm^3/Sm3$

S saturation, *dimensionless*

S_{wi} initial water saturation, *dimensionless*

S^* crossover-saturation, *dimensionless*

V matrix cell bulk volume, m^3

Z height of displacing fluid front in matrix, L, m

α welltest/ core ratio, *dimensionless*

γ specific gravity, *dimensionless*

$\Delta\rho$ density difference, mL^{-3}, kg/m^3

θ contact angle, *degree*

μ viscosity, $mL^{-1}T^{-1}$, cP

ρ density, mL^{-3}, kg/m^3

σ sigma/ shape factor, m^{-2}

Υ interfacial tension, $L^{-1}t^{-2}$

ϕ porosity, *dimensionless*

Subscripts

x,y,x dimensions

f fracture

g gas

ma matrix

max maximum

nwe non-wetting phase

o oil

r residual

w water

we wetting phase

Abbreviations

CPU Central Processing Unit

FWL Free Water Level

GOC Gas Oil Contact

GOR Gas Oil Ratio

MW Mixed Wet

OOIP Original Oil In Place

OW Oil-Wet

OWC Oil Water Contact

PLT Production Logging Tool

PVT Pressure Volume Temperature

RF Oil Recovery Factor

SCAL Special Core Analysis

SOW Strongly Oil-Wet

SWW Strongly Water-Wet

WAG Water Alternating Gas

References

Abdallah, W., Buckley, J. S., Carnegie, A., Edwards, J., Herold, B., Fordham, E., Graue, A., Habashy, T., Seleznev, N., Signer, C., et al. (1986). Fundamentals of wettability. *Technology*, 38(1125-1144):268.

Allan, J., Sun, S. Q., et al. (2003). Controls on recovery factor in fractured reservoirs: lessons learned from 100 fractured fields. In *SPE Annual Technical Conference and Exhibition*. Society of Petroleum Engineers.

Atarah, J. J. A. (2011). The use of flotation technology in produced water treatment in the oil & gas industry. Master's thesis, University of Stavanger, Norway.

Barenblatt, G. I., Zheltov, I. P., and Kochina, I. N. (1960). Basic concepts in the theory of seepage of homogeneous liquids in fissured rocks [strata]. *Journal of Applied Mathematics and Mechanics*, 24(5):1286–1303.

Barkve, T., Firoozabadi, A., et al. (1992). Analysis of reinfiltration in fractured porous media. In *SPE Annual Technical Conference and Exhibition*. Society of Petroleum Engineers.

Bourdon, L., Coca, S., Alessio, L., et al. (2004). Karst identification and impact on development plan. In *SPE Asia Pacific Oil and Gas Conference and Exhibition*. Society of Petroleum Engineers.

Carrillat, A., Hunt, D., Randen, T., Sonneland, L., and Elvebakk, G. (2005). Automated mapping of carbonate build-ups and palaeokarst from the norwegian barents sea using 3d seismic texture attributes. In *Geological Society, London, Petroleum Geology Conference series*, volume 6, pages 1595–1611. Geological Society of London.

Chilingar, G. V. and Yen, T. (1983). Some notes on wettability and relative permeabilities of carbonate reservoir rocks, ii. *Energy Sources*, 7(1):67–75.

Chima, A., Geiger, S., et al. (2012). An analytical equation to predict gas/water relative permeability curves in fractures. In *SPE Latin America and Caribbean Petroleum Engineering Conference*. Society of Petroleum Engineers.

de la Porte, J. J., Kossack, C. A., Zimmerman, R. W., et al. (2005). The effect of fracture relative permeabilities and capillary pressures on the numerical simulation of naturally fractured reservoirs. In *SPE annual technical conference and exhibition*. Society of Petroleum Engineers.

Dejam, M., Ghazanfari, M. H., and Masihi, M. (2009). Theoretical modeling of reinfiltration process in naturally fractured reservoirs: a comparative study on traveling liquid bridges and continuum film flow approaches. In *SPE/EAGE Reservoir Characterization & Simulation Conference*.

Di Donato, G., Huang, W., Blunt, M., et al. (2003). Streamline-based dual porosity simulation of fractured reservoirs. In *SPE Annual Technical Conference and Exhibition*. Society of Petroleum Engineers.

Elvebakk, G., Hogstad, K., Hunt, D., Pajchel, K., Rafaelsen, B., and Robak, H. (2003). Upper carboniferous–lower permian gipsdalen group karstified reservoir carbonates of the loppa high, barents sea: Reservoir potential and drilling challenges (abs.). In *Conference on Petroleum Exploration and Production in Environmentally Sensitive Areas, Ålesund, Norway*.

Fernø, M. A. (2008). *A study of capillary pressure and capillary continuity in fractured rocks*. PhD thesis, Department of Physics and Technology, University of Bergen, Norway.

Festoy, S. and van Golf-Racht, T. (1989). Gas gravity drainage in fractured reservoirs through new dual-continuum approach (includes associated papers 20296 and 20390). *SPE Reservoir Engineering*, 4(03):271–278.

Firoozabadi, A. et al. (2000). Recovery mechanisms in fractured reservoirs and field performance. *Journal of Canadian Petroleum Technology*, 39(11).

Firoozabadi, A., Hauge, J., et al. (1990). Capillary pressure in fractured porous media (includes associated papers 21892 and 22212). *Journal of Petroleum Technology*, 42(06):784–791.

Firoozabadi, A., Markeset, T., et al. (1994). An experimental study of the gas-liquid transmissibility in fractured porous media. *SPE Reservoir Engineering*, 9(03):201–207.

Fisher, G., Hunt, D., Colpaert, A., Wall, B. G., and Henderson, J. (2010). Comprehensive karst delineation from 3d seismic data. *Proceedings AAPG GEO*.

Fung, L. S. (1991). Simulation of block-to-block processes in naturally fractured reservoirs. *SPE reservoir engineering*, 6(04):477–484.

Fung, L. S.-K., Collins, D. A., et al. (1991). An evaluation of the improved dual porosity model for the simulation of gravity effects in naturally fractured reservoirs. *Journal of Canadian Petroleum Technology*, 30(03).

Ghorayeb, K., Holmes, J. A., et al. (2005). Black oil delumping. In *SPE Annual Technical Conference and Exhibition*. Society of Petroleum Engineers.

Hill, A., Thomas, G., et al. (1985). A new approach for simulating complex fractured reservoirs. In *Middle East Oil Technical Conference and Exhibition*. Society of Petroleum Engineers.

Horie, T., Firoozabadi, A., Ishimoto, K., et al. (1990). Laboratory studies of capillary interaction in fracture/matrix systems. *SPE Reservoir Engineering*, 5(03):353–360.

Hughes, R. G. and Blunt, M. J. (2000). Pore scale modeling of rate effects in imbibition. *Transport in Porous Media*, 40(3):295–322.

Hunt, D., Elvebakk, G., Rafaelsen, B., Pajchel, K., Hogstad, K., Robak, H., and Randen, T. (2003). Paleokarst recognition and 3-d distribution—new insights from the upper paleozoic, loppa high, barents sea (abs.). In *European Association of Geoscientists and Engineers 65th Conference and Exhibition, Stavanger, Norway*.

Karpyn, Z. T., Halleck, P. M., Grader, A. S., et al. (2006). Fracture-matrix transport dominated by capillary-driven flow in layered sandstone. In *SPE/DOE Symposium on Improved Oil Recovery*. Society of Petroleum Engineers.

Kazemi, H., Merrill Jr, L., Porterfield, K., Zeman, P., et al. (1976). Numerical simulation of water-oil flow in naturally fractured reservoirs. *Society of Petroleum Engineers Journal*, 16(06):317–326.

Killough, J. et al. (1976). Reservoir simulation with history-dependent saturation functions. *Society of Petroleum Engineers Journal*, 16(01):37–48.

Kjøsnes, V. A. A. (2012). Effects of fracture capillary pressure and non-straight relative permeability lines. Master Thesis, NTNU.

Kleppe, J. (2017). Lecture notes tpg4160 - reservoir simulation; introduction to compositional simulation (hand-out note 14). Retrieved 24/5/2017 from http://www.ipt.ntnu.no/ kleppe/TPG4160/note14.pdf.

Kleppe, J., Delaplace, P., Lenormand, R., Hamon, G., Chaput, E., et al. (1997). Representation of capillary pressure hysteresis in reservoir simulation. In *SPE Annual Technical Conference and Exhibition*. Society of Petroleum Engineers.

Kossack, C., Gurpinar, O., et al. (2001). A methodology for simulation of vuggy and fractured reservoirs. In *SPE Reservoir Simulation Symposium*. Society of Petroleum Engineers.

Kossack, C. A. et al. (2006). Simulation of gas/oil displacements in vuggy and fractured reservoirs. In *SPE Annual Technical Conference and Exhibition*. Society of Petroleum Engineers.

Kriebernegg, M. and Heinemann, Z. E. (1996). A new model for history dependent saturation functions in reservoir simulation. In *ECMOR V-5th European Conference on the Mathematics of Oil Recovery*.

Lake, L. W. (1989). Enhanced oil recovery.

Larssen, G., Elvebakk, G., Henriksen, L. B., Kristensen, S., Nilsson, I., Samuelsberg, T., Svånå, T., Stemmerik, L., and Worsley, D. (2002). Upper palaeozoic lithostratigraphy of the southern norwegian barents sea. *Norwegian Petroleum Directorate Bulletin*, 9:76.

Loucks, R. (1999). Paleocave carbonate reservoirs: Origins, burial-depth modifications, spatial complexity, and reservoir implications. volume 83,11.

Lu, H. (2008). *Investigation of recovery mechanisms in fractured reservoirs*. PhD thesis, Department of Earth Science and Engineering, Imperial College London.

Lundin (2017). Lundin petroleum corporate presentation.

Madsen, T., Abtahi, M., et al. (2005). Handling the oil zone on troll. In *Offshore Technology Conference*. Offshore Technology Conference.

Maidebor, V. (1973). Production from fractured oil reservoirs. *IFP 21 820*, (1 and 2).

Meehan, D. N. et al. (2011). Using analog reservoir performance to understand eor opportunities in type i fractured reservoirs. In *SPE Enhanced Oil Recovery Conference*. Society of Petroleum Engineers.

Mikkelsen, J., Norheim, T., Sagatun, S., et al. (2005). The troll story. In *Offshore Technology Conference*. Offshore Technology Conference.

Morrow, N. R. et al. (1990). Wettability and its effect on oil recovery. *Journal of Petroleum Technology*, 42(12):1–476.

Noroozi, M., Moradi, B., Bashiri, G., et al. (2010). Effects of fracture properties on numerical simulation of a naturally fractured reservoir. In *Trinidad and Tobago Energy Resources Conference*. Society of Petroleum Engineers.

NPD (2010). Guidelines for plan for development and operation of a petroleum deposit (pdo) and plan for installation and operation of facilities for transport and utilisation of petroleum (pio). Norwegian Petroleum Directorate.

NPD (2015). Delineation of oil and gas discovery 7220/11-1 in the barents sea - 7220/11-3 and 7220/11-3 a. Norwegian Petroleum Directorate. http://www.npd.no/en/news/Exploration-drilling-results/2015/722011-3-og-722011-3-A/ [Online: accessed Jan 6 2017].

NPD (2016a). Deepening of appraisal well 7220/11-3 a in the barents sea – 7220/11-3 ar. http://www.npd.no/en/news/Exploration-drilling-results/2016/722011-3-AR/ [Online: accessed Jan 5 2017].

NPD (2016b). Factmaps. Norwegian Petroleum Directorate. http://www.npd.no/no/Kart/Faktakart/ [Online: accessed 29 Dec 2016].

NPD and MPE (2016). Norsk petroleum 7220/11-1 (alta). Norwegian Petroleum Directorate and Ministry of Petroleum & Energy. http://www.norskpetroleum.no/en/facts/discoveries/722011-1-alta/ [Online: accessed 16 Dec 2016].

Orlopp, D. et al. (1988). Casablanca oilfield, spain: A karsted carbonate trap at the shelf edge. In *Offshore Technology Conference*. Offshore Technology Conference.

Petrowiki (2016). Relative permeability.

Pooladi-Darvish, M., Firoozabadi, A., et al. (1998). hu. In *Annual Technical Meeting*. Petroleum Society of Canada.

Reiss, L. H. (1980). *The reservoir engineering aspects of fractured formations*, volume 3. Editions Technip.

Romm, E. (1966). Fluid flow in fractures.

Sayago, J., Di Lucia, M., Mutti, M., Cotti, A., Sitta, A., Broberg, K., Przybylo, A., Buonaguro, R., and Zimina, O. (2012). Characterization of a deeply buried paleokarst terrain in the loppa high using core data and multiattribute seismic facies classification. *AAPG bulletin*, 96(10):1843–1866.

Schlumberger (2016). Software, petrel 2016.

Schlumberger Ltd, . (2015). *Eclipse Manual*, version 2015.2 edition.

Siggerud, E. I. H. (2015). Lecture Notes TPG4177 - Carbonate Reservoir Characterization.

Skjaeveland, S., Siqveland, L., Kjosavik, A., Hammervold, W., Virnovsky, G., et al. (1998). Capillary pressure correlation for mixed-wet reservoirs. In *SPE India Oil and Gas Conference and Exhibition*. Society of Petroleum Engineers.

Sonier, F., Souillard, P., Blaskovich, F., et al. (1988). Numerical simulation of naturally fractured reservoirs. *SPE reservoir engineering*, 3(04):1–114.

SPE (2015). Petrowiki - ekofisk field. Society of Petroleum Engineers.

Sylta, K.-E. H. (2010). Primary drainage capillary pressure curves in heterogeneous carbonates with ultracentrifuge and nmr. Master's thesis, The University of Bergen.

Sylte, J., Thomas, L., Rhett, D., Bruning, D., Nagel, N., et al. (1999). Water induced compaction in the ekofisk field. In *SPE Annual Technical Conference and Exhibition*. Society of Petroleum Engineers.

Tan, T. et al. (1990). Representation of hysteresis in capillary pressure for reservoir simulation models. *Journal of Canadian Petroleum Technology*, 29(04).

Torsaeter, O. and Silseth, J. (1985). The effects of sample shape and boundary conditions on capillary imbibition. In *North Sea Chalk Symp., Stavanger*.

Treiber, L., Owens, W., et al. (1972). A laboratory evaluation of the wettability of fifty oil-producing reservoirs. *Society of petroleum engineers journal*, 12(06):531–540.

Uleberg, K. and Kleppe, J. (1996). Dual porosity, dual permeability formulation for fractured reservoir simulation. In *Norwegian university of science and technology, trondheim RUTH seminar, stavanger*.

Van Dijkum, C., Walker, T., et al. (1991). Fractured reservoir simulation and field development, natih field, oman. In *SPE Annual Technical Conference and Exhibition*. Society of Petroleum Engineers.

van Golf-Racht, T. D. (1982). *Fundamentals of fractured reservoir engineering*, volume 12. Elsevier.

van Heel, A. P., Boerrigter, P. M., van Dorp, J. J., et al. (2008). Thermal and hydraulic matrix-fracture interaction in dual-permeability simulation. *SPE Reservoir Evaluation & Engineering*, 11(04):735–749.

Warren, J., Root, P. J., et al. (1963). The behavior of naturally fractured reservoirs. *Society of Petroleum Engineers Journal*, 3(03):245–255.

Appendix B

ECLIPSE Data Files

A complete set of ECLIPSE data files for the base case examples of gas, water and WAG injection schemes are delivered in an attache ZIP file: "BjergaT_Appendix_datafiles". This folder also contains SCHEDULE and PROPS include files for all simulation cases run with the thesis. Included in this appendix are Base Case data files for the main file, mentioned include files, in addition to other include files that are frequently altered to give the results presented in this thesis and include files that contain essential information about the model and/or simulations, e.g. GRID.INC, SOL.INC and SUM.INC

Data files that are not included in appendix, but included in the attached ZIP file:

1. 'GRID.GRDECL'
2. 'PERMX.GRDECL'
3. 'PERMY.GRDECL'
4. 'PERMZ.GRDECL'
5. 'PORO.GRDECL'
6. 'ACTNUM.GRDECL'
7. 'SATNUM.GRDECL'
8. 'PVTNUM.GRDECL'
9. 'ROCKNUM.GRDECL'
10. 'EQLNUM.GRDECL'
11. 'FIPNUM.GRDECL'

Main Data File, .DATA

data.txt

```
-- Format      : ECLIPSE keywords ASCII
-- Exported by : Petrel 2015.5 64-bit Schlumberger
-- User name   : jpnorgard
-- Date        : Wednesday, February 01 2017 10:39:36
-- Project     : Alta_sektor_DP_JPN.pet

RUNSPEC

EQLDIMS                                 -- Generated : Petrel
  2 /

TITLE                                   -- Generated : Petrel
'Alta DP Sektor Model'

WELLDIMS                                -- Generated : Petrel
  2 12 4 3 /

START                                   -- Generated : Petrel
  1 DEC 2023 /

DISGAS                                  -- Generated : Petrel

WATER                                   -- Generated : Petrel

OIL                                     -- Generated : Petrel

GAS                                     -- Generated : Petrel

PETOPTS                                 -- Generated : Petrel
INITNNC /

GRAVDR                                  -- Generated : Petrel

NODPPM                                  -- Generated : Petrel

DUALPORO                                -- Generated : Petrel

MONITOR                                 -- Generated : Petrel

MULTOUT                                 -- Generated : Petrel

METRIC                                  -- Generated : Petrel

DIMENS                                  -- Generated : Petrel
```

```
  35 18 184 /

TABDIMS                              -- Generated : Petrel
  2 2 1
GRID

INCLUDE                              -- Generated : Petrel
'A_S2_DPSP_DZ_0_GRID.INC' /

NOECHO                               -- Generated : Petrel

INCLUDE                              -- Generated : Petrel
'A_S2_DPSP_DZ_0_GRID.GRDECL' /

INCLUDE                              -- Generated : Petrel
'A_S2_DPSP_DZ_0_PROP_PERMX.GRDECL' /

INCLUDE                              -- Generated : Petrel
'A_S2_DPSP_DZ_0_PROP_PERMY.GRDECL' /

INCLUDE                              -- Generated : Petrel
'A_S2_DPSP_DZ_0_PROP_PERMZ.GRDECL' /

INCLUDE                              -- Generated : Petrel
'A_S2_DPSP_DZ_0_PROP_PORO.GRDECL' /

INCLUDE                              -- Generated : Petrel
'A_S2_DPSP_DZ_0_PROP_ACTNUM.GRDECL' /

INCLUDE                              -- Generated : Petrel
'A_S2_DPSP_DZ_0_PROP_SIGMAV.GRDECL' /

INCLUDE                              -- Generated : Petrel
'A_S2_DPSP_DZ_0_PROP_SIGMAGDV.GRDECL' /

INCLUDE                              -- Generated : Petrel
'A_S2_DPSP_DZ_0_PROP_DZMTRXV.GRDECL' /

ECHO                                 -- Generated : Petrel

EDIT

PROPS

INCLUDE                              -- Generated : Petrel
'A_S2_DPSP_DZ_0_PROPS.INC' /

REGIONS
```

```
NOECHO                                -- Generated : Petrel

INCLUDE                               -- Generated : Petrel
'A_S2_DPSP_DZ_0_PROP_SATNUM.GRDECL' /

INCLUDE                               -- Generated : Petrel
'A_S2_DPSP_DZ_0_PROP_PVTNUM.GRDECL' /

INCLUDE                               -- Generated : Petrel
'A_S2_DPSP_DZ_0_PROP_ROCKNUM.GRDECL' /

INCLUDE                               -- Generated : Petrel
'A_S2_DPSP_DZ_0_PROP_EQLNUM.GRDECL' /

INCLUDE                               -- Generated : Petrel
'A_S2_DPSP_DZ_0_PROP_FIPNUM.GRDECL' /

ECHO                                  -- Generated : Petrel

SOLUTION

INCLUDE                               -- Generated : Petrel
'A_S2_DPSP_DZ_0_SOL.INC' /

SUMMARY

INCLUDE                               -- Generated : Petrel
'A_S2_DPSP_DZ_0_SUM.INC' /

SCHEDULE

INCLUDE                               -- Generated : Petrel
'A_S2_DPSP_DZ_0_SCH.INC' /
```

Include File: GRID.INC

data.txt

```
INIT                                    -- Generated : Petrel

DPGRID                                  -- Generated : Petrel

GRIDFILE                                -- Generated : Petrel
  0 0 /

GRIDUNIT                                -- Generated : Petrel
  METRES /

MAPUNITS                                -- Generated : Petrel
  METRES /

MAPAXES                                 -- Generated : Petrel
  482293.69 7993098.73 482293.69 7994098.73 483293.69 7994098.73 /

MINPORV                                 -- Generated : Petrel
  0.01 /

PINCH                                   -- Generated : Petrel
  /
```

Include File: DZMTRXV.GRDECL

data.txt

```
BOX                                   -- Generated : Petrel
--Matrix Box
  1 35 1 18 1 92 /

DZMTRXV                               -- Generated : Petrel
  57960
ENDBOX                                -- Generated : Petrel
```

Include File: SIGMAGDV.GRDECL

data.txt

```
BOX                                   -- Generated : Petrel
--Matrix Box
  1 35 1 18 1 92 /

SIGMAGDV                              -- Generated : Petrel
  57960
ENDBOX                                -- Generated : Petrel
```

Include File: SIGMAV.GRDECL

data.txt

```
BOX                                     -- Generated : Petrel
--Matrix Box
  1 35 1 18 1 92 /

SIGMAV                                  -- Generated : Petrel
  57960
ENDBOX                                  -- Generated : Petrel
```

Include File: PROPS.INC

data.txt

```
SCALECRS
  YES/

PVTW                                  -- Generated : Petrel
         196.6       1.0184  3.3635E-005      0.68636  6.7216E-005 /
         196.6       1.0184  3.3635E-005      0.68636  6.7216E-005 /

PVDG
-- Dry gas
--             Pg                     Bg         my_g      -- Generated : Petrel
            25      0.04657     0.012383
            50     0.022521     0.013109
            75     0.014656     0.013869
           100     0.010809     0.014787
           125     0.008565     0.015902
           150     0.007122     0.017228
           175     0.006133     0.018764
         196.6     0.005511     0.020246
           200     0.005427     0.020491
           225     0.004908     0.022387
           250     0.004517      0.02443
           275     0.004221     0.026604
           300     0.003995       0.0289
  /
            25      0.04657     0.012383
            50     0.022521     0.013109
            75     0.014656     0.013869
           100     0.010809     0.014787
           125     0.008565     0.015902
           150     0.007122     0.017228
           175     0.006133     0.018764
         196.6     0.005511     0.020246
           200     0.005427     0.020491
           225     0.004908     0.022387
           250     0.004517      0.02443
           275     0.004221     0.026604
           300     0.003995       0.0289
  /

DENSITY                               -- Generated : Petrel
         826.3       1168.7      0.93884 /
         826.3       1168.7      0.93884 /

ROCKOPTS                              -- Generated : Petrel
```

```
  1
ROCK                                  -- Generated : Petrel
      400.0000   5.787E-005 /

--        RS              POIL           FVFO
PVTO                                  -- Generated : Petrel
        17.635           25       1.1117        1.042
                            50       1.1086        1.077
                            75       1.1056         1.11
                           100       1.1029        1.143
                           125       1.1003        1.176
                           150       1.0978        1.207
                           175       1.0955        1.238
                         196.6       1.0935        1.264
                           200       1.0932        1.268
                           225       1.0911        1.298
                           250       1.0891        1.327
                           275       1.0872        1.356
                           300       1.0854        1.384
                           305        1.085        1.389
                           310       1.0846        1.395 /
        32.176           50       1.1518        0.904
            75       1.1482        0.935
           100       1.1449        0.966
           125       1.1417        0.997
           150       1.1388        1.026
           175        1.136        1.056
         196.6       1.1337         1.08
           200       1.1333        1.084
           225       1.1308        1.112
           250       1.1285         1.14
           275       1.1262        1.167
           300        1.124        1.194
           305       1.1236        1.199
           310       1.1232        1.205 /
        45.154           75       1.1845        0.792
           100       1.1805        0.821
           125       1.1768        0.849
           150       1.1733        0.877
           175         1.17        0.905
         196.6       1.1674        0.928
           200       1.1669        0.932
           225        1.164        0.958
           250       1.1612        0.984
           275       1.1586         1.01
           300       1.1561        1.035
           305       1.1556         1.04
           310       1.1551        1.045 /
         58.39          100       1.2172        0.697
```

```
   125       1.2129        0.724
   150       1.2088         0.75
   175        1.205        0.776
 196.6       1.2019        0.797
   200       1.2014        0.801
   225        1.198        0.825
   250       1.1948         0.85
   275       1.1918        0.874
   300       1.1889        0.897
   305       1.1883        0.902
   310       1.1878        0.907 /
72.032          125       1.2506        0.617
   150       1.2459        0.641
   175       1.2414        0.665
 196.6       1.2378        0.685
   200       1.2373        0.688
   225       1.2334        0.711
   250       1.2297        0.734
   275       1.2262        0.756
   300       1.2229        0.778
   305       1.2223        0.782
   310       1.2216        0.787 /
 86.18          150        1.285        0.548
                175       1.2798         0.57
               196.6      1.2757        0.589
                200       1.275        0.592
                225       1.2705        0.613
                250       1.2663        0.634
                275       1.2623        0.654
                300       1.2585        0.675
                305       1.2578        0.679
                310       1.2571        0.683 /
100.93          175       1.3205        0.489
               196.6       1.3157        0.506
                200        1.315        0.509
                225       1.3098        0.528
                250        1.305        0.548
                275       1.3004        0.567
                300       1.2961        0.585
                305       1.2953        0.589
                310       1.2945        0.593 /
114.24        196.6       1.3524        0.444
                200       1.3516        0.447
                225       1.3458        0.465
                250       1.3403        0.483
                275       1.3352          0.5
                300       1.3304        0.518
                305       1.3295        0.521
                310       1.3285        0.525 /
```

```
      116.38          200       1.3576        0.438
         225       1.3516        0.456
         250        1.346        0.473
         275       1.3408        0.491
         300       1.3359        0.508
         305        1.335        0.511
         310       1.3341        0.515 /
       132.7          225       1.3965        0.393
         250       1.3901        0.409
         275       1.3842        0.425
         300       1.3786        0.441
         305       1.3775        0.444
         310       1.3765        0.447 /
       150.1          250       1.4379        0.353
         275        1.431        0.368
         300       1.4247        0.382
         305       1.4235        0.385
         310       1.4223        0.388 /
      168.69          275       1.4819        0.319
         300       1.4746        0.332
         305       1.4732        0.334
         310       1.4718        0.337 /
      188.58          300       1.5288        0.288
         305       1.5272         0.29
         310       1.5257        0.293 /
/
      17.635           25       1.1117        1.042
          50       1.1086        1.077
          75       1.1056         1.11
         100       1.1029        1.143
         125       1.1003        1.176
         150       1.0978        1.207
         175       1.0955        1.238
       196.6       1.0935        1.264
         200       1.0932        1.268
         225       1.0911        1.298
         250       1.0891        1.327
         275       1.0872        1.356
         300       1.0854        1.384
         305        1.085        1.389
         310       1.0846        1.395 /
      32.176           50       1.1518        0.904
          75       1.1482        0.935
         100       1.1449        0.966
         125       1.1417        0.997
         150       1.1388        1.026
         175        1.136        1.056
       196.6       1.1337         1.08
         200       1.1333        1.084
```

```
   225       1.1308       1.112
   250       1.1285        1.14
   275       1.1262       1.167
   300        1.124       1.194
   305       1.1236       1.199
   310       1.1232       1.205 /
45.154          75      1.1845       0.792
   100       1.1805       0.821
   125       1.1768       0.849
   150       1.1733       0.877
   175         1.17       0.905
 196.6       1.1674       0.928
   200       1.1669       0.932
   225        1.164       0.958
   250       1.1612       0.984
   275       1.1586        1.01
   300       1.1561       1.035
   305       1.1556        1.04
   310       1.1551       1.045 /
 58.39         100      1.2172       0.697
   125       1.2129       0.724
   150       1.2088        0.75
   175        1.205       0.776
 196.6       1.2019       0.797
   200       1.2014       0.801
   225        1.198       0.825
   250       1.1948        0.85
   275       1.1918       0.874
   300       1.1889       0.897
   305       1.1883       0.902
   310       1.1878       0.907 /
72.032         125      1.2506       0.617
   150       1.2459       0.641
   175       1.2414       0.665
 196.6       1.2378       0.685
   200       1.2373       0.688
   225       1.2334       0.711
   250       1.2297       0.734
   275       1.2262       0.756
   300       1.2229       0.778
   305       1.2223       0.782
   310       1.2216       0.787 /
86.18          150       1.285       0.548
   175       1.2798        0.57
 196.6       1.2757       0.589
   200        1.275       0.592
   225       1.2705       0.613
   250       1.2663       0.634
   275       1.2623       0.654
```

```
          300       1.2585        0.675
          305       1.2578        0.679
          310       1.2571        0.683 /
       100.93          175       1.3205        0.489
        196.6       1.3157        0.506
          200        1.315        0.509
          225       1.3098        0.528
          250        1.305        0.548
          275       1.3004        0.567
          300       1.2961        0.585
          305       1.2953        0.589
          310       1.2945        0.593 /
       114.24        196.6       1.3524        0.444
          200       1.3516        0.447
          225       1.3458        0.465
          250       1.3403        0.483
          275       1.3352          0.5
          300       1.3304        0.518
          305       1.3295        0.521
          310       1.3285        0.525 /
       116.38          200       1.3576        0.438
          225       1.3516        0.456
          250        1.346        0.473
          275       1.3408        0.491
          300       1.3359        0.508
          305        1.335        0.511
          310       1.3341        0.515 /
        132.7          225       1.3965        0.393
          250       1.3901        0.409
          275       1.3842        0.425
          300       1.3786        0.441
          305       1.3775        0.444
          310       1.3765        0.447 /
        150.1          250       1.4379        0.353
          275        1.431        0.368
          300       1.4247        0.382
          305       1.4235        0.385
          310       1.4223        0.388 /
       168.69          275       1.4819        0.319
          300       1.4746        0.332
          305       1.4732        0.334
          310       1.4718        0.337 /
       188.58          300       1.5288        0.288
          305       1.5272         0.29
          310       1.5257        0.293 /
/

FILLEPS                          -- Generated : Petrel
```

```
--          Sw             Krelw          Krelo               Pc,OW
-- Table 1 for Matrix, table 2 for Fractures
SWOF                                  -- Generated : Petrel
          0.12            0            1      0.83324
          0.15   0.00027233      0.85083      0.50966
       0.19556   0.00068587       0.6243      0.33749
           0.2   0.00096829       0.6091      0.32069
       0.27111     0.005487      0.36595      0.22055
           0.3      0.01047      0.30155      0.17986
       0.34667     0.018519      0.19753      0.15045
           0.4     0.036432      0.12534      0.11683
       0.42222     0.043896      0.09526      0.10935
       0.49778     0.085734     0.039018      0.08392
           0.5      0.08757     0.038234     0.083172
       0.57333      0.14815     0.012346     0.072071
       0.64889      0.23525    0.0024387     0.060634
       0.72444      0.35117   0.00015242     0.049196
           0.8          0.5            0     0.037759
             1            1            0            0
  /
             0            0            1            0
             1            1            0            0
  /


--          Sg             Krelg          Krelo               Pc,OG
-- Table 1 for Matrix, table 2 for Fractures
SGOF                                  -- Generated : Petrel
             0            0            1            0
          0.05            0      0.73676            0
       0.12875       0.0125      0.43188            0
        0.2075         0.05      0.23312            0
       0.28625       0.1125      0.11242            0
         0.365          0.2     0.046048            0
       0.44375       0.3125      0.01457            0
        0.5225         0.45     0.002878            0
       0.60125       0.6125   0.00017987            0
          0.68          0.8  7.1057E-064            0
          0.88            1            0            0
  /
             0            0            1            0
             1            1            0            0
  /
```

Include File: SCH.INC

data.txt

```
RUNCTRL
DTMAX 3 /
DTINITIAL 0.001      /
DTMIN 0.00001        /
/

RPTSCHED                              -- Generated : Petrel
  FIP WELLS /

RPTRST                                -- Generated : Petrel
  BASIC=3 FLOWS FREQ PCOW PCOG /

SKIP                                  -- Generated : Petrel
--Hint: Select wells on the input tree, drop in with the blue arrow, then add rules with the rule po

ENDSKIP                               -- Generated : Petrel

WELSPECS                              -- Generated : Petrel
--'OP' is the simulation well name used to describe flow from 'OP'
--'GI 2' is the simulation well name used to describe flow from 'GI 2'
--
--Well    Grp       WH/HeelI J  RD PHASE
  OP      PROD      22        5 1  'GI 2' 'NOT USED'  2       13 1  /

COMPDAT                               -- Generated : Petrel
   OP 22 5 159 159 OPEN 1   OP 22 6 159 159 OPEN 1   OP 22 7 159 159 OPEN 1   OP 22 8 159 159 OPEN 1

GRUPTREE                              -- Generated : Petrel
  'NOT USED' FIELD /
  PROD FIELD /
  INJ FIELD /
  /

WCONPROD                              -- Generated : Petrel
  OP OPEN GRUP 1500.00 1  /

GCONINJE                              -- Generated : Petrel
  FIELD GAS VREP 1  /

WECON                                 -- Generated : Petrel
  OP 10.00 1  /

WCONINJE                              -- Generated : Petrel
  'GI 2' GAS OPEN GRUP 1  /
```

```
WTEST                                   -- Generated : Petrel
  OP 7.0000 P 0 0.0000 /
  /

DATES                                   -- Generated : Petrel
  11 DEC 2023 /
  /

DATES                                   -- Generated : Petrel
  21 DEC 2023 /
  /

DATES                                   -- Generated : Petrel
  31 DEC 2023 /
  /

DATES                                   -- Generated : Petrel
  10 JAN 2024 /
  /

DATES                                   -- Generated : Petrel
  20 JAN 2024 /
  /

DATES                                   -- Generated : Petrel
  30 JAN 2024 /
  /

DATES                                   -- Generated : Petrel
  9 FEB 2024 /
  /

DATES                                   -- Generated : Petrel
  19 FEB 2024 /
  /

DATES                                   -- Generated : Petrel
  29 FEB 2024 /
  /

DATES                                   -- Generated : Petrel
  10 MAR 2024 /
  /

DATES                                   -- Generated : Petrel
  20 MAR 2024 /
  /
```

```
DATES                                   -- Generated : Petrel
  30 MAR 2024 /
  /

DATES                                   -- Generated : Petrel
  9 APR 2024 /
  /

DATES                                   -- Generated : Petrel
  19 APR 2024 /
  /

DATES                                   -- Generated : Petrel
  29 APR 2024 /
  /

DATES                                   -- Generated : Petrel
  9 MAY 2024 /
  /

DATES                                   -- Generated : Petrel
  19 MAY 2024 /
  /

DATES                                   -- Generated : Petrel
  29 MAY 2024 /
  /

DATES                                   -- Generated : Petrel
  8 JUN 2024 /
  /

DATES                                   -- Generated : Petrel
  18 JUN 2024 /
  /

DATES                                   -- Generated : Petrel
  28 JUN 2024 /
  /

DATES                                   -- Generated : Petrel
  8 JUL 2024 /
  /

DATES                                   -- Generated : Petrel
  18 JUL 2024 /
  /

DATES                                   -- Generated : Petrel
```

```
  28 JUL 2024 /
  /

DATES                                   -- Generated : Petrel
  7 AUG 2024 /
  /

DATES                                   -- Generated : Petrel
  17 AUG 2024 /
  /

DATES                                   -- Generated : Petrel
  27 AUG 2024 /
  /

DATES                                   -- Generated : Petrel
  6 SEP 2024 /
  /

DATES                                   -- Generated : Petrel
  16 SEP 2024 /
  /

DATES                                   -- Generated : Petrel
  26 SEP 2024 /
  /

DATES                                   -- Generated : Petrel
  6 OCT 2024 /
  /

DATES                                   -- Generated : Petrel
  16 OCT 2024 /
  /

DATES                                   -- Generated : Petrel
  26 OCT 2024 /
  /

DATES                                   -- Generated : Petrel
  5 NOV 2024 /
  /

DATES                                   -- Generated : Petrel
  15 NOV 2024 /
  /

DATES                                   -- Generated : Petrel
  25 NOV 2024 /
```

```
  /

DATES                                   -- Generated : Petrel
  1 DEC 2024 /
  /

DATES                                   -- Generated : Petrel
  1 JUN 2025 /
  /

DATES                                   -- Generated : Petrel
  1 DEC 2025 /
  /

DATES                                   -- Generated : Petrel
  1 JUN 2026 /
  /

DATES                                   -- Generated : Petrel
  1 DEC 2026 /
  /

DATES                                   -- Generated : Petrel
  1 JUN 2027 /
  /

DATES                                   -- Generated : Petrel
  1 DEC 2027 /
  /

DATES                                   -- Generated : Petrel
  1 JUN 2028 /
  /

DATES                                   -- Generated : Petrel
  1 DEC 2028 /
  /

DATES                                   -- Generated : Petrel
  1 JUN 2029 /
  /

DATES                                   -- Generated : Petrel
  1 DEC 2029 /
  /

DATES                                   -- Generated : Petrel
  1 JUN 2030 /
  /
```

```
DATES                                   -- Generated : Petrel
  1 DEC 2030 /
  /

DATES                                   -- Generated : Petrel
  1 JUN 2031 /
  /

DATES                                   -- Generated : Petrel
  1 DEC 2031 /
  /

DATES                                   -- Generated : Petrel
  1 JUN 2032 /
  /

DATES                                   -- Generated : Petrel
  1 DEC 2032 /
  /

DATES                                   -- Generated : Petrel
  1 JUN 2033 /
  /

DATES                                   -- Generated : Petrel
  1 DEC 2033 /
  /

DATES                                   -- Generated : Petrel
  1 JUN 2034 /
  /

DATES                                   -- Generated : Petrel
  1 DEC 2034 /
  /

DATES                                   -- Generated : Petrel
  1 JUN 2035 /
  /

DATES                                   -- Generated : Petrel
  1 DEC 2035 /
  /

DATES                                   -- Generated : Petrel
  1 JUN 2036 /
  /
```

```
DATES                                   -- Generated : Petrel
  1 DEC 2036 /
  /

DATES                                   -- Generated : Petrel
  1 JUN 2037 /
  /

DATES                                   -- Generated : Petrel
  1 DEC 2037 /
  /

DATES                                   -- Generated : Petrel
  1 JUN 2038 /
  /

DATES                                   -- Generated : Petrel
  1 DEC 2038 /
  /

DATES                                   -- Generated : Petrel
  1 JUN 2039 /
  /

DATES                                   -- Generated : Petrel
  1 DEC 2039 /
  /

DATES                                   -- Generated : Petrel
  1 JUN 2040 /
  /

DATES                                   -- Generated : Petrel
  1 DEC 2040 /
  /

DATES                                   -- Generated : Petrel
  1 JUN 2041 /
  /

DATES                                   -- Generated : Petrel
  1 DEC 2041 /
  /

DATES                                   -- Generated : Petrel
  1 JUN 2042 /
  /

DATES                                   -- Generated : Petrel
```

```
  1 DEC 2042 /
  /

DATES                                   -- Generated : Petrel
  1 JUN 2043 /
  /

DATES                                   -- Generated : Petrel
  1 DEC 2043 /
  /
```

Include File: SOL.INC

data.txt

```
EQUIL                                -- Generated : Petrel
         1878        196.6         1924            0         1878           0 1 0 0 /
         1878        196.6         1924            0         1878           0 2 0 0 /

RSVD                                 -- Generated : Petrel
         1878       114.24
         1888        113.5
         1898       112.76
         1908       112.08
         1918       111.34
         1928       110.67
         1938       109.93
         1948       109.25
         1958       108.51
  /
         1878       114.24
         1888        113.5
         1898       112.76
         1908       112.08
         1918       111.34
         1928       110.67
         1938       109.93
         1948       109.25
         1958       108.51
  /

RPTRST                               -- Generated : Petrel
  BASIC=3 FLOWS PCOW PCOG /

RPTSOL                               -- Generated : Petrel
  RESTART=2 FIP /
```

Include File: SUM.INC

data.txt

```
WBP4                                    -- Generated : Petrel
 /

WSTAT                                   -- Generated : Petrel
 /

FWGR                                    -- Generated : Petrel

WWGR                                    -- Generated : Petrel
 /

GWGR                                    -- Generated : Petrel
 /

FWCT                                    -- Generated : Petrel

WWCT                                    -- Generated : Petrel
 /

GWCT                                    -- Generated : Petrel
 /

FRV                                     -- Generated : Petrel

WTHP                                    -- Generated : Petrel
 /

TIMESTEP                                -- Generated : Petrel

FRS                                     -- Generated : Petrel

FVPR                                    -- Generated : Petrel

WVPR                                    -- Generated : Petrel
 /

GVPR                                    -- Generated : Petrel
 /

FVPT                                    -- Generated : Petrel

WVPT                                    -- Generated : Petrel
 /
```

```
GVPT                                -- Generated : Petrel
 /

FVIR                                -- Generated : Petrel

WVIR                                -- Generated : Petrel
 /

GVIR                                -- Generated : Petrel
 /

FVIT                                -- Generated : Petrel

WVIT                                -- Generated : Petrel
 /

GVIT                                -- Generated : Petrel
 /

WPI                                 -- Generated : Petrel
 /

FWPR                                -- Generated : Petrel

WWPR                                -- Generated : Petrel
 /

GWPR                                -- Generated : Petrel
 /

FOPR                                -- Generated : Petrel

WOPR                                -- Generated : Petrel
 /

GOPR                                -- Generated : Petrel
 /

FGPR                                -- Generated : Petrel

WGPR                                -- Generated : Petrel
 /

GGPR                                -- Generated : Petrel
 /

WEPR                                -- Generated : Petrel
 /
```

```
FWPT                                -- Generated : Petrel

WWPT                                -- Generated : Petrel
 /

GWPT                                -- Generated : Petrel
 /

FOPT                                -- Generated : Petrel

WOPT                                -- Generated : Petrel
 /

GOPT                                -- Generated : Petrel
 /

FGPT                                -- Generated : Petrel

WGPT                                -- Generated : Petrel
 /

GGPT                                -- Generated : Petrel
 /

FPR                                 -- Generated : Petrel

FWIP                                -- Generated : Petrel

FOIPG                               -- Generated : Petrel

FGIPL                               -- Generated : Petrel

FOIP                                -- Generated : Petrel

FOIPL                               -- Generated : Petrel

FGIP                                -- Generated : Petrel

FGIPG                               -- Generated : Petrel

FWIR                                -- Generated : Petrel

WWIR                                -- Generated : Petrel
 /

GWIR                                -- Generated : Petrel
 /
```

```
FOIR                                -- Generated : Petrel

WOIR                                -- Generated : Petrel
 /

GOIR                                -- Generated : Petrel
 /

FGIR                                -- Generated : Petrel

WGIR                                -- Generated : Petrel
 /

GGIR                                -- Generated : Petrel
 /

FWIT                                -- Generated : Petrel

WWIT                                -- Generated : Petrel
 /

GWIT                                -- Generated : Petrel
 /

FOIT                                -- Generated : Petrel

WOIT                                -- Generated : Petrel
 /

GOIT                                -- Generated : Petrel
 /

FGIT                                -- Generated : Petrel

WGIT                                -- Generated : Petrel
 /

GGIT                                -- Generated : Petrel
 /

FGOR                                -- Generated : Petrel

WGOR                                -- Generated : Petrel
 /

GGOR                                -- Generated : Petrel
 /

WBHP                                -- Generated : Petrel
```

/
